# Evaluating the Performance of Thermally and UV Aged Firefighters' Protective Clothing Using both Destructive and Non-Destructive Methods

A Thesis Submitted to the College of

Graduate and Postdoctoral Studies

In Partial Fulfilment of the Requirements

For the Degree of Master of Science

In the Department of Mechanical Engineering

University of Saskatchewan

Saskatoon

By

Mackenzie Fulton

# Permission to Use

In presenting this dissertation in partial fulfilment of the requirements for a Postgraduate degree from the University of Saskatchewan, I agree that the Libraries of this University may make it freely available for inspection. I further agree that permission for copying of this dissertation in any manner, in whole or in part, for scholarly purposes may be granted by the professor or professors who supervised my dissertation work or, in their absence, by the Head of the Department or the Dean of the College in which my thesis work was done. It is understood that any copying or publication or use of this thesis/dissertation or parts thereof for financial gain shall not be allowed without my written permission. It is also understood that due recognition shall be given to me and to the University of Saskatchewan in any scholarly use which may be made of any material in my dissertation.

Requests for permission to copy or to make other uses of materials in this dissertation in whole or part should be addressed to:

Head of the Department of Mechanical Engineering
University of Saskatchewan
Saskatoon, Saskatchewan S7N 5A9
Canada

OR

Dean
College of Graduate and Postdoctoral Studies
University of Saskatchewan
Room 116 Thorvaldson Building, 110 Science Place
Saskatoon, Saskatchewan S7N 5C9
Canada

# Disclaimer

The names of certain commercial products were exclusively used to meet the dissertation and/or exhibition requirements for the degree of Master of Science at the University of Saskatchewan. Reference in this dissertation to any specific commercial products, process, or service by trade name, trademark, manufacturer, or otherwise, does not constitute or imply its endorsement, recommendation, or favoring by the University of Saskatchewan. The views and opinions of the author expressed herein do not state or reflect those of the University of Saskatchewan, and shall not be used for advertising or product endorsement purposes.

# Abstract

Firefighters' protective clothing (e.g. coat and pants) are multi-layer ensembles consisting of an outer shell, moisture barrier, and thermal liner. Strict material performance and manufacturing conditions exist for new firefighter protective clothing constructions, but evaluation of in-use or worn protective clothing lacks these defined metrics. A need currently exists for the development of a quantitative, material-property based method of determining the remaining useful life of firefighters' protective clothing. A non-destructive testing method is desirable due to the high replacement cost of firefighters' protective clothing. Additionally, a non-destructive testing procedure developed in laboratory conditions could be adapted for field use and allow for material performance history tracking by individual firefighters. Guidelines and specific performance indicators could then be developed for a detailed garment retirement procedure for future implementation in fire departments. This information would be extremely useful to many firefighting departments in Canada and around the world.

This study considered destructive and non-destructive textile testing of aged outer shell materials of firefighters' clothing. Three types of outer-shell Kevlar®/PBI fabric types were examined and mechanical strength was used to evaluate remaining fabric performance following thermal and UV ageing procedures. Thermal exposures were chosen based on data obtained from thermogravimetric testing and exposure conditions faced by firefighters. A scanning electron microscope was used to evaluate microstructural changes in the fabrics following thermal and UV ageing procedures. A fiber microstructure crack-development process based on ageing was outlined using this information. Near infrared (NIR) reflectance readings were obtained through the use of a spectrophotometer and related to the remaining material strength of the aged fabrics.

Different methods of interpreting NIR spectral results were compared. These included reflectance shifts, absorbance feature characteristic changes (e.g. feature area and peak prominence/width), and slope change based on a normalized-difference index method. Absorbance feature area and characteristic changes showed promise at explaining thermochemical changes in the specimens following ageing. However, the normalized-difference index slope changes showed the best potential for characterizing the remaining tensile strength for all three fabrics.

# Acknowledgements

I would like to sincerely thank Prof. David Torvi for his continuous guidance and support throughout my program. His passion for fire protection engineering and financial support are greatly appreciated. I would like to specially thank Prof. Scott Noble from the Department of Mechanical Engineering for his guidance in infrared spectroscopy and spectral analysis. His strong background in optics and results interpretation were invaluable in many stages of my completed thesis. Prof. Jane Batcheller with the Department of Human Ecology at the University of Alberta was very knowledgeable in the set-up and troubleshooting of the equipment in the laboratory. I learned a great deal about textile properties and experimental procedures under her guidance. Technical support from both Mr. Ahmed Tiamyu and Mr. Nanfang Zhao in using the scanning electron microscope and interpretation guidance from Prof. Akindele Odeshi is appreciated. Technical support from Professor Robert Scott from the Department of Chemistry in using the thermogravimetric analyzer is appreciated. Support from Melanie Fauchoux, Reisha Peters, and Chris Bespflug is acknowledged.

Examination of my advisory committee members is acknowledged. I wish to extend deep thanks to my family and friends for their support during my academic program. Your constant encouragement and interest in my research activities was always welcome and appreciated.

Financial support from Natural Science and Engineering Research Council of Canada (NSERC), Department of Mechanical Engineering, and College of Graduate and Postdoctoral Studies at the University of Saskatchewan is greatly appreciated. Donation of fabrics by Diane Hess from PBI Performance Products, Inc. is also acknowledged.

# Table of Contents

# List of Tables

# List of Figures

# List of Symbols

## English Letters

| | |
|---|---|
| $A$ | Absorbance |
| $A_n$ | Normalized feature area |
| $P_n$ | Normalized feature prominence |
| $T_i$ | Initial temperature |
| $\% TS$ | Percentage of original tensile strength |

## Greek Letters

| | |
|---|---|
| $\Delta T$ | Temperature increase |
| $\rho$ | Diffuse Reflectance |
| $\rho_o$ | Original or unaged diffuse reflectance |
| $\rho_n$ | Diffuse reflectance at ageing condition $n$ |
| $\rho_{1160}$ | Reflectance reading at the 1160 nm wavelength when calculating a normalized difference index |
| $\rho_{1360}$ | Reflectance reading at the 1360 nm wavelength when calculating a normalized difference index |

# List of Abbreviations and Acronyms

| | |
|---|---|
| AATCC | American Association of Textile Chemists and Colorists |
| AFM | Atomic Force Microscopy |
| ASTM | American Society for Testing and Materials |
| ATR | Attenuated Total Reflectance |
| CCHR | Conductive and Compressed Heat Resistance |
| CFD | Computational Fluid Dynamics |
| CGSB | Canada General Standards Board |
| CHTC | Convective Heat Transfer Coefficient |
| CIE | International Commission on Illumination |
| CRE | Constant Rate of Extension |
| DAQ | Data Acquisition System or Systems |
| EN | European Standard from European Committee for Standardization |
| FTIR | Fourier Transform Infrared Spectroscopy |
| IR | Infrared |
| ISO | International Standards Organization |
| LSCM | Laser Scanning Confocal Microscopy |
| NDI | Normalized Difference Index |
| NDT | Non-destructive test or testing |
| NFPA | National Fire Protection Association |
| NIR | Near-Infrared Spectrum of Light |
| OS | Outer Shell Material of Firefighters' Protective Clothing |
| P&ID | Process and Instrumentation Diagram |
| PBI | Polybenzimidazole |
| PPE | Personal Protective Clothing |
| Pt | Platinum |
| RGB | Red-Green-Blue |
| RH | Relative Humidity (%) |
| RPP | Radiative Protective Performance |

| | |
|---|---|
| RS | Ripstop Fabric Type |
| SEM | Scanning Electron Microscope or Microscopy |
| SFH | Standard Fading Hours, unit of UV exposure |
| SPHERE | Simulated Photodegradation via High energy Radiant Exposure |
| TGA | Thermogravimetric Analysis |
| TPP | Thermal Protective Performance |
| UofS | University of Saskatchewan |
| UV | Ultra-Violet Light Radiation |
| XRD | X-Ray Diffraction |

# 1. Introduction[1]

The prevention and suppression of fires is the main goal of active firefighting departments around the world. In 2015 the United States had over 1.3 million reported fires resulting in an estimated $14.3 billion worth of property damage (National Fire Protection Association 2016). On average this means a fire department was responding to a fire every 23 seconds in 2015 in the United States. Similar statistics for a majority of Canadian provinces from 2003 – 2007 show that 42,753 fires resulted in 226 deaths and about $1.5 billion in direct property damage (Wijayasinghe 2011). With these statistics in mind the importance of the firefighting profession and structural firefighting techniques is very clear. Firefighters rely on their personal protective equipment (PPE) ensembles (pants, coats, gloves, boots, helmets, visors, self-contained breathing apparatus (SCBA)) when responding to active fires. These full ensembles are designed to be durable, resist intense thermal exposure from heat and flames, reduce the impact of liquid sprays or steam, prevent ripping or tearing from sharp/abrasive surface contact, and still provide a high degree of user mobility for the performance of firefighting activities.

The firefighting occupation comes with inherent risks. These risks should be minimized in order to ensure the continued safety of firefighters in their hazardous workplace. One of the major issues facing a fire professional is the ongoing condition of their turnout or thermal protective gear. When entering a fire-filled compartment firefighters deserve to know how well their main source of protection is going to actually protect them under the wide variety of working conditions. The protective clothing (i.e. pants and coats) a firefighter wears is a critical piece of equipment in the prevention of injury or death while responding to a fire. These multi-layer protective clothing ensembles have been specifically designed to withstand elevated thermal exposure conditions. Typical constructions consist of an external outer shell, moisture barrier, and an inner thermal or comfort liner. Inner thermal or comfort layers provides the firefighter with insulation against heat or cold while the moisture barrier is designed to prevent the passage of liquids while allowing some vapour diffusion. The outer shell material provides initial protection against heat, flames, abrasive or sharp surfaces, and would be the most

[1] A portion of this chapter has been published in Advanced Characterization and Testing of Textiles (Fulton, Rezazadeh and Torvi 2017). The author was responsible for updating and adding new information to the previous literature review conducted by Rezazadeh (2011).

accessible material to analyze using a non-destructive test. Therefore, this outer layer material will be the main focus of this current research. Outer shell materials are typically made from Nomex®[2], Kevlar®[2], and PBI blends in varying material compositions due to their high strength and flame resistant abilities. More information on the other layer materials can be found in previous work by Thorpe (2004) and Rezazadeh (2014).

Strict standards must be met before a piece of firefighters' clothing enters active service (NFPA 1971 2013). However, end users are not only interested in the performance of textiles when they are new, but the continuing performance of textiles, and the products that contain these materials, over their entire useful life. The same level of quantitative guidelines are absent when trying to evaluate the condition or remaining service life of in-use clothing (NFPA 1851 2014). According to NFPA 1851 (2014) these high-performance articles of clothing are typically retired after a manufacturer stated useful lifespan has been reached (typically 5 – 10 years), when the cost of repair becomes too onerous (higher than replacement cost), or if there is contact with CBRN terrorism agents (chemicals, biological agents, and radioactive materials). Additionally, an ensemble may be retired after significant visual signs of ageing (rips, tears, severe discoloration) appear. In applications such as protective clothing the continuing performance and the ability to determine replacement timelines will have a significant impact of the safety of end users. There is a current need for improved methods of evaluating the performance and remaining active life of in-use firefighters' protective clothing and for a better understanding of the ageing process of outer shell materials.

One particular important issue with evaluating performance of in-use textiles is that most standard tests are destructive. Therefore, in many applications these tests cannot be practically used to evaluate the performance of in-use clothing, especially when this clothing is expensive; such as firefighters' protective clothing. To address this issue, non-destructive tests are being developed to provide information to aid in evaluating in-use textiles and determining whether or not to replace individual products. This is already being done in many other engineering applications, such as the evaluation of urban infrastructure.

[2] Commercial products are identified in this thesis in order to adequately specify the results of research. In no case should this identification imply recommendation or endorsement by the author, nor does it suggest the product or material identified is the best choice for the purpose of research.

These introductory sections (Section 1.1 – 1.12) will briefly review textile ageing processes, as well as how these processes impact important aspects of textile performance. Recent research to quantify the effects of ageing on textile performance will be discussed, along with standard and non-standard tests that can be used to evaluate the continuing performance of textiles. In many cases, the same tests that are used to evaluate the textiles when new are used to determine the change in one or more specific performance aspects of used textiles. The scope and objectives of this current research are then outlined in Section 1.13.

## 1.1. Textile Ageing

A general definition of ageing, which can be applied to firefighters' protective clothing, is the accumulation of all changes in a system with the passage of time (Timiras, Quay and Vernadakis 1995). These changes are irreversible and usually cause a decline in performance or loss of functionality. However, some features, such as thermal protective performance or aesthetics, may improve as a result of ageing (Johnson 2005).

Degradation is defined as weakening and loss of properties that are necessary for satisfactory performance due to changes that occur as a result of the ageing process (Slater 1991). It is possible for textile degradation to occur prior to field use. However, this introductory section will primarily focus on ageing that occurs after textiles have experienced use and on methods used to evaluate used thermal protective clothing for firefighters and other workers.

Slater (1991) discusses the main causes of degradation of textiles and the mechanisms by which this degradation can occur. Some degradation may occur before a product reaches the end user as a result of the processing of textiles, either in the various stages of production of a fabric (Zhao, et al. 2012; Zhang, et al. 2014), or during dyeing or finishing. Once a product reaches the end user, some degradation may also occur during storage. Often degradation that occurs during either normal or severe use is of primary concern to the end user and may have a large impact on performance (Cloud and Lowe 1995). For example, for firefighters' protective clothing this degradation may be caused by a number of factors including:

- mechanical action (e.g., abrasion),

- environmental conditions (e.g., exposure to ultra-violet (UV) radiation, weathering, moisture),
- cleaning and maintenance procedures, and
- exposure to high temperatures and/or heat fluxes.

In some cases, end users are concerned with ageing of textiles simply for aesthetic purposes (Slater 1991). However, in other cases the ageing of textiles may lead to a decrease in user safety. For example, thermal protective fabrics commonly used for outer shells (OS) in firefighters' protective clothing have been shown to degrade with wear associated with normal use as well as exposures to high temperatures and other conditions (Thorpe, 2004; Davis, et al. 2010; Rezazadeh, 2014). Therefore, it is very important for firefighters to understand how their protective clothing may degrade with use.

Severe damage to firefighters' protective clothing and other textiles (tears, fading, and brittleness) are immediately evident during visual inspection. However, it has been shown the level of damage to the textiles may not be completely reflected by visible degradation. Slater (1986) found that performance may degrade below accepted levels before visual cues appear on a textile surface. For clarification Slater (1986) defined two levels of degradation in fabrics: a functional level and a visual level (Figure 1.1). The functional level is the limit below which the material performance of a fabric no longer meets performance or functional requirements. The visual level, which usually does not coincide with the functional level, is the point at which visual indicators of deterioration (colour fade, tears) become visually apparent (Slater 1986).

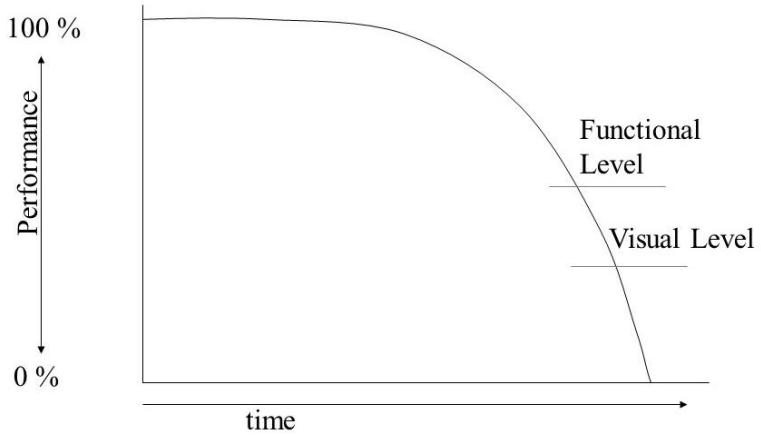


*Figure 1.1 Performance difference between the functional and visual level (adapted from Slater 1986)*

This could bring about severe consequences in specialized applications, such as firefighters' protective clothing, if degradation past the functional level occurred before the visible level. For example, Davis, et al. (2010) could not determine any evidence of deterioration in mechanical strength of exposed specimens through visual inspection or basic physical manipulation. However, measured values of tensile and tear strength of these aged fabrics were found to be significantly lower than new fabrics. Hence, it is possible that visual and manual inspection of a garment for physical damage (rips/cuts, tears, seam/thread discontinuities) and thermal damage (charring, burn holes) will not identify an unacceptable level of deterioration (Thorpe 2004).

Detailed discussions on the individual ageing degradation mechanisms (e.g. UV radiation, thermal exposures) can be found in previous work by Slater (1991), Rezazadeh and Torvi (2011), and Rezazadeh (2014). In order to understand the overall effects of ageing on individual textile products the effects of a number of factors will need to be understood (Rezazadeh 2014) including:

- the type of material used to manufacture the textile;
- the nature of conditions under which textiles are used, including exposures to high temperatures and heat fluxes, chemicals, and ultraviolet radiation;
- wear, pilling, and abrasion patterns; and
- the specific maintenance procedures used for the textiles.

These factors may vary considerably even for textiles that are used for similar applications. Sections 1.3 – 1.12 discuss methods that can be used to evaluate the effects of textile ageing on performance in the laboratory and under field conditions.

## 1.2. Background Chemistry of Outer Shell Materials

This section covers a brief introduction of outer shell material base chemical components with a focus on Kevlar® and PBI structures that are the main focus of this current study. More background information on these and other clothing layer materials are contained in previously reported work (Torvi, 1997; Thorpe 2004; Rezazadeh 2014).

Kevlar® and PBI are key textile fabrics for flame resistant applications, such as firefighting, due to their inherent ability to char when exposed to extreme temperatures rather than melting,

dripping, or igniting. Additionally, these high performance textiles are better at retaining their characteristics and resisting thermal decomposition under thermal exposure than other textiles. Repeating aromatic groups create a stiff molecule orientation that results in a very stable structure with the desirable thermal characteristics outlined above (Torvi 1997).

Kevlar® belongs to the poly(phenyleneisophthal-amide) group that has a chemical structure in the form of long-chain polyamide with amide linkages (-CO-NH-) of which more than 85% are connected directly to two aromatic rings (Federal Trade Commission 2009). Components in this class fall into two broad categories called *meta* and *para* oriented phenylene which differ in the location of the amide position within the phenylene group. These meta and para pre-cursors describe the relative position of substituents (other than hydrogen) in relation to each other on an aromatic hydrocarbon structure. Further details on the structure of these organic chemicals can be found in Rezazadeh (2014).

Kevlar® is a registered trademark version (DuPont 2016) of a polyamide (aramid) fibre that has the poly(para-phenyleneisophthal-amide) rod-like molecular structure shown in Figure 1.2.

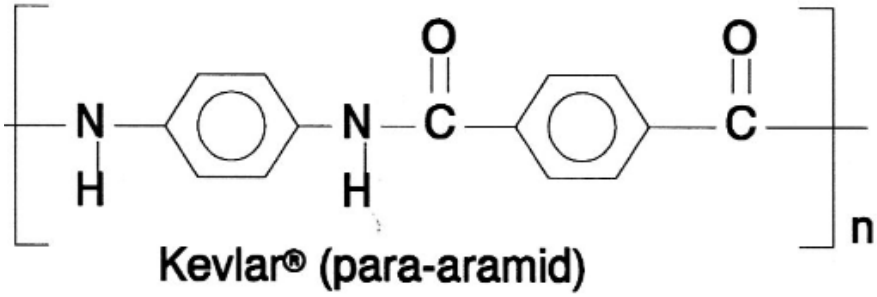


*Figure 1.2 Chemical structure of Kevlar® (Torvi 1997)*

PBI is the abbreviation for the synthetic aromatic polymer called polybenzimidazole. This material comes in the form of a long-chain aromatic polymer (i.e. reoccurring imidazole groups) with the chemical structure - $(C_{20}N_4H_{12})_n$- (Federal Trade Commission 2009) shown in Figure 1.3. PBI has a high chemical resistance and desirable performance properties in addition to similar flame resistant properties found in Kevlar®. These factors combine to make PBI an

appropriate choice for the outer shell materials of firefighters' protective clothing (Rezazadeh 2014).

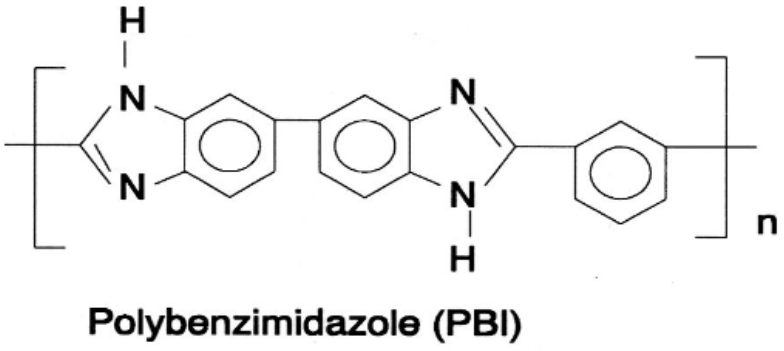


*Figure 1.3 Chemical structure for PBI (Torvi 1997)*

## 1.3. Tests for Textile Ageing

A study of the effects of ageing on textile performance generally involves two phases. The first phase is either sampling in-use textiles or using laboratory tests to simulate the expected ageing processes in the field. The second phase is to evaluate the performance of the textile, and to compare this performance to the same textile when it was originally new, or to some performance standard. This section will first describe full-scale field-fire experiments conducted and the exposure data obtained from each. Next, some of the ways that are used to simulate ageing of textiles in the laboratory will be discussed. Methods of evaluating performance, most of which are destructive tests included in standards for new textiles, are briefly described in this section. Examples of research in which these and other methods have been used to evaluate the effects of ageing on performance of textiles are then provided.

## 1.4. Firefighting Conditions and Full Scale Fire Testing

It is very important to understand the similarities and differences between exposures in the laboratory and field when interpreting the results of performance testing. Field conditions will often expose a fabric to repeated and combined degradation factors over an extended lifetime. This is especially true in firefighting due to the variable residential and industrial materials that may be burning at any given fire event. On the other hand, many laboratory testing procedures and testing devices are based on only one specific type of exposure. Bridging the gap between

controlled laboratory conditions and real-world situations is an ongoing area of active research. Some examples of textile ageing research are summarized in Tables 1.1 – 1.3.

Selecting appropriate ageing protocols is key to obtaining laboratory results that can be related to expected performance in the field. For example, variations between individual fire departments and individual firefighter roles make for a wide range of expected exposure conditions, in terms of both exposure intensity and frequency. One method that has been used in the past is to classify the heat flux and temperature exposures that firefighters are subjected to as routine, ordinary, and emergency conditions (Abbott and Schulman, 1976; Veghte, 1988; Donnelly, et al. 2006; Thorpe, 2004). For each of these classifications, a temperature and heat flux range is given, which can then be used to set heat flux and temperature exposure levels for thermal ageing in a laboratory environment. For example, a thermal manikin test (Figure 1.4) specifies a heat flux of 84 kW/m$^2$ to simulate a flash-fire environment (ASTM F1930-15 2015). A more detailed breakdown of this process is outlined by Rezazadeh (2014) who used information from the literature and measurements made in field fire tests to develop laboratory exposures to simulate the range of conditions that firefighters face during their duties. Temperature ranges outlined by Thorpe (2004) and originally described by Veghte (1988) can be found below in Figure 1.4.

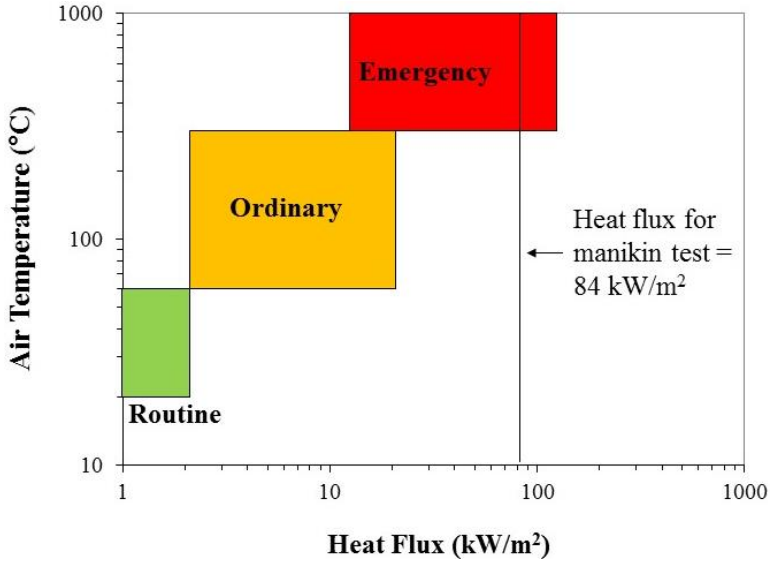


*Figure 1.4 Classification of firefighting conditions (Thorpe 2004)*

Therefore, quantifying real world exposure conditions is important when designing laboratory exposures. Full-scale fire testing of structures is relatively expensive and rarely performed, but the large amount of information obtained can be very valuable. For example, data obtained from the St. Lawrence burns (Shorter and McGuire 1958) has been in use for decades and has played a vital role in the development of spatial separation equations used in building codes in Canada and other countries. The environments a firefighter must face have been investigated by a number of authors (e.g. Veghte 1988; Udayraj, et al. 2016). Full scale fire data has also been obtained by the University of Saskatchewan to better classify these conditions for the purposes of this and other fire research. Three full scale tests conducted by the Univeristy of Saskatchewan are briefly described along with implications into the current research project.

### 1.4.1. Edmonton Full Scale Fire Test

Previous work by the research group at the University of Saskatchewan includes a full-scale fire test conducted in Edmonton, Alberta (Threlfall, Torvi and Thorpe 2004). This procedure consisted of a number of room-fire tests followed by the complete burn of the single story housing structure. Figure 1.5 shows the progression of fire development from the initial igintion source to the entire housing structure.

Heat flux measurements were recorded using different heat flux gauges located 4 m away from the open first story window. However, proximity to the fire required these instruments to be moved 11 minutes following ignition in order to prevent equipment damage. The recorded data (Figure 1.6) from this experiment shows that heat flux levels ranging from 15 – 20 $kW/m^2$ may occur outside of a house fire and could be considered within the working range of the firefighter. This data matched well with published classifications of the thermal hazard conditions present in the firefighting occupation (Figure 1.4).


*Figure 1.5 Fire development from the Edmonton full scale house fire (Threlfall, et al. 2004)*

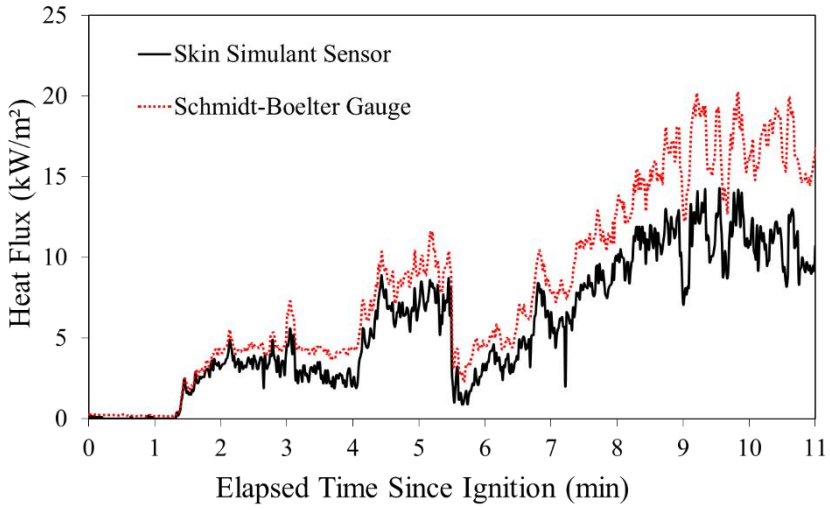


*Figure 1.6 Heat flux measurements recorded during a full scale house fire in Edmonton, Alberta (Threlfall, et al. 2004)*

## 1.4.2. Prince Albert Full Scale Fire Test

The Prince Albert Fire Department and the Saskatchewan Association of Fire Chiefs had the opportunity for live training using a donated house located south of Prince Albert. The house appeared to be a modified version of an Eatons' Eadwin style two story house (Winnipeg Architecture 1913) with an additional constructed entryway (Figure 1.7). Housing dimensions and other background information can be found in Fulton, et al. (2017b). Heat flux measurements were obtained from a water-cooled Schmidt-Boelter gauge located 8 m (26'2") away from the outside wall, 1.30 m (51") above the ground, and centered in the middle of the first-floor window. Temperature measurements of the fire (e.g. back wall through the window) were made using an infrared (IR) thermometer.

*Figure 1.7 Prince Albert full scale fire test before (left) and during (right) fire experiment (Fulton, et al. 2017b)*

Heat flux measurements are shown in Figure 1.8. Heat fluxes follow an exponential increase, sustain levels above 22 kW/m$^2$ near the height of the fire and reach a peak of about 28 kW/m$^2$. Temperatures measured by the IR thermometer through the first story window can be found in Figure 1.9. Heat flux and temperature measurements obtained in this study showcase the field exposure conditions a firefighter may experience when responding to a house fire.

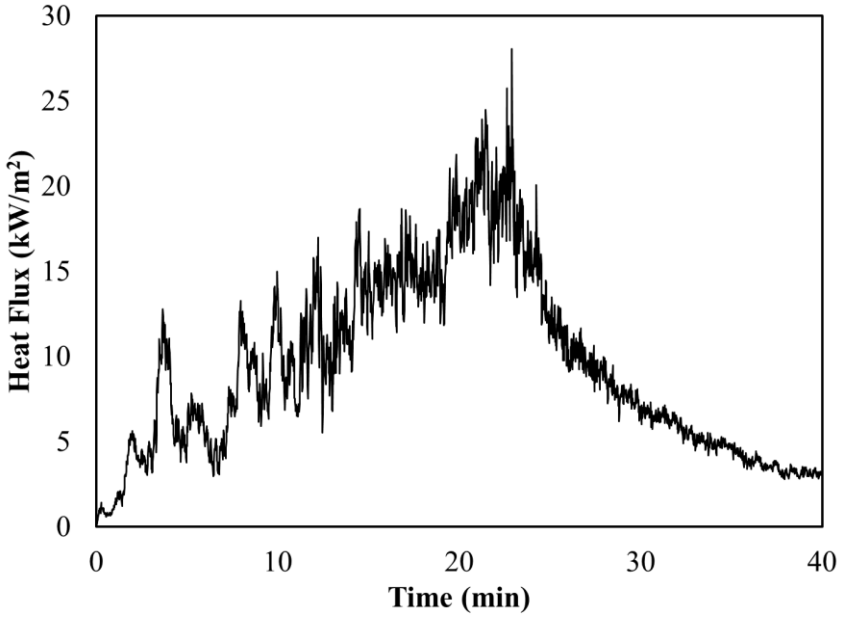


*Figure 1.8 Experimental heat flux measurements 8 m away from a first story window and 1.3 m above ground-level during a full-scale house fire (Fulton, et al. 2017b)*

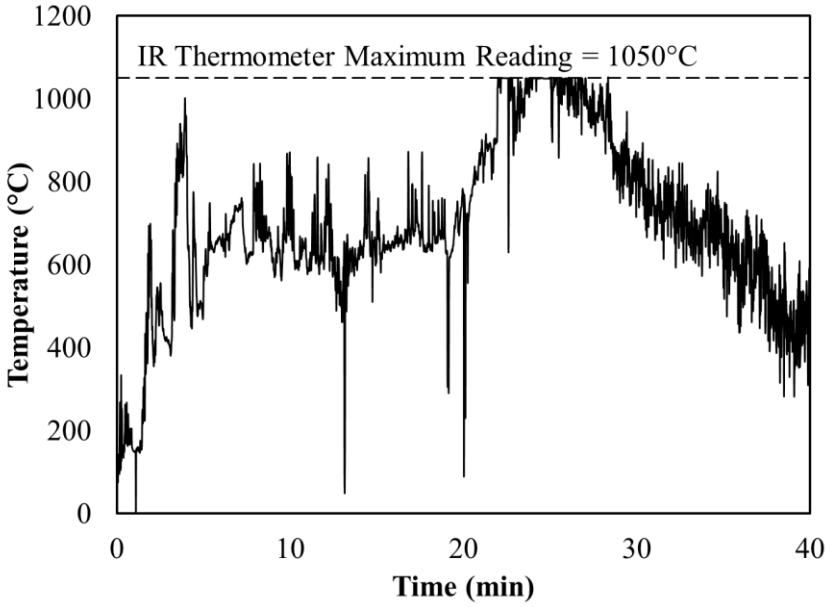


*Figure 1.9 Temperatures measured through the first story window using an IR thermometer (Fulton, et al. 2017b)*

## 1.4.3. University of Saskatchewan Dorm Room Fire Tests

In September 2016 live fire demonstrations were conducted at the University of Saskatchewan in order to promote fire safety on campus. Temperatures were measured in two

mock dormitory constructions that represented a sprinklered kitchen and an unsprinklered bedroom that are shown below in Figure 1.10. Thermocouples (24 gauge, Type K) mounted on the ceiling and on a thermocouple tree near the doorway recorded room temperatures. Additional information and room dimensions can be found in the original paper by Fulton, et al. (2017a). Figure 1.11 shows the different fire conditions during the time of peak temperature measurements for each room.


*Figure 1.10 Pre-test images of the constructed (left) sprinklered kitchen and (right) unsprinklered bedroom (Fulton, et al. 2017a)*

*Figure 1.11 Images near peak temperature measurements for fire demonstrations in (left) kitchen and (right) bedroom constructions (Fulton, et al. 2017a)*

More detail on testing procedures and temperature results for the sprinklered room are contained within the original paper. Relevant data to this current work is the rapid temperature increase in the unsprinklered room in Figure 1.12 and 1.13. A rapid temperature increase to 700 - 800°C recorded at the ceiling of the unsprinklered bedroom showcases the rapidly changing thermal conditions a firefighter may face in the field. The relatively low temperatures observed in the sprinklered kitchen shows the variability that a firefighter may experience in the field.

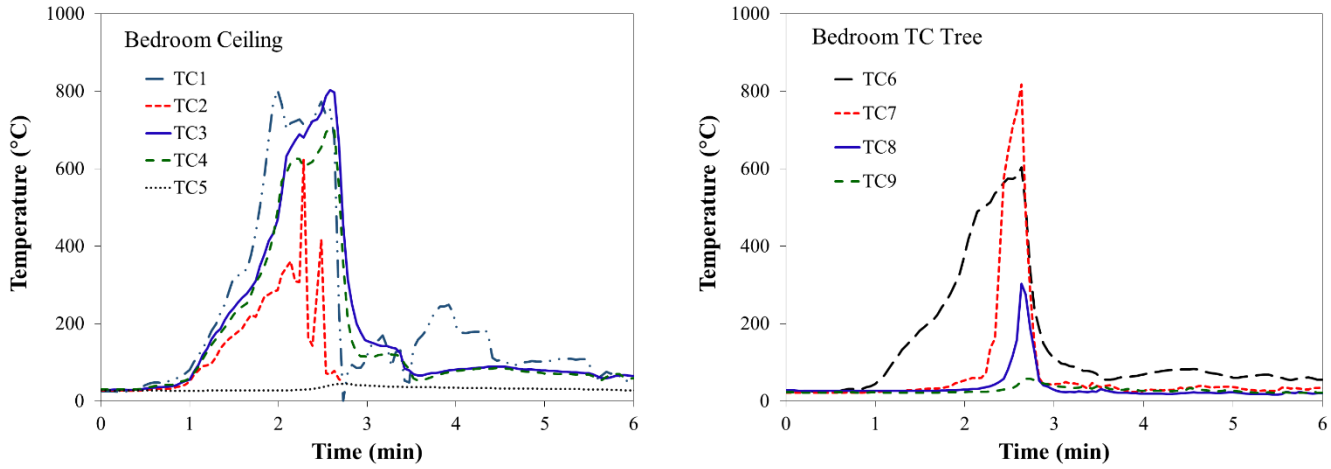


*Figure 1.12 Temperature measurements obtained from (left) across the ceiling and (right) inside the door of the unsprinklered bedroom (Fulton, et al. 2017a)*

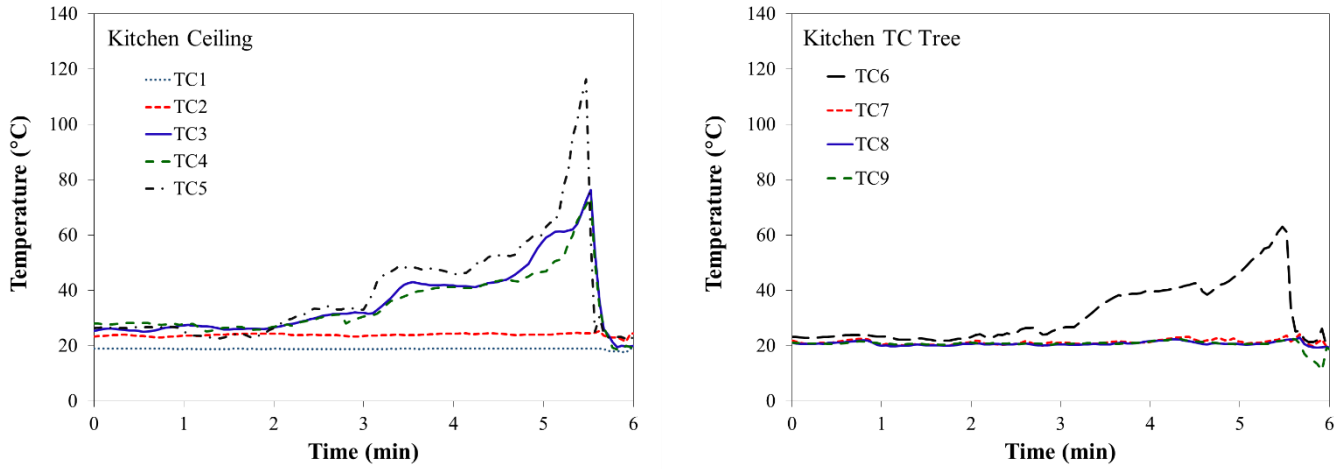


*Figure 1.13 Temperature measurements obtained from (left) across the ceiling and (right) inside the door of the sprinklered kitchen (Fulton, et al. 2017a)*

## 1.5. Methods to Simulate Ageing

### 1.5.1. Weathering, environmental, and UV ageing

Laboratory simulated UV exposures require the use of specialized weathering equipment such as a Simulated Photodegradation via High energy Radiant Exposure (SPHERE) device or a xenon-arc lamp (Davis, et al. 2010). Conversions between sun irradiance to actual outdoor exposure will vary from machine to machine, but one example related to firefighting protective clothing can be found in Davis, et al (2010). Further information on outdoor weathering conditions and photodegradation predictions can be found in a comparison study performed by Pickett and Sargent (2009).

Sunlight is considered to be one of the most important weathering factors in protective clothing; near UV light delivers a large amount of energy on a per-photon basis which corresponds to covalent-bond energy levels of many chemical structures (Nazare, et al. 2012). Moreover, sunlight has a tendency to react with organic polymers, leading to fiber embrittlement and a loss of tensile properties. The photo-oxidation process proceeds through reactions involving chain scissions (coupled with oxidation), cross-linking, and finally depolymerisation leading to a decrease in molecular weight (Nazare, et al. 2012). Recently, Nazare, et al. (2012) conducted research into the individual impact of UV irradiation at ambient conditions on the chemical and mechanical degradation of polyaramid and PBI protective clothing fabrics. These high-performance fabrics, especially polyaramids, are very susceptible to UV degradation. Between the fabric samples examined PBI blends showed less deterioration in tear and tensile strength tests when compared to polyaramid specimens. After 14 days of UV irradiation from the SPHERE device both specimens tested lost up to 87% of their initial tear strength.

Research has shown that although flame resistance properties of fabrics deteriorate through exposure to ultra violet radiation, the mechanical strength of fabrics deteriorates even more severely. Such a loss in mechanical strength may be more notable during the early stages of exposure. For example, Davis, et al. (2010) found the largest single percentage decrease in tear strength for their specimens occurred following the very first single day of UV irradiation exposure. In addition, the effect of the incident radiation on the temperature of the specimen

during an exposure should be considered since the level of thermal energy absorbed by the specimen may be comparable with the energy absorbed due to ultra violet radiation. It may be particularly important for wildland firefighters' protective clothing, which could be exposed to solar radiation in a high temperature environment for a relatively long period

The UV ageing process of firefighter clothing is thought to take place through the photo-oxidation of the textile structures through free-radicals resultant from the incident radiation light source (Houshyar, et al. 2015). Houshyar, et al. (2015) found that that performance characteristics evaluated using a loss of tensile and tear strength, reduction to abrasion resistance, and extensions in break locations were all negatively impacted with sunlight exposure. High tenacity fibres (e.g. PBI and polyaramids) are known to be photosensitive, due to their bond scissions via free radical generation, in a manner similar to commercially available polymers. Brittle fibres and fractures can be observed in these fabric specimens following UV exposure. Additional etching and roughness of the microstructure were shown to become visible with increasing exposure times with degradation starting at the fibre-skin and continuing to core-cracking. This material transition could be the result of microstructural composition changes. New FTIR spectroscopy peaks of product gases from thermogravimetric analysis (TGA) of UV aged samples indicated the formation of alcohol, acid, and amides in these textile structures (Houshyar, et al. 2015). Arrieta, et al.'s (2011b) investigation of hydrolytic and photochemical ageing of a Kevlar/PBI blend contains a detailed explanation of the Photo-Fries bond rearrangement. This inherent photosensitivity is an area for future research and material improvement. A summary of previous UV ageing research is contained in Table 1.1.

*Table 1.1 Examples of research on effects of UV ageing (Fulton, Rezazadeh and Torvi 2017)*

| **Investigator(s)** | **Textiles tested** | **Ageing method(s)** | **Parameters studied** |
|---|---|---|---|
| Day, et al. (1988) | outer shell and moisture barrier fabrics for firefighters' protective clothing | xenon-arc lamp, 60°C and 30% RH | - colour fastness<br>- mechanical properties (tensile, tear strength)<br>- flame resistance (char length/afterflame time)<br>- thermal protection |

*Table 1.1 Continued*

| Investigator(s) | Textiles tested | Ageing method(s) | Parameters studied |
|---|---|---|---|
| Barnett and Slater (1991) | cotton/nylon blends | xenon-arc exposure at specific temperature and relative humidity (RH) with and without water spray | - mechanical properties (tensile and tear strength)<br>- abrasion resistance |
| Poli, et al (2006) | polymer coatings for protecting low porosity stones | xenon-arc lamp | - water-repellence |
| Zhang, et al. (2006) | outer shell for firefighters' protective clothing | carbon-arc lamp, 40°C and 45% RH | - mechanical properties (tensile, tear strength)<br>- XRD and SEM<br>- calorimetry<br>- ATR-FTIR chemical changes |
| Davis, et al. (2010) | inherently flame resistant fabrics | mercury-arc lamp, 50°C and 50% RH | - mechanical properties (tensile, tear strength)<br>- UV transmission and protection<br>- microscopy |
| Arrieta, et al. (2011b) | outer shell for firefighters' protective clothing | UV (50-80°C) and hydrolytic ageing environmental chamber (50-80°C, 60-80% RH) | - mechanical properties (breaking force)<br>- ATR-FTIR chemical changes |
| Nazare, et al. (2012) | outer shell for firefighters' protective clothing | moisture influence (dried versus 50% RH) and SPHERE mercury-arc lamp UV ageing at 50°C and 50% RH | - ATR-FTIR chemical changes<br>- UV protection factor<br>- performance properties (stretching, tear resistance, elasticity) |
| Aidani, et al. (2013) | moisture barrier with Nomex® backing | UV (50-80°C) exposure with Weather Tester | - mechanical properties (tensile, tear strength)<br>- chemical changes (FTIR)<br>- X-ray diffraction, SEM<br>- calorimetry<br>- atomic force microscopy<br>- vapour permeability |
| Houshyar, et al. (2015) | outer shell for firefighters' protective clothing | weather-O-meter xenon lamp UV exposure, 40°C and 50% RH (ASTM G155) | - mechanical properties (tensile, tear strength)<br>- abrasion resistance (Martindale method)<br>- FTIR, SEM, TGA results<br>- photo/UV degradation ageing process |

## 1.5.2. Thermal Ageing

Firefighters and other workers can be exposed to both high temperatures and heat fluxes. Therefore, many research studies on ageing of these types of fabrics focus on thermal exposures (Day, Cooney and Suprunchuk 1988). Intensity, temperature, duration of exposure, and frequency of exposure will all influence ageing of fabrics (Rezazadeh 2014). One other piece of information that is valuable when evaluating thermal ageing is information on expected temperatures that a textile may reach during exposure, and temperatures that are necessary for changes to occur to the textile (e.g., dye loss and onset of thermal-chemical changes). This information can be used to understand the possible material or chemical structure changes that may result from thermal exposure.

Laboratory procedures can be largely grouped into two main categories; full scale (Section 1.4) or bench scale tests. Full scale tests have the advantage of being able to test large structures or ensembles, but have a relatively large cost and significant testing facility requirements. In textile testing a thermal manikin apparatus capable of exposing an entire garment to an incident heat flux (e.g. 84 $kW/m^2$ in Figure 1.4) would be considered a full scale test (ASTM F1930-15 2015). Bench scale tests are less expensive and facilities are more widely available. However, usually only a small representative sample may be tested in a bench scale apparatus. Numerous bench scale tests have been adapted to test high performance textiles such as firefighters' protective clothing.

Examples of tests that can be used to thermally age fabrics include thermal protection performance (TPP) (ASTM F2700-08 2013) or radiative protective performance (RPP) (ASTM F1939-15 2015) procedures included in NFPA 1971 (2013) and other standards used to evaluate new fabrics. Depending on the standard, specimens are exposed to a heat flux provided from a primarily convective (e.g., laboratory burner), primarily radiative (e.g., quartz tubes), or combined convective/radiative exposure. The differences in convective and radiative components and wavelengths of thermal radiation should be considered when comparing laboratory and field exposures (Torvi, Rezazadeh and Bespflug 2016). Others have used different radiative heat sources to produce heat fluxes, such as the heater from the cone calorimeter, a

piece of fire testing equipment typically used to test building materials (ASTM E1354-16a 2016; Torvi, et al. 2016). Thermal ageing can also be performed using constant-temperature ovens.

Bench scale tests do not account for clothing features (zippers, ties, loops, stitching) that would be found in a full scale garment. Full scale testing facilities may include life-sized thermal mannequins that can be used to gain significant insight into thermal protective clothing performance (ASTM F1930-15 2015). Many of these high-tech thermal mannequins are stationary, but recent research has been conducted into the influence of movement or occupant sweat generation on protective performance during emergency fire scenarios (Sipe, 2004; Udayraj, et al. 2016).

Table 1.2 provides a summary of examples of work on effects of thermal ageing and continues a previous review (Rezazadeh and Torvi 2011). Research has shown that flame resistance and mechanical properties of fabrics deteriorate more severely through thermal exposure than other aspects of performance (Rezazadeh and Torvi 2011). Such a loss in mechanical strength is more noticeable during the early stages of exposure, while a loss in flame resistance properties may take much longer to occur (Wang and Li 2015a). Wang and Li (2015a) and others have noted that in some cases there can be an initial increase in TPP values after low thermal exposures.

*Table 1.2 Examples of research on effects of thermal ageing (Fulton, Rezazadeh and Torvi 2017)*

| Investigator(s) | Thermal ageing method | Duration | Parameters studied |
|---|---|---|---|
| Day, et al. (1988) | exposure to 150 - 250°C in an oven | 5 minutes - 7 days | - thermal shrinkage and weight loss<br>- flame resistance (char length/afterflame time)<br>- TPP<br>- tear strength |

*Table 1.2 Continued*

| Investigator(s) | Thermal Ageing Method | Duration | Parameters studied |
|---|---|---|---|
| An, et al. (1989) | convective exposure at 94°C in an oven<br>conductive exposure at 94°C on a metal plate | - 4 hr.<br>- 5 min. | - mass per unit area<br>- mechanical properties (tensile, tear strength, bending flexibility)<br>- chemical permeation resistance |
| Iyer, et al. (1999, 2006) | exposure to 150-550 °C in a furnace | 0.5-7000 hr.<br>(1-12 stages) | - X-ray diffraction pattern<br>- weight loss<br>- mechanical properties (tensile strength)<br>- microstructural features |
| Jain and Vijayan (2002) | exposure to 200-400 °C in a furnace | 0.5-2000 hr.<br>(1 stage) | - X-ray diffraction pattern<br>- weight loss<br>- mechanical properties (tensile strength)<br>- microstructural features |
| Thorpe (2004) | exposure to 5 - 30 $kW/m^2$ using radiant panel | 30-3600 s | - conductive and compressed heat resistance (CCHR) rating<br>- mechanical properties (tensile, tear strength)<br>- water penetration resistance |
| Rossi, et al. (2008) | two exposures to 40 $kW/m^2$ (quartz tubes) or 80 $kW/m^2$ (Meker burner) | 17-33 s | - required time for 12 or 24 °C temperature rise of a test sensor ($t_{12}$ or $t_{24}$)<br>- mechanical properties (tensile, tear strength) |
| Arrieta, et al. (2010) | extended exposure, temperatures from 190-320°C | from hours for high temperatures and weeks for low temperatures | - mechanical properties (breaking strength, thermal life)<br>- FTIR |
| Aidani, et al. (2011) | oven from 190-320°C | 1-1056 hours | - mechanical properties (tensile, tear strength, ASTM D5587)<br>- vapour permeability |
| Rezazadeh (2014) | exposures to cone calorimeter (10 – 40 $kW/m^2$)<br>multiple exposures at 20 $kW/m^2$ (15-150s) | 10 – 2600 s | - mechanical properties (tensile, tear strength)<br>- SEM evaluation<br>- water vapour permeability/penetration<br>- TPP<br>- colorimetry<br>- NIR reflectance |

*Table 1.2 Continued*

| Investigator(s) | Thermal Ageing Method | Duration | Parameters studied |
|---|---|---|---|
| Ozgen and Pamuk (2014) | oven from 220-300°C | 1-30 days | - mass loss<br>- mechanical properties (tensile strength) |
| Wang and Li (2015a) | repeated high heat flux exposure 84 kW/m$^2$ using a traversing thermal mannequin or a bench scale apparatus | repeated 3 s exposures for both bench and mannequin test | - TPP<br>- mechanical properties (tensile, tear strength, shrinkage, fabric thickness)<br>- SEM evaluation |
| Cui, et al. (2015) | exposure from a quartz tube (6.5 and 9.7 kW/m$^2$) | 5-30 minutes | - mechanical properties (tensile, tear strength and elongation at break)<br>- TPP<br>- SEM evaluation<br>- FTIR-Raman spectroscopy |

## 1.5.3. Other Ageing Factors – Mechanical Action and Laundering

Textiles and products containing textiles are used in physical activities which may result in abrasion. For example, textiles used in clothing can be subjected to large mechanical forces when they are in contact with other surfaces, and individual layers of fabric within clothing system can also be in contact with each other (Rezazadeh and Torvi 2011). Mechanical wear can also occur from laundering of fabrics (Vanderschaaf, Batcheller and Torvi 2015). In firefighting contact with sharp or abrasive objects (e.g. broken wall material, nails or screws, broken glass) may occur. One concern is that research has shown that the actual abrasion of textiles cannot be completely simulated in the laboratory. Slater (1987) clarified how different tests used to simulate abrasion produce different modes of degradation in the fabrics. More information on mechanical abrasion and abrasion testing can be found in a recent literature review (Fulton, Rezazadeh and Torvi 2017).

The repeated washing and drying of textile garments has been known to have a detrimental impact on both aesthetics and textile performance (Slater 1991). Even a single incorrect washing

procedure may have an immediate destructive impact on some types of clothing (Loftin 1992). Therefore, manufacturers will provide instructions on cleaning, and standards organizations have published detailed guidelines for cleaning and maintenance (Stull, et al. 1996); specific guidelines exist for firefighter clothing including NFPA 2113 (2015) and NFPA 1851 (2014). Both of these NFPA standards make reference to either ASTM F2757-09 (2016) or ASTM F1449 (2015). As fabrics can also become soiled and contaminated with use, determining the effectiveness of cleaning and maintenance procedures is also an important aspect of ageing (Fulton, Rezazadeh and Torvi 2017).

## 1.6. Field Studies

Some studies will involve testing of textiles that have been used in the field. These textiles will experience combined exposures to a number of factors, which may include UV degradation, high intensity thermal exposures, mechanical wear and other factors over a period of time. These field studies offer a wealth of information, but major disadvantages include the time required to obtain the specimens necessary to perform the research and the absence of detailed information on the exposure conditions over the lifetime of the garments.

In some industries, organizations will take a sample of garments from their inventory and use these to assess the condition of other garments that are still in use. For firefighters' protective clothing this approach would be prohibitively expensive. There have been some research studies that have examined used firefighting equipment (Vogelpohl and Easter 1997). These studies may take a relatively long period of time and require the cooperation of active firefighting departments with a variety of used garments. This research is particularly important as some firefighters have a preference towards wearing aged and worn gear even though it may not be clear whether these ensembles continue to provide required protection levels (McQuerry, et al. 2015). A summary of select field study results can be found in Table 1.3.

*Table 1.3 Summary of field studies (Fulton, Rezazadeh and Torvi 2017)*

| Investigator(s) | Textiles tested | Ageing method(s) | Parameters studied |
|---|---|---|---|
| Makinen (1992) | firefighters' protective clothing | specimens taken from new and in-use clothing (4-10+ years of service) laundering in the laboratory | - flame resistance<br>- mechanical properties (tensile, tear strength)<br>- abrasion resistance |
| Vogelpohl (1996) | 20 used firefighters' protective clothing specimens | specimens donated from active service and training programs (1-5$^{+}$ years of service) | - NFPA 1971 requirements<br>- mechanical properties (tensile, tear strength, seam strength)<br>- flame resistance<br>- water resistance<br>- abrasion resistance, zipper operation resistance |
| Vogelpohl and Easter (1997) | evaluated used firefighters' protective clothing | 1-5$^{+}$ years in service | - flame resistance (char length/afterflame time)<br>- TPP<br>- water absorption and penetration resistance<br>- mechanical properties (tensile, tear strength) |
| House and Squire (2004) | firefighters' protective hood | 15-20 days of use (including daily laundering) at firefighter school | - estimated burn injury after 1-10 s thermal mannequin exposures |
| Cinnamon (2013) | 108 used firefighters' protective clothing specimens | field studies, specimens in active service for 10-20 years | - age (vs 10 year retirement guidelines)<br>- TPP<br>- mechanical properties (tensile, tear strength, seam strength)<br>- water penetration<br>- visual inspection results (NFPA 1971; NFPA 1851) |
| McQuerry, et al. (2015) | 108 used firefighters' protective clothing specimens | field studies, specimens in active service for 2-10 years | - age (vs 10 year retirement guidelines)<br>- TPP<br>- mechanical properties (tensile, tear strength, seam strength)<br>- water penetration<br>- visual inspection results (NFPA 1971; NFPA 1851) |

## 1.7. Methods to Evaluate Performance

Destructive testing methods for evaluating performance criteria of new textiles can be adapted to evaluate aged textiles. Studies are often based on standards used to specify performance for new textiles (e.g., NFPA 1971 (2013), CAN/CGSB-155.1 (2001), EN 367 (1992), EN 469 (2005), ISO 13506 (2008), ISO 6942 (2002)). For example, NFPA 1971 (2013) outlines over fifty destructive test methods, which are used to evaluate protective ensembles for structural and proximity firefighting. Tests include the constant-rate-of-extension (CRE) tensile tests (ASTM D2261 2013; ASTM D5034 2013), and flammability testing methods (ASTM D1230-10e1 2016; ASTM D6413/D6413M-15 2015) which expose a textile specimen to a standardized flame using a specialized mounting apparatus. In a similar manner, aged firefighters' protective fabrics can be tested for a number of aspects of performance including:

- thermal protection,
- flammability,
- thermal shrinkage resistance,
- heat resistance,
- water resistance,
- dimensional stability, and/or
- tear strength.

Supplemental information provided by thermogravimetric analysis (TGA), microscopy and other methods can help to interpret test results and explain the effects of ageing on performance. Further microscopic evaluations (e.g. SEM) can also give valuable information on the microstructural changes taking place during ageing processes (Rezazadeh 2014).

## 1.8. Non-Destructive Evaluation

As noted earlier, most standard tests used to evaluate textiles are destructive, and therefore are not suitable for evaluation of in-use textile products. A non-destructive test (NDT) technique is an evaluation method that gauges the current state of a material without influencing future performance (Rezazadeh 2014). NDT methods may impact the material structure in some form, but these changes are often small enough to have a negligible influence on future performance.

For example, magnetic particle testing can be used to find defects and stress corrosion cracking in a ferromagnetic material structures while the magnetic flux has no influence on future performance of the tank, vessel, or pipeline in question.

### 1.8.1. Purpose of NDT Methods

In NDT methods particular properties of a material are used to indicate deterioration in performance. Measurements of these properties are then used to determine deterioration of the material, and possibly to estimate the remaining life of the material. Shull (2002) states that these selected physical properties must deteriorate with use and the physical degradation process must be known. NDT techniques are being used extensively in many areas of engineering to evaluate in-use conditions of materials and to estimate remaining service life (Shull 2002). Although the interest level in the non-destructive evaluation of textile structures has been high for quite some time (e.g. Onions and Slater 1967) work continues to develop new NDT methods for textile applications, or to apply NDT methods used in other branches of engineering and science.

Several NDT methods that have been studied for use in evaluating protective and other textiles are described in the sections below. Emphasis is placed on techniques that are based on colour measurements and near infrared spectroscopy to match similar studies previously performed (Thorpe 2004; Rezazadeh 2014). Examples of how the results of these tests can be correlated with those from destructive tests are also given. Further information on these and other NDT methods can be found in previous work (Rezazadeh 2014; Fulton, et al. 2017)

### 1.8.2. Visual Inspection

One NDT method used in textile applications is visual inspections. For example, NFPA 1851 (2014) provides information on various levels of visual inspection of in-use firefighter's protective clothing. After each use, individual end users can look for visual indications of possible damage including soiling, contamination, and physical damage, such as tears and rips. Specially trained individuals can conduct more advanced inspections on a regular basis or as a result of an initial visual inspection.

While NFPA 1851 is heavily reliant on visual inspections, a few other NDT procedures are also provided for evaluating the clothing. The inner layer of this clothing, which includes both the moisture barrier and thermal liner, is evaluated by using a light source and subjectively determining the amount of light that passes through the liner. Brighter areas may indicate a deficiency in the insulating layers. In another test method, which is also applicable to the inner layer, a cup of a water-alcohol mixture is poured on the moisture barrier side of the inner layer and the other side is visually inspected for leakage. In the third test method, the substrate of the moisture barrier is exposed to water pressure of 6.9 kPa (1 psi) and water leakage on the other side is determined visually.

## 1.8.3. Colour Measurements

Many visual inspections are based on colour changes, such as those that occur when firefighter's protective clothing is exposed to high heat fluxes and temperatures (Figure 1.14). However, colour differences made during visual inspections are subjective (Randall 1998). Therefore, NDT methods for textiles based on colour measurements have been considered in previous studies (Thorpe 2004).


*Figure 1.14 Examples of Colour Fade of Royal Blue Nomex® IIIA Specimens after Different Thermal Exposures (Rezazadeh 2014)*

The discoloration of the fabric as a result of a thermal or other exposure, such as shown in Figure 1.14, can be expressed as a colour difference and related to mechanical or other physical properties. Thorpe (2004) used both a colorimeter and images from a computer scanner to

measure colour differences after exposures in the laboratory. Emphasis was placed on the computer scanner, as it was felt that this equipment would be easily available to firefighters. Discoloration, or colour difference, was defined as the colour difference between a new and exposed specimen, measured using two distinct colour measurement systems, RGB and CIE L*a*b colour space. He found that tensile strength of the outer shell (OS) fabrics could be correlated with colour measurements.

Rezazadeh (2014) continued this work on colour measurement by assessing the technique using fabrics with a range of initial colour. Two trends in correlations between colour change and tensile strength were observed. The first trend was observed for yellow, red and undyed (light brown) fabrics where the colour difference continually increased as dye was removed and char appeared (Figure 1.15). The second trend was observed for blue and black fabrics (e.g., Figure 1.16), for which the colour difference increased as dye was removed, but then decreased when char appeared. While this method shows promise, Thorpe (2004) identified a number of issues that would need to be addressed. A collection of baseline colour changes for a variety of protective fabrics would need to be developed, and the sensitivity of the results to deposition of contaminants in the fabric and the required level of resolution of specimen image would need to be determined.

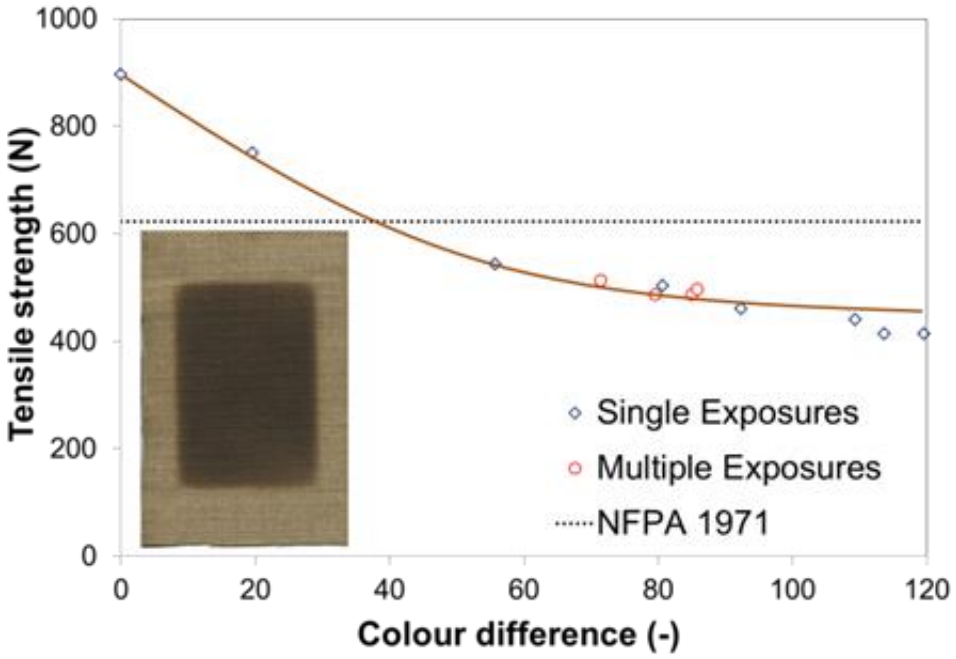


*Figure 1.15 Correlation between Colour Difference and Tensile Strength of Kevlar®/PBI Outer Shell Measured after Single and Multiple Exposures of Firefighters' Ensemble to 20 kW/m$^2$ (Rezazadeh 2014)*

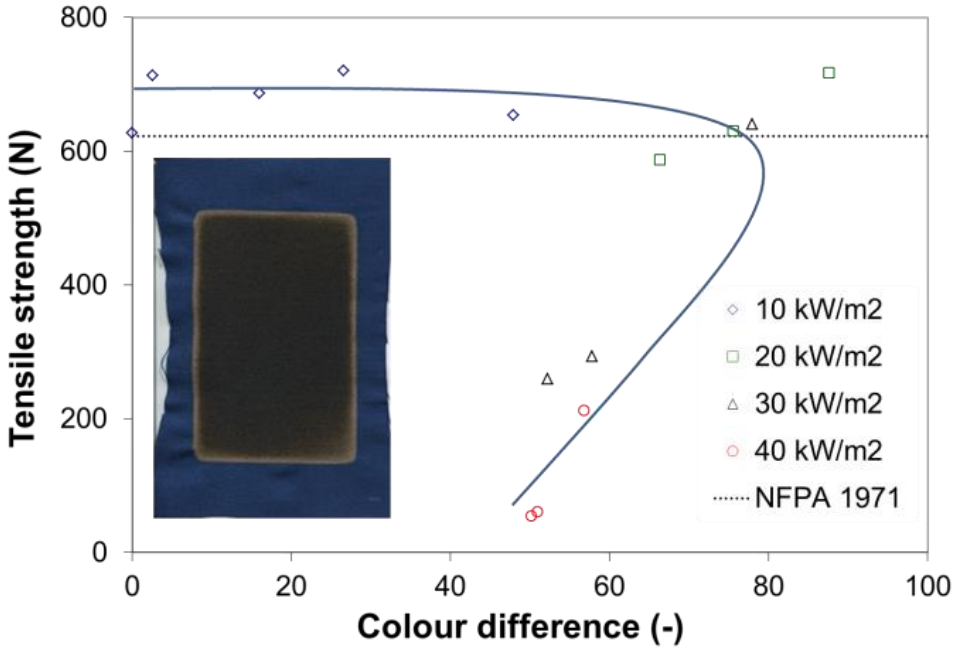


*Figure 1.16 Correlation between Colour Difference and Tensile Strength of Royal Blue Nomex® Fabric Measured after Exposures to 10 - 40 kW/m$^2$ (Rezazadeh 2014)*

Digital image analysis can also be based on other visual parameters besides colour changes. For example, Hadjianfar, et al. (2010) used digital image analysis to measure textile lustre properties. The appearance of textile materials can often be classified by lustre (gloss, glitter, sheen, shine, etc.), but in practice it is difficult to obtain theoretical and experimental lustre values. Commercial devices, such as glarimeters and glossimeters, are available. However, Hadjianfar, et al. (2010) created a new method that takes diffuse and scattered light from fabrics into account. This method can produce consistent results based on derived luminance values of textile images taken by a high-quality camera and a diffused non-polarized lighting system.

### 1.8.4. Near Infrared Spectroscopy

Infrared spectroscopy has been used for identification of compounds and investigation of material composition in agricultural and other applications since the initial development of the technology (McClure 2004). Peak intensity changes in the transmission spectrum (e.g. reflectance or absorbance) can also be used to study degradation in materials or to analyze decomposition products. Examples of specific wavelengths or wavelength ranges that can be related to particular structural features, or changes that occur as a result of ageing, can be found in Goddu and Delker (1960), Mosquera, et al. (1994), Chalmers and Griffiths (2001), McClure (2004), and Arrieta, et al. (2010, 2011a, 2011b).

Infrared spectroscopy has been used in various areas of engineering and science. Researchers in the field of heritage conservation (Richardson, et al. 2008; Garside, et al. 2011) compared the absorption spectra of new and aged silk specimens after exposure to heat, light, and humidity. These groups correlated tensile strength of specimens to changes in the intensity of peaks in the water absorption bands in the spectra of new and used specimens. Dispersive infrared spectroscopy was used by Gu, et al. (2008) to compare degradation of an epoxy coating when exposed to ultraviolet radiation both in the laboratory and the field. Many researchers have investigated methods of using infrared spectroscopy to evaluate or predict properties of wood, including density (Mora 2009), moduli of rupture and elasticity (Kludt 2003), compressive strength (Kelley 2003) and stiffness and tensile strength (Hedrick, et al. 2007).

Ghosh, et al. (1990) used dispersive IR spectroscopy in the wavelength region of 1100 – 2500 nm to determine the amount of resin in cotton fabrics. This group then developed a model to predict the amount of fixed resin in these cotton samples based on changes in absorbance spectra. In a similar spectroscopy application Fortier, et al. (2014) used attenuated total reflectance FTIR (ATR-FTIR) to evaluate the percentage change in moisture content of oven dried cotton in order to determine if oxidation of the cotton structure was occurring.

A number of previous researchers have used IR spectroscopy in applications related to protective fabrics and clothing. For example Davis, et al. (2010) used FTIR within the wavelength region of 5500 – 12500 nm to investigate degradation of PBI, Nomex®, and Kevlar® fabrics after exposure to ultraviolet radiation. After 13 days of exposure the group found that tensile strength decreased by up to 40% and confocal microscopy revealed significant surface decomposition accompanied with a switch from ductile to brittle failure of the fibers (Davis, et al. 2010). Nazare, et al. (2012) used FTIR spectroscopy within wavelength region of 2800 – 3400 nm and 5500 – 6200 nm to explain mechanical property changes in PBI, Nomex®, and Kevlar® fabrics after exposure to UV conditions combined with a hot and humid chamber. These conditions were thought to reflect active firefighting and storage conditions. The group (Nazare, et al. 2012) used the infrared spectra of new and aged specimens to correlate spectral changes with chemical composition of the aged specimens and reductions in mechanical properties. After 14 days of UV irradiation the fabrics in this study lost up to 87% of their original tear strength which the group attributed to photooxidative reactions changing the chemical composition of the polyaramid and polybenzimidazole fabrics (Nazare, et al. 2012).

Using FTIR within the wavelength region of 2500 – 20000 nm Arrieta, et al. (2011b) found that thermal degradation of 60% Kevlar®/40% PBI fabrics after thermal ageing exposure from 190 to 320°C could not be detected in the absorbance peaks. The variation of the absorbance peaks was subtle even though the tensile strength of the specimens decreased noticeably after a certain level of ageing. However, Arrieta, et al. (2011b) showed that ATR-FTIR results in this range could be correlated with UV ageing of Kevlar®/PBI blended fabrics. Decreases in mechanical strength after exposure to both UV radiation and humidity were correlated with ATR-FTIR measurements of the aged specimens. Cai and Yu (2015) used FTIR spectroscopy in

the wavelength region of 2500 – 25000 nm to analyse the volatiles produced during thermal degradation of Kevlar® and Nomex® specimens.

Washer, et al. (2009) examined the effects of incident UV and thermal exposures on Raman spectra. The vibrational modes of the spectral peaks were thought to change in direct relation to deterioration of the fibre. For example, the Kevlar® molecular structure has a series of aromatic rings bonded by oxygen and hydrogen in a monomer. This results in a series of vibrational modes (both stretching and axial extension) for C-C, H-O, and H-C bonds. An example of the resultant vibrational modes from Raman spectroscopy of Kevlar® can be found in Washer, et al. (2009). Although these results are based from Raman spectroscopy similar techniques for relating near infrared spectral results to fundamental chemical components of a scanned specimen have been widely utilized in the past (McClure 2004).

This previous work (Washer, et al. (2009)) also showed that spectral results can be related to base chemical structures and chemical change in protective fabrics. Washer, et al. (2009) showed that the average peak intensity of aged specimens decreased in comparison with that of unaged specimens while the average bandwidth of peaks in the spectrum of aged specimens increased. However, Washer, et al. inferred that peaks located at a Raman shift of 1613 $cm^{-1}$ may be due to stretching of vibrational modes in the C-C phenyl ring shifting due to this bond's sensitivity to applied stress and strain. This differs from the peak shift located at 1649 $cm^{-1}$ which Washer, et al. (2009) believe stems from the stretching of the C=O bond. A more detailed coverage of the chemical composition of Kevlar® can also be found in this paper. McClure (2004) states that many still make use of a spectral-structure correlation table for NIR regions originally created by Goddu and Delker (1960). A more recent study of wavelength specification and the limitations of various laboratory instruments is covered by Chalmers and Griffiths (2001). A full classification of the anticipated spectral results for thermal ageing chemical changes for Kevlar® can be found in Mosquera, et al.'s (1994) original work.

Rezazadeh (2014) demonstrated that near infrared spectroscopy has the potential to be used to predict tensile strength of fabrics used in the outer shell of firefighters' protective clothing. Figure 1.17 shows the shifts in reflectance spectra that were observed for the same royal blue

Nomex® fabric shown in Figure 1.14 after exposures to 40 kW/m$^2$. Correlations were developed using multi-variable linear regression models, and it was found that a model based on reflectance values at three wavelengths could be used to predict tensile strength. For example, Figure 1.18 compares predicted and measured tensile strength values for one fabric. In this case, the regression model was developed using reflectance at 1600, 1750 and 2425 nm and tensile strength values measured after exposures to 10 – 40 kW/m$^2$ (e.g. points shown using open squares in Figure 1.18). The model was then used to predict tensile strength for a second set of fabrics exposed to 5, 15 and 25 kW/m$^2$ based on reflectance at the same three wavelengths (shown using solid squares). The model did a very good job of predicting tensile strengths around 600 N, but was much less successful at predicting lower tensile strengths. One reason for the lower success in this range of tensile strength is that a much larger fraction of the data used to develop the regression model was for higher tensile strength values rather than for values of 400 N or less. Nevertheless, this research demonstrated that a practical device, which would measure reflectance at even a small number of wavelengths, could be a viable way to predict tensile strength of in-use protective clothing. Understanding which particular wavelengths can be correlated to fabric property changes or degradation will be important for the development of practical tools that can be used to evaluate in-use fabrics and other products in the field.

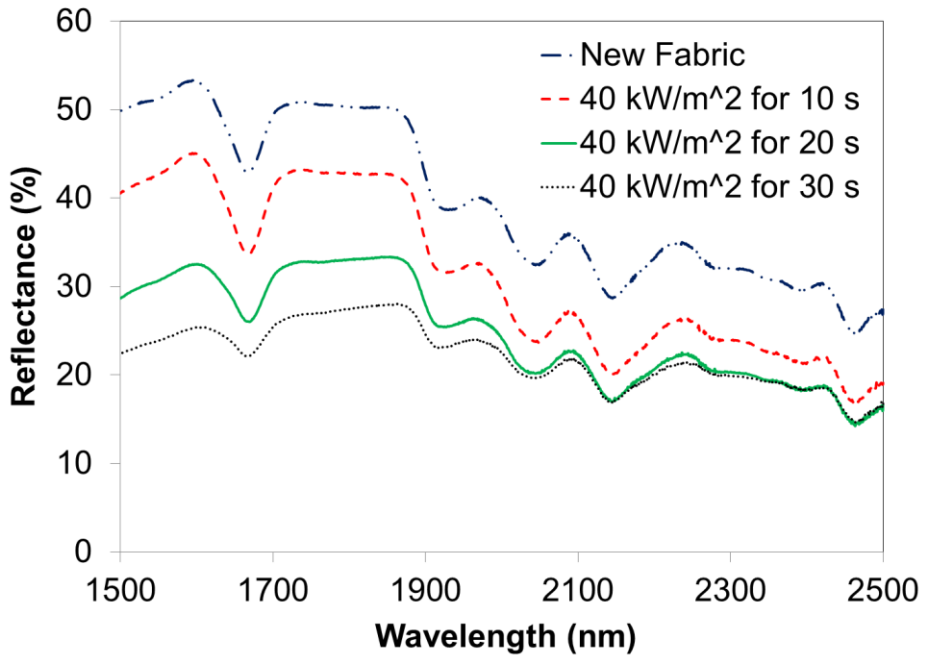


*Figure 1.17 Infrared reflectance spectrum of a royal blue Nomex® fabric specimen after various lengths of exposed to 40 kW/m$^2$ (Rezazadeh 2014)*

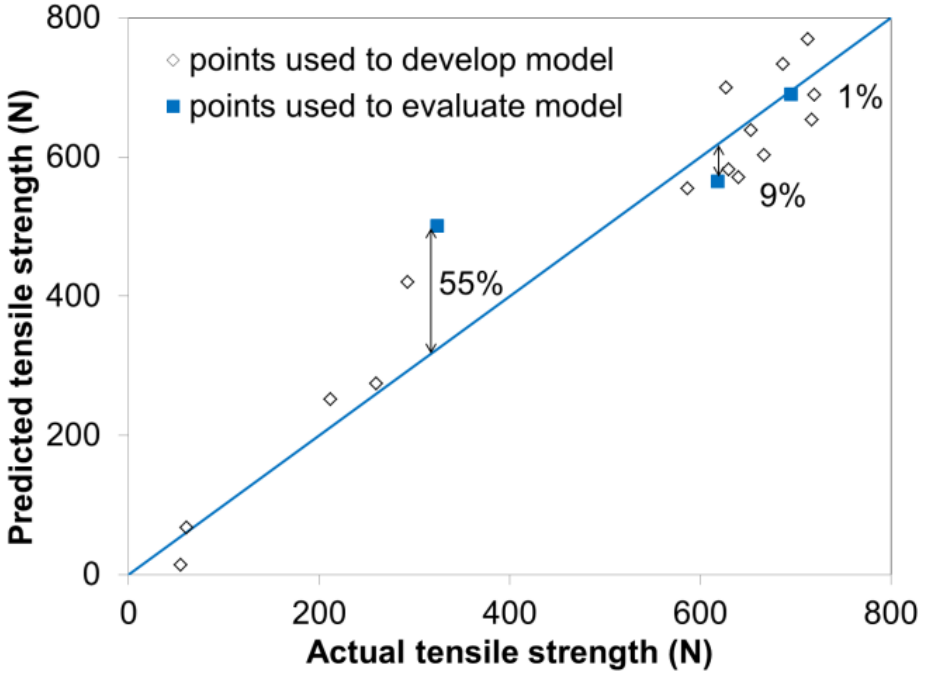


*Figure 1.18 Comparison of tensile strength measurements for thermally aged royal blue Nomex® fabrics with values predicted using three-wavelength regression model (Rezazadeh 2014)*

Portable NIR evaluation tools have been in development for a number of decades in a number of areas, including the agricultural and medical fields (McClure 2004). Portable textile evaluation methods based on NIR measurements have been developed successfully by Rodgers, et al. (2010) for the evaluation of cotton fibre micronaire, a key property of evaluating cotton fiber fineness (i.e. air permeability of compressed cotton). Rodgers, et al. (2010) found that results from handheld device matched well with benchtop NIR devices; certain spectral shifts were noted, but could be minimized with baseline correction methods. The development of a portable NIR method for evaluating the condition of firefighters' protective clothing would be of great use to many fire departments and protective clothing manufacturers. However, more research in the ageing process and material degradation of protective clothing is currently needed before a commercial device can be envisioned.

## 1.9. Scope and Objectives of Research

The main purpose of this research project is to examine the effects of artificial ageing performed in a laboratory setting on the performance of single outer shell protective clothing specimens. This will be done in an attempt to simulate real exposure conditions present in the firefighting service. Artificial ageing will take the form of exposures to a primary radiative heat source for controlled lengths of time, and ultraviolet light (UV). A broad range of thermal exposure levels will be selected to represent different fire service working conditions. Ultra-violet light exposures were limited when compared to the number of thermal exposures conducted. Fabric specimens examined in this research are selected from common materials used in outer shell layers of firefighters' protective clothing (i.e. 60/40% Kevlar®/PBI blends). These outer shell materials will act as the first line of defense in real firefighting activities and will be the most accessible to any developed inspection procedures. Additionally, degradation of these outer shell materials below performance requirements is also expected to lead to damage of the inner layers in full multi-layer protective clothing ensembles. Following ageing procedures the performance of the fabrics will be evaluated using both destructive and non-destructive methods. Tensile testing (NFPA 1971 2013; ASTM D5034 2013) will be used as the main means of destructive testing to evaluate the tensile strength of the aged fabrics and will be the main performance characteristic used for comparison. Near-infrared spectroscopy and interpretation of diffuse reflectance results will be the main method of non-destructive testing.

This research has been conducted to address gaps in the available literature regarding the effects of ageing process on firefighters protective clothing, and the current lack of quantitative retirement guidelines for in-use firefighters clothing.

The summarized objectives of this current research are:

- To evaluate the impact of thermal and ultra-violet ageing exposure conditions on the performance of firefighters' outer shell protective fabrics with specific focus on remaining mechanical strength as a key performance indicator;
- to examine microstructural changes in the fabrics resultant from thermal and UV ageing;

- to evaluate near-infrared techniques as a non-destructive testing method of the aged fabrics combined with physical interpretations based on scanning electron microscopy of the aged fabrics;
- to correlate different non-destructive results to physical changes or remaining performance characteristics of the aged fabrics wherever possible and suggest new avenues for future research.

This thesis will describe all testing methods performed, experimental results, and implications to future research. Chapter 1 covers initial background information considered critical to understanding the ageing and evaluation process of in-use firefighter's clothing. Chapter 2 describes the outer shell materials examined in this current study and experimental instrumentation utilized at the University of Saskatchewan and the University of Alberta. Chapter 3 covers the experimental results from thermal and UV ageing procedures along with tensile testing results of the aged specimens, images of the aged specimens, and results from a microstructural examination completed using a scanning electron microscope. Chapter 4 details non-destructive near-infrared results and compares several methods of analysis in their ability to predict or explain the effects of ageing. Chapter 5 covers the conclusions and implications of this research.

# 2. Methods and Materials

This section covers background information on the textile specimens, experimental testing apparatuses, and specific testing procedures utilized in this study.

## 2.1. Outer Shell Textile Specimen Characteristics

Firefighting ensembles are typically multi-layer constructions consisting of an outer shell (OS), a moisture barrier, and an internal thermal comfort liner. This investigation will examine OS specimens since they should be the most impacted by any external ageing factors and will be the most accessible location for an eventual commercial device. Additionally, the outer shell construction is known to provide a large percentage of a garment's thermal protection (Atalay, Bahadir and Kalaoglu 2015). OS textiles can vary in construction materials and this study will examine materials that utilize Kevlar® and PBI.

Textile specimens were classified as Ripstop (RS) Natural, Ripstop Black, and SCI PBI Max constructions each containing a 60/40% Kevlar®/PBI blend. The natural and black constructions were initially believed to be the same weave pattern (this was later found to be inaccurate) and were chosen to examine the impact of material dye. The RS constructions make use of a raised rib pattern that helps to prevent rips and tears in the fabric structure. The PBI Max construction is a relatively new product and was selected to examine the impact of a new weave pattern and the introduction of a filament yarn structure. A summary table of key material characteristics obtained using devices at the University of Alberta Department of Human Ecology testing facility can be found in Table 2.1. Material density measurements were averaged over five specimens and made using 50 mm die-punch disks with the use of a Denver M310 (Denver, CO) electronic scale according to ASTM D3766 (2013). Thickness measurements were averaged over five specimens and made using a 1 kPa pressure-foot driven Custom Scientific Instrument CS-55-225 (Whippany, NJ) with an accuracy of ± 0.001 inch. Yarn structures and patterns were analyzed using a Seiwa Optical Correct Tokyo® No.628471 microscope. The different weave patterns will also result in a different air permeability rating for each fabric. A Frazier 2000 Air Permeability Tester (Hagerstown, MD) with a 69.85 mm (2.75") opening was used according to ASTM D737 (2016) and CAN/CGSB-4.2 No. 36 (1997) testing standards in order to obtain

averaged (e.g. five trials for each fabric type) air permeability readings for each fabric type. A 4 mm orifice was used for both RS Natural and Black fabrics while a 2 mm orifice was used for the SCI PBI Max due to this tight twill weave fabric structure.

*Table 2.1 Key fabric characteristics*

| Characteristic | RS Natural | RS Black | SCI PBI Max |
|---|---|---|---|
| Mass/unit area, $g/m^2$ | 272 | 274 | 260 |
| Average thickness, mm (inch) (uncertainty) | 0.69 ± 0.03 (0.027 ± 0.001) | 0.80 ± 0.03 (0.031 ± 0.001) | 0.54 ± 0.05 (0.021 ± 0.002) |
| Air Permeability ($L/m^2 \cdot s$) (uncertainty) | 145.6 ± 12.0 | 69.2 ± 9.0 | 50.1 ± 2.0 |
| Fabric count | 17 warp x 14 weft | 22 warp x 19 weft | 19 warp x 19 weft |
| Weave | Plain | Plain | 2/1 Twill |
| Yarn structure | zzS twist | zzS twist | z and zzS twist |

A number of comments can be made to help explain differences in the structure of these textiles. On the RS constructions the raised ribs (e.g. grid pattern) in the weave contribute to an overall greater thickness measurement over the SCI PBI Max. For the fabric count, the RS Natural is a plain weave with paired warp every $10^{th}$ end and paired weft every $8^{th}$ shot. Conversely, the RS Black is a plain weave with a group of three warp every $9^{th}$ end and a group of three weft every $9^{th}$ shot. Both RS constructions are two-ply, spun staple yarns with a zzS twist pattern. On the other hand, the SCI PBI Max has two different types of yarn that are used for both the warp and the weft (e.g. a bright yellow yarn alternates with two darker, natural coloured yarns). The natural yarns in this construction are two-ply, spun staple yarns with a zzS twist pattern while the yellow yarn is a smooth multi-filament yarn with a z twist. Additionally, the 2/1 twill weave pattern of the SCI PBI Max provides a strong fabric structure that allows for "shifting" and movement within the fabric structure (e.g. more space between yarn loops allows for a larger spread of force over the textile structure). This increased material strength was evident by "pulling" observed when cutting out fabric specimens.

## 2.2. Specimen Conditioning and Preconditioning

The fabric samples originally arrived factory-treated on 4 m rolls. A 2 m section was cut from each roll and laundered according to CAN/CGSB 4.2 No. 58-2004 with a double rinse medium temperature wash of 50°C combined with 20.2 g of Tide Condensed detergent. This standard washing procedure should be sufficient to remove factory finishing. A tumble dry without heat was used to dry the fabrics after washing. Leaving a 2 m unlaundered section of fabric on the original roll will allow for comparisons to "as-received" conditions in future studies that may examine the influence of factory surface finishes.

Following laundering, specimens were cut into 145 x 150 mm rectangles in order to fit into both UV and thermal ageing testing brackets. Marking for the cutting template was completed on the non-face side of each textile. Specimen number labels were placed in the top left while an arrow in the bottom right indicated the warp direction of the cut specimen. The warp thread runs in perpendicular to the weft direction of the textile roll. A diagram depicting the difference between the two thread conditions of the textiles considered in this study can be found in Figure 2.1. Cutting of specimens was completed leaving 5 cm to the selvedge and 30 cm to the factory cut-edge. Cutting from the middle section of the fabric roll allows this 30 cm distance from the factory cut-edge to act as a protective barrier for the inner fabric (e.g. UV exposures could age the fabric during transport, discolouration of the SCI PBI Max protective barrier was evident following the drive to Edmonton, AB). Following ageing procedures these 145 x 150 mm rectangles were further cut down to 35 x 150 mm specimen sizes; providing for three test strips (A, B, and C in Figure 2.2).

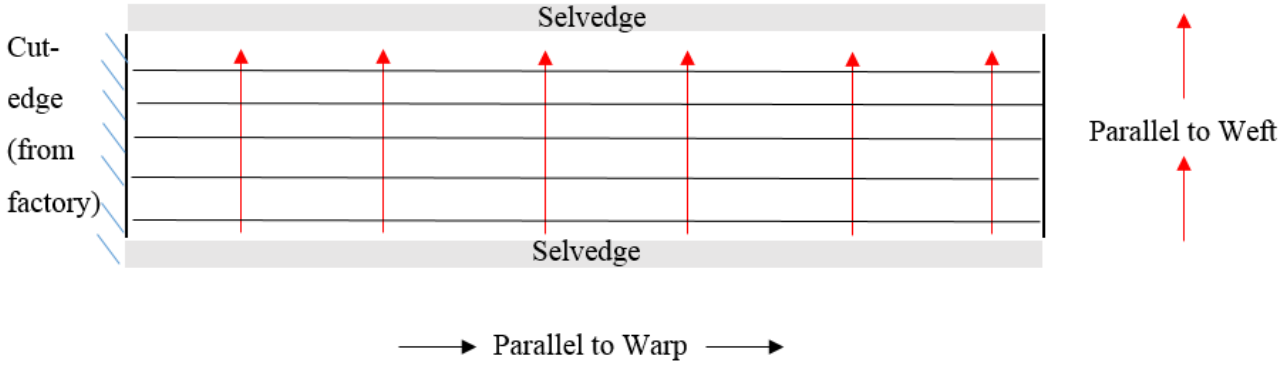


*Figure 2.1 Warp and weft directions of selected textiles*

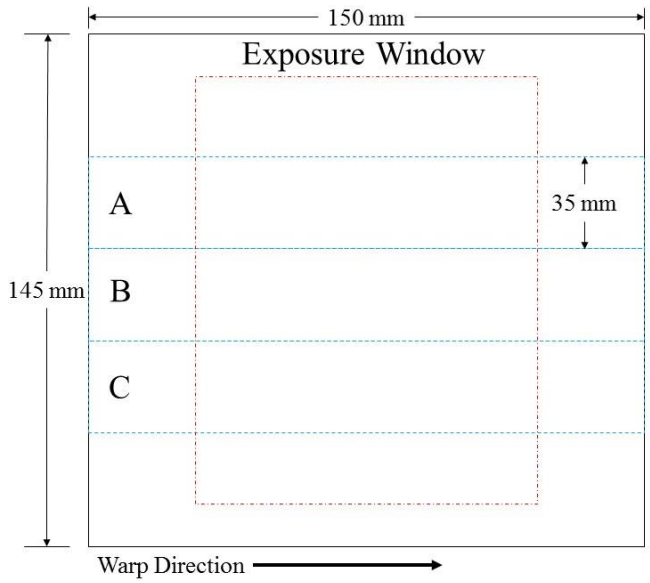


*Figure 2.2 Sketch of aged specimen dimensions and test sample sizing*

Cutting order was established in an increasing diagonal pattern rather than taking randomized sample patches across the textile surface. This selected cutting method allows for comparison along similar warp-wise strands and also allows for thermal ageing specimens to be in-line for comparison (Figure 2.3). This cutting pattern allowed for 57 individual specimens from each 2 m sample and a total of 171 individual tensile testing strips per fabric type.

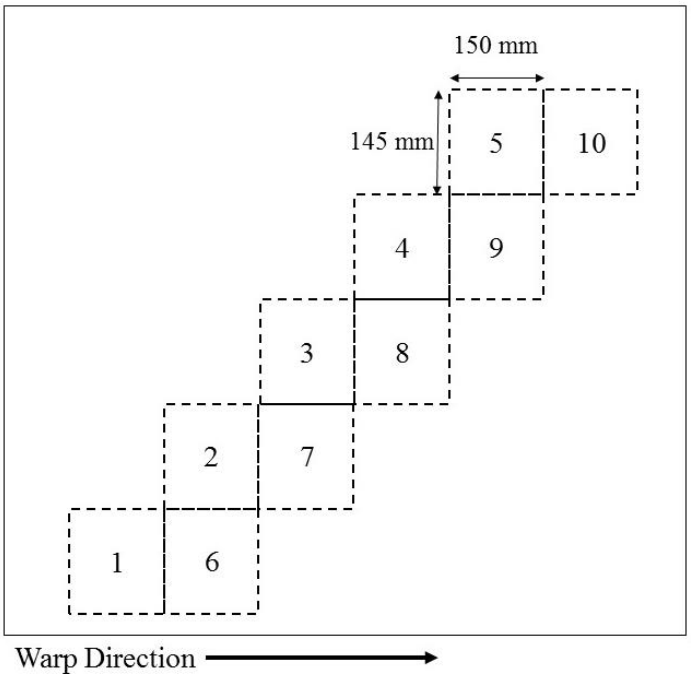


*Figure 2.3 Example sketch of increasing diagonal cutting pattern for fabric specimens*

Prior to any testing or property measurements specimens were preconditioned at 22 ± 2°C and 65 ± 5% RH (ASTM D1776 2016) and transported to testing devices using individually sealed plastic bags. These conditions were achieved at the University of Alberta using their environmentally controlled laboratory and at the University of Saskatchewan using a small conditioning chamber utilizing a magnesium salt (MgCl) and water mixture (0.6 – 0.8 g/L salt concentration) in a manner similar to ASTM E104 (2012).

## 2.3. Thermogravimetric Analysis

Thermogravimetric analysis (TGA) is a test method involving the continuous heating of a very small sample of a material specimen in either an oxygen, nitrogen, or other purge gas (e.g. argon, xenon) rich environment. In this research oxygen was selected in order to better reflect results that would be achieved with thermal ageing. TGA is often utilized in conjunction with spectroscopy in order to gain information on decomposition chemical reactions taking place (ASTM E1131-08 2014). Recording the mass-loss over time gives information on the thermochemical degradation processes for a material; these changes in mass can then be used to determine temperatures at which physical and thermo-chemical changes of the textile structure occur. This testing method was used on the OS specimens in order to determine temperature ranges necessary for specimen degradation, which also helped to select the incident heat fluxes required for thermal ageing. Each fabric (e.g. Ripstop Black, Ripstop Natural, and SCI PBI Max) was tested three times in order to gain information on the repeatability of the TGA test for these protective fabrics.

The Department of Chemistry at the University of Saskatchewan (UofS) has a TA Instruments Q5000 (TA Instruments 2006) system with a TGA/SDTA85 module (Figure 2.4) and an autosampler. This TGA device is based on a counter-balance system in an inert gas flow of oxygen or nitrogen at 10 mL/minute. The Q5000 balance mechanism has a specimen weight capacity up to 1.0 g, a resolution of 0.1 μg, and an accuracy ≤ ± 0.1% (TA Instruments 2006). Tests were carried out using a compressed air purge of 25 mL/minute at heating rates of 20°C/minute up to a temperature of 900°C. Individual masses of the test specimens ranged from 6 – 12 mg and were held in high temperature 100 μL platinum crucibles. The crucible was

cleaned using acetone and a chem-wipe swabbing in between each individual trial. Plotted along with the TGA results for percentage mass loss are derivative mass loss percentage curves which simplify data interpretation. Detailed results and discussion are contained in Section 3.1.

*Figure 2.4 Q5000 TGA testing apparatus*

## 2.4. Cone Calorimeter

Cone calorimeters have become a standard small-scale scientific apparatus utilized by various research groups conducting fire research (ASTM E1354-16a 2016). This device can record a number of valuable pieces of information (e.g. mass loss over time, ignition/extinguishment time, smoke/soot production, exhaust gas analysis, temperatures, heat release rates) when materials are subjected to an incident heat flux provided from a 16 mm diameter conical heater element. The UofS Fire Testing Technologies Dual Cone Calorimeter (Figure 2.5) makes use of both the internal and an external Agilent 34970A DAQ with HP 34970A Multiplexers for data acquisition and can provide heat flux levels from 0 – 100 $kW/m^2$ from a conical heater element. This conical heater element can be positioned either vertically or horizontally in the cone calorimeter and in the UofS apparatus a specially designed air-cooled

shutter system protects specimens from unintended heating until the start of heat flux exposure is desired. Reinsertion of this air-cooled shutter also ends the test following a desired exposure time. Power supply accuracy specifications will vary and can be found in the available literature (Hewlett-Packard Company 1999). During active testing a ventilation system and laboratory roof-mounted fume hood above the cone calorimeter evacuates gaseous by-products resultant from specimen pyrolysis or off-gassing following heat flux exposure.

*Figure 2.5 UofS cone calorimeter in horizontal orientation*

The cone calorimeter vertical mounting slide, pictured below in Figure 2.6, has a number of air-gaps that are not present in the standard quartz tube apparatus (ASTM F1939-15). However, for lower heat flux and subsequent temperature ranges the vertical orientation of the cone calorimeter has been shown to perform well for experimental testing procedures in previous studies performed at the UofS (Thorpe 2004; Rezazadeh 2014). A specially designed specimen holder (Torvi, Rezazadeh and Bespflug 2016) was used to hold fabrics in place during thermal exposure (Figure 2.6).

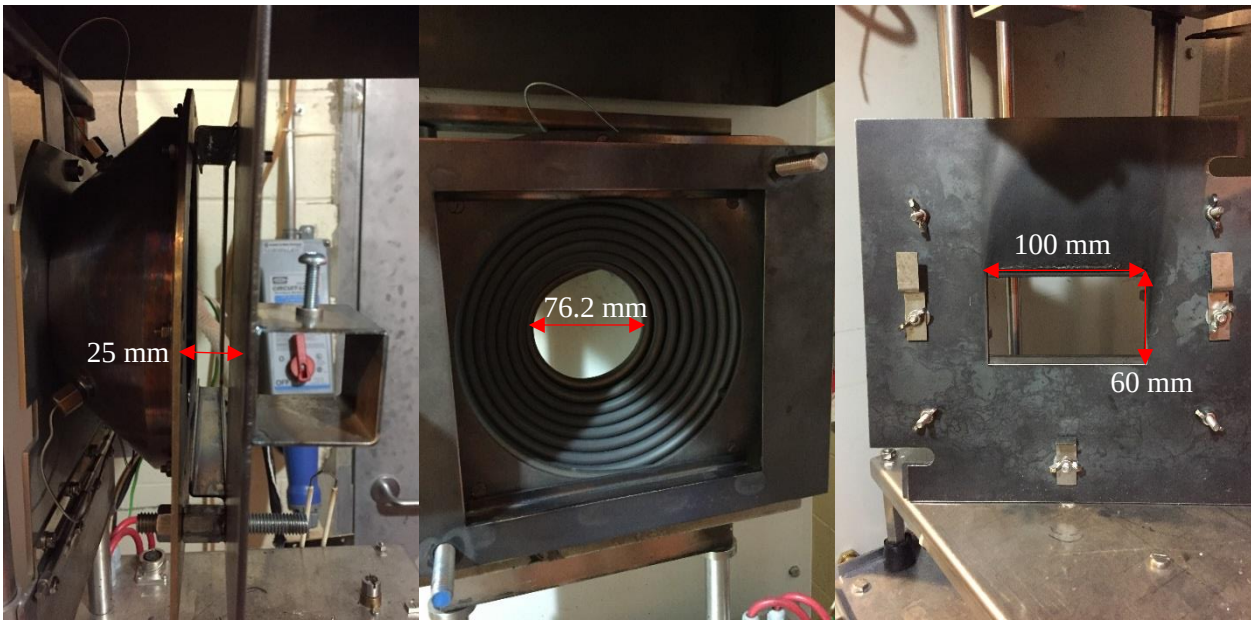


*Figure 2.6 Side view of the vertical mounting apparatus (left) for the cone calorimeter, large central air gap (middle) of the radiative cone, and (right) specimen holder*

## 2.5. Thermal Ageing with the Cone Calorimeter

Previous research has shown the radiative heat flux provided by this cone calorimeter is very uniform across the exposure window (Rezazadeh 2014). A previous undergraduate student at the UofS named Thomas Ingold (Rezazadeh 2014) marked the exposure area of this particular cone calorimeter using a 2.5 x 2.5 cm grid system and measured the distribution of an incident 35 kW/m$^2$ heat flux starting from point zero in the centre of the exposure window. This previously completed work (Rezazadeh 2014) showed that outer edge heat flux levels were still 90% of the nominal heat flux provided by the cone calorimeter for a 7.5 x 7.5 cm exposure window. This uniform exposure has a number of benefits for the current study when compared to other thermal ageing methods such as isothermal ovens. For a period of time following specimen placement in an oven there will be a recovery time period. This recovery time could introduce critical errors in short exposure periods and add uncertainty to longer exposures. Moreover, individual ovens may contain temperature gradients which depend on and vary with the internal size of the heated compartment. Thermal ageing of multiple fabric specimens at one time (e.g. multiple specimens on mounting racks) may increase the severity of these gradients by creating defined isothermal layers within the oven. Additionally, the cone calorimeter provides a one-sided heat flux exposure in contrast to an oven's exposure on all sides of a specimen. In

firefighting the exterior side of an OS material will be exposed to intense thermal radiation while the inner side of the OS will be in contact with the inner layers (moisture barrier, inner comfort liner) and the firefighters' body. Therefore, use of a cone calorimeter to provide a heat flux exposure may better represent real fire conditions that would be faced in field suppression activities. This is why the current research has focused on heat flux levels provided from the conical heater element of a cone calorimeter for thermal ageing procedures.

The thermal ageing procedure for each specimen was performed using a method that was similar to previous research (Thorpe 2004; Rezazadeh, 2014). Material specimens were cut to size from larger fabric rolls as previously mentioned and were conditioned for 24 hours at 22 ± 2°C and 65 ± 2% relative humidity (RH) in a conditioning chamber (ASTM E104-02). These conditions were created using a magnesium chloride and tap water solution (0.6 – 0.8 g/L) in a contained chamber (ASTM E104-02). All specimens were tested in the cone calorimeter within 5 minutes of exposure to ambient conditions. For calibration purposes a water cooled Schmidt-Boelter heat flux gauge (GTW-10-32-485A, Medtherm, Huntsville, AL) was mounted 25 mm behind the heating element to verify each heat flux before testing. This working gauge was also calibrated against a laboratory reserve gauge (Appendix A) prior to use. An air-cooled shutter then allowed for specimen mounting with minimal exposure to the heat fluxes from the cone heater prior to the start of testing. With the cooled shutter removed fabric specimens were then exposed to 60 s of continuous thermal ageing conditions while temperature measurements were recorded on the back of the fabric using a Minolta Cyclops 300bAF (Dronfield, UK) infrared (IR) thermometer with a maximum range of 1050°C. A Canon Vixia HF R500 video camera was used to take a visual recording of each heat flux exposure. Heat fluxes were chosen to match ordinary and early stage emergency conditions as outlined in Sections 1.4 and 1.5. Thermal ageing exposures ranged from 0 – 70 kW/m$^2$ and are detailed further in Section 3.2.

## 2.6. UV Ageing – Weatherometer

UV ageing was performed at the University of Alberta using an Atlas xenon Arc Weatherometer in the Department of Human Ecology. Specimens in this trial were aged for 40, 80, or 160 standard fading hours (SFH) to match initial investigations performed by an undergraduate student at the UofS (Chris Bespflug) and conducted under conditions outlined in

CAN/CGSB – 4.2 No. 183-97/ISO 105-B02:1994 standards. A total of fifteen 145 x 150 mm specimens of each of the three fabrics were used for UV exposure in the Weatherometer (five specimens per fabric type for each of three UV exposures). Once the required exposure time had been reached for a set of aged fabrics the Weatherometer was powered down, the selected specimens removed from the device, and the Weatherometer was restarted to continue ageing the longer duration specimens. After 40 SFH of exposure five specimens of each fabric were removed from the chamber. This removal process was completed following an additional 40 hours of UV exposure to get the 80 SFH exposure specimens and then another set was removed after 160 hours of UV exposure for the 160 SFH exposure specimens. This Weatherometer apparatus uses a water-cooled xenon lamp with a borosilicate inter glass filter and soda-lime outer filter to give a spectral distribution similar to that of sunlight passed through a window glass. It is capable of simulating solar radiation and providing a full spectrum of light irradiance of 1.1 W/($m^2$/nm) at 420 nm. The xenon bulbs and filter system were recently replaced in this Weatherometer at the University of Alberta.

All UV fabric specimens were mounted around individual paper cards to add rigidity during mounting procedures and prevent slippage of the fabrics during the ageing process. This card will not impact the UV ageing process since the folded pieces on the back of the specimen are not intended to be UV aged. The interior of the UV chamber with paper-cards mounted in the specimen holders and a side view of the control panel of the Weatherometer is shown in Figure 2.7. All UV specimens were cut and mounted at the same time within the Weatherometer.

The age of the device leads to some occasional operating errors that cause the device to activate a safety shut-down procedure. Impure conditioning water, excess high temperatures, low temperatures, and a wide variety of other events will cause the device to power down. For the 40 and 80 SFH trials the device ran without incident. However, when attempting the 160 SFH trials the Weatherometer would shut down on high-temperature conditions during its warm-up phase. After some trouble shooting and purge water cycling this issue seemed to be mostly resolved, but may have caused a small amount of additional ageing during the 160 SFH trial from the repeated start-up and shut-down procedures during the trouble shooting. The goal of the final exposure (e.g. 160 SFH) was extended UV ageing condition and this small amount of intermittent ageing

during troubleshooting (e.g. lamp/device start-up, over-temperature shut-down, and restarting process) is expected to be negligible to final 160 SFH results in this current study.

*Figure 2.7 Interior view of the Weatherometer UV chamber (left) and side-mounted control panel (right) at the University of Alberta*

## 2.7. Tensile Testing – Instron 5565

Tensile testing of the OS specimens was performed according to NFPA 1971 (2013) which recommends the use of the standard ASTM D5035 (2015). An Instron 5565 tensile testing apparatus (Figure 2.8) with a load capacity of 5 kN was used after being zeroed and balanced before the start of each trial set. The entire Instron apparatus was recently calibrated by an Instron technician in August, 2016 and the device was used for testing in November, 2016. Specimen samples were mounted in anti-slip jaws and subjected to a Constant-Rate-of-Extension (CRE) at 60 mm/min rather than the specified 300 mm/min (ASTM D5035 2015) in order to gain more information from more intensely aged and damaged specimens. The strip-jaws had dimensions of 25.4 mm x 76.2 mm (1” x 3”) and a pneumatic clamping system set at 517.1 kPa (75 psi). A fixed gauge length of 75 mm was used. Slippage of the jaw clamping system remains a common problem with this testing method (Rezazadeh 2014) and increases the uncertainty of test results. For the Ripstop constructions this did not seem to be an issue, but the SCI PBI Max

trials required the use of some sandpaper grips (100 – 150 grit) in order to provide extra grip on the filament yarn.


*Figure 2.8 Instron 5565 tensile testing apparatus located in an environmentally controlled laboratory in the Department of Human Ecology at the University of Alberta*

## 2.8. NIR Spectroscopy – Cary UV-Vis-NIR Spectrophotometer

As previously mentioned specimens were preconditioned utilizing a manner similar to ASTM E104 (2012) for 24 hours at 22 ± 2°C and 65 ± 2% relative humidity and were tested within 5 minutes of removal from the conditioning chamber. The UofS has a 16 mm aperture UV-Vis-NIR spectrophotometer (Varian (now Agilent), Cary 5G Palo Alto, CA) equipped with an integrating sphere configured for diffuse reflectance which was used to expose OS specimens to the equipment's light source. Prior to testing, a baseline calibration run was completed using a reading from a reference disk (SRS-99) with a known absolute reflectance in contrast to a completely blocked zero-line reading. NIR reflectance results were acquired by taking an average of two, using different areas of the same aged specimen for each. These results were

nearly identical (< 0.5% difference) which confirms the previously mentioned uniformity of ageing of the individual fabric specimens across all cases considered in this study. The interrogation area was the exposed area of the 150 mm x 35 mm non-pared down specimens prepared for tensile testing.

Aged OS specimens were subjected to incident light in the wavelength region from 400 – 2000 nm at a scan rate of 600 nm/min and 1 nm intervals and 2 nm spectral band width. This range was selected to include the visible light spectrum (400 – 750 nm) as well as the NIR spectrum (800 – 2000 nm). The equipment slit height and beam mode were set to "reduced" and "double", respectively. The software package in use also allowed for the automatic baseline correction from zero reflectance. Since lower wavelength regions are sensitive to colour change (Schwanninger, Rodrigues and Fackler 2011) only the reflectance spectrum from 800 – 2000 nm are shown in Chapter 4 for thermal ageing and UV ageing results.

## 2.9. Scanning Electron Microscope – JEOL JSM 6010

The use of a JEOL JSM 6010 (Akishima, JA) scanning electron microscope (SEM) allowed for an in-depth view of the textiles' microstructures. Comparison of unaged and aged OS specimens were used to reveal the development of microstructure damage (e.g. pits, holes, cracks, fissures). This SEM study was conducted in two parts; an initial attempt at examining the fabric macrostructure followed by a more detailed examination of the microstructure at higher magnifications. Resolutions of 50 μm have been used to capture signs of microstructure damage in previous studies (Rezazadeh 2014) and justified selection of this magnification level for an initial investigation. A more detailed investigation of surface features could be achieved at higher resolutions (e.g. 4 μm used by Jain, et al. (2002) for Nomex®) and was done in the second part of this SEM study. High vacuum conditions were briefly investigated without the use of a surface coating, but did not yield any reliable results. A conductive double-sided tape was used to mount specimens onto brass piles for placement on the viewing platform. Initial images were acquired under low vacuum conditions of 40 Pa, a spot size of 60, 15 kV back-scattered electron (BES) settings, 350x magnification, and a resolution of 50 μm following focusing at the 700x magnification level. However, this level of focus failed to provide meaningful insight. These initial attempts are contained in Appendix C for completeness.

# 3. Experimental Results – Ageing, Tensile Testing, and SEM

Methods of ageing firefighters' clothing and outer shell materials was discussed in Section 1.5 – 1.6 along with comparisons between field and laboratory conditions in Section 1.4. This section contains details on the thermal and ultraviolet light ageing testing methods performed on the RS Natural, RS Black, and SCI PBI Max fabrics with tensile testing results and scanning electron microscopy microstructure images.

## 3.1. Thermogravimetric Analysis

TGA testing was completed for all specimens from October 3-5$^{th}$, 2016 at a heating rate of 20°C/minute. Prior to each test, the high temperature platinum pan was cleaned and tared to acquire a zero reading for the empty sample pan. The Q5000 TGA tester had the ability to make use of an autosampler, but only one platinum pan was used during this experimental procedure. During testing the mounting of the platinum holder was found to be a key experimental step. Any offset on the sample hook would cause the holder to spin or oscillate in the freestream and introduce noise into the results. Additional data noise may have been resultant from nearby trenching construction activities in the area outside the Thorvaldson Laboratory 246. The balance on this device is sensitive enough to record vibrations from these activities.

Three trials were conducted for each respective fabric type to gain information on the repeatability of the TGA testing procedure (Figures 3.1 – 3.3). Specimen size was found to be a key parameter for repeatable results. Specimens with a mass between 6 – 8 mg were found to yield consistent results. For Ripstop constructions, this size roughly correlates to one "square" on the fabric once the edges have been rounded to fit the platinum holder. Larger specimen sizes (> 10 mg) introduced noise in derivative mass results near the end of the test (e.g. Figure 3.2). Aside from this effect in larger specimen trials, the thermochemical decomposition patterns at different temperature ranges appear to be fairly consistent when comparing trials of one specimen against one another. Water evaporates out of the porous textile structure around 100°C and is evident from the small jump in derivative mass loss around this temperature. All fabrics saw a reaction around 300°C that may be due to a dye-removal event. However, this reaction

around 300°C appears in fabrics without the presence of dye so there should be some other explanation. Subsequent material decomposition changes take place between 450 – 550°C. More details on correlations between the thermochemical decomposition process and infrared results are given in in Sections 4.1 – 4.3. When temperatures reach the upper range of the test (> 700°C) all of the material has been consumed and this is evident in the TGA results. Therefore, TGA results are only shown up to 700°C even though temperatures ranged up to 900°C during testing. TGA mass-loss trends for RS Natural, RS Black, and SCI PBI Max specimens can be found in Figures 3.1 – 3.3. The derivative weight from trial one of the RS Natural (e.g. Figure 3.1) has not been included to improve readability (i.e. the spike-loss of material between 450 – 550°C is not repeatable and was due to nearby construction/groundwork in area).

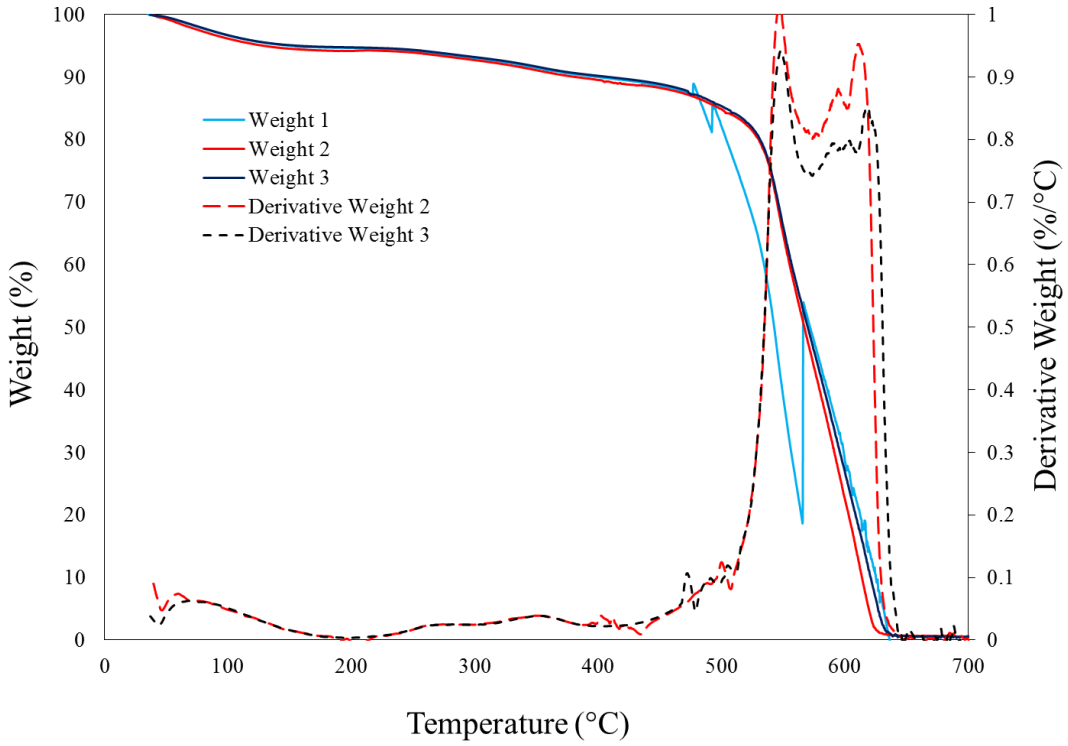


*Figure 3.1 TGA results for RS Natural*

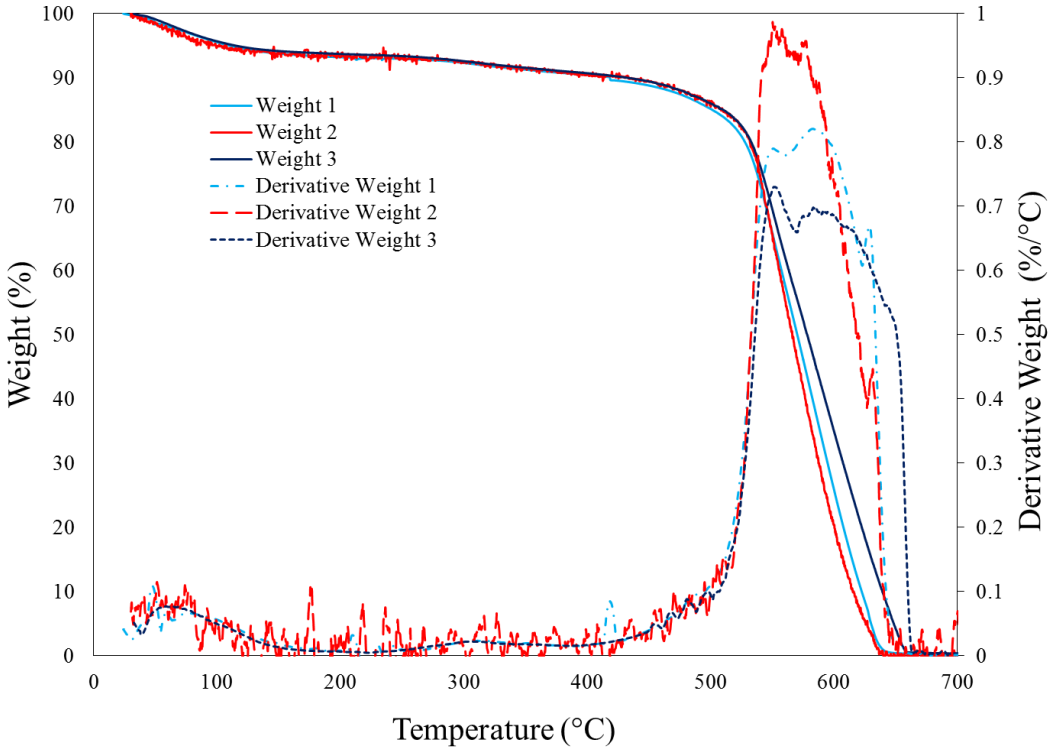


*Figure 3.2 TGA results for RS Black*

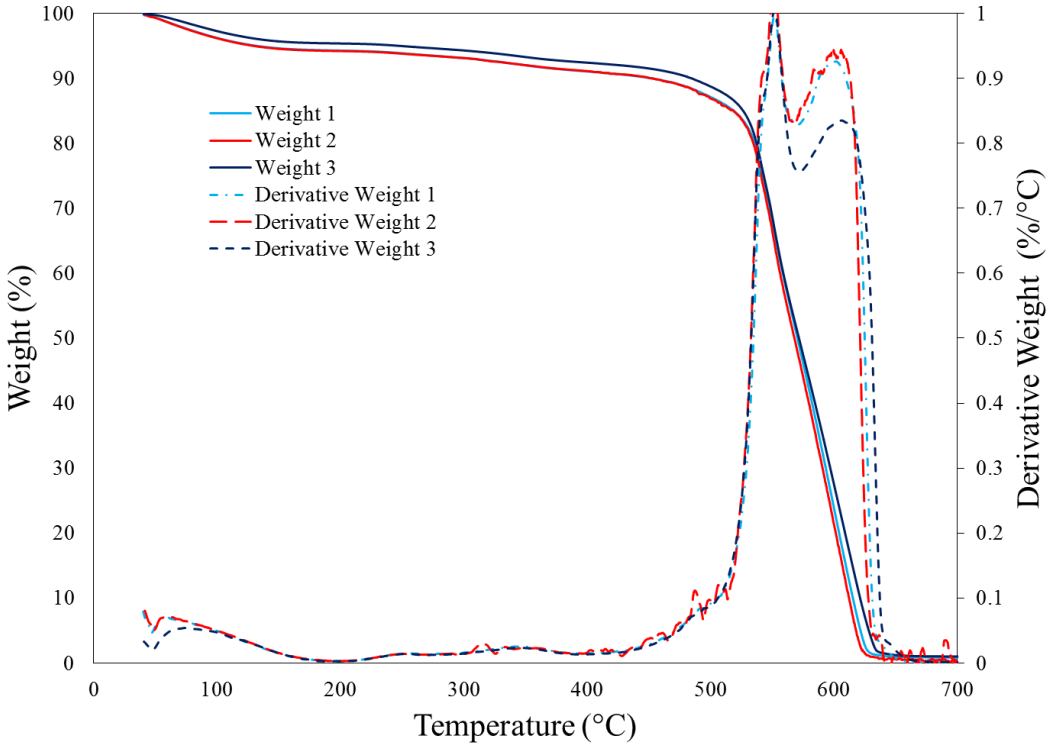


*Figure 3.3 TGA results for SCI PBI Max*

## 3.2. Temperature Measurements – Thermal Ageing

Fabrics were subjected to a wide range of incident heat flux levels, which were selected based on previous research (Sections 1.5.2 and 2.4) and temperatures at which thermochemical reactions occurred based on TGA data. Temperatures on the back of the fabrics were recorded using an infrared thermometer. Before thermal ageing each specimen was preconditioned according to ASTM D1776 (2016) for a minimum of 24 hours in a conditioning chamber at the previously mentioned 22 ± 2°C and 65 ± 5% RH. A thermal ageing condition of 10 kW/m$^2$ (i.e. which produced a fabric temperature of 200°C) was selected in order to establish a baseline ageing temperature that related to ordinary working conditions of a firefighter (Figure 1.4). This also matched TGA results which indicated the earliest onset of thermochemical changes following the evaporation of the entrained moisture within the fabric structure at approximately 100°C (Figure 3.1 – 3.3). The selected heat flux ageing levels were 10, 15, 20, 25, 30, 35, 40, 45, 50, 60, and 70 kW/m$^2$. The heat fluxes produced a wide range of temperatures over which the thermochemical reactions of the fabrics were expected to occur based on the TGA results (e.g. approximately 200°C to 700°C). The heating rate of this cone calorimeter exposure is much higher than TGA procedures, but the temperatures recorded on the back of the fabrics reach an approximate steady-state temperature shortly after the air-cooled shutter has been removed. An example temperature trace showing repeatability and averaged results for the RS Natural can be found in Figure 3.4a. Temperatures for RS Black and SCI PBI Max are nearly identical (Figure 3.5 – 3.6). Figure 3.7 shows a comparison of the steady state temperatures reached for the 30 and 60 kW/m$^2$ exposures for all fabric types. Initial temperatures, temperature increases, and standard deviations can be found in Table 3.1. The decrease in temperature during the final 10 s of all exposure conditions is a result of the operator placing the air-cooled shutter system in the cone calorimeter bracket in preparation for the end of the thermal exposure. This operation was performed with 10 s remaining in the test in order to ensure a consistent 60 s exposure time across all trials.

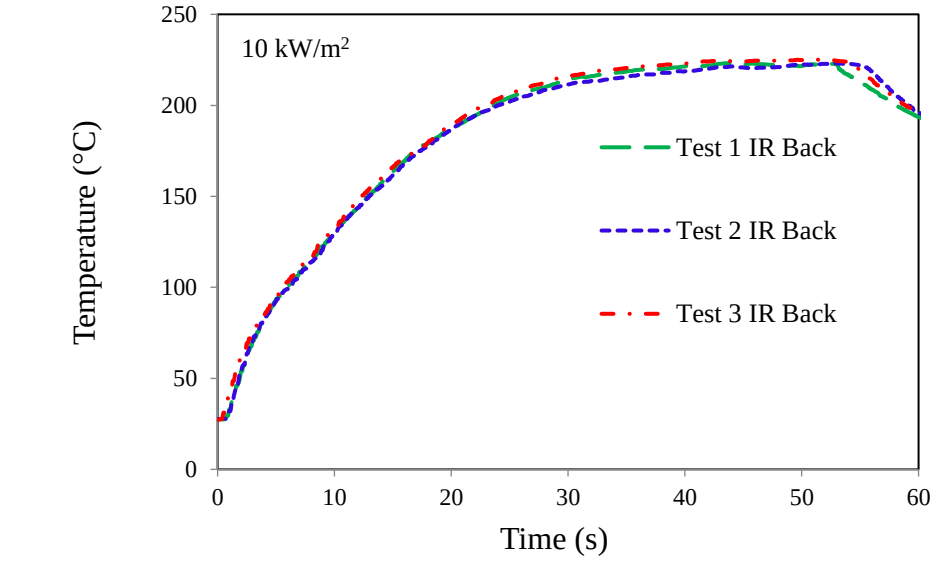


(a)

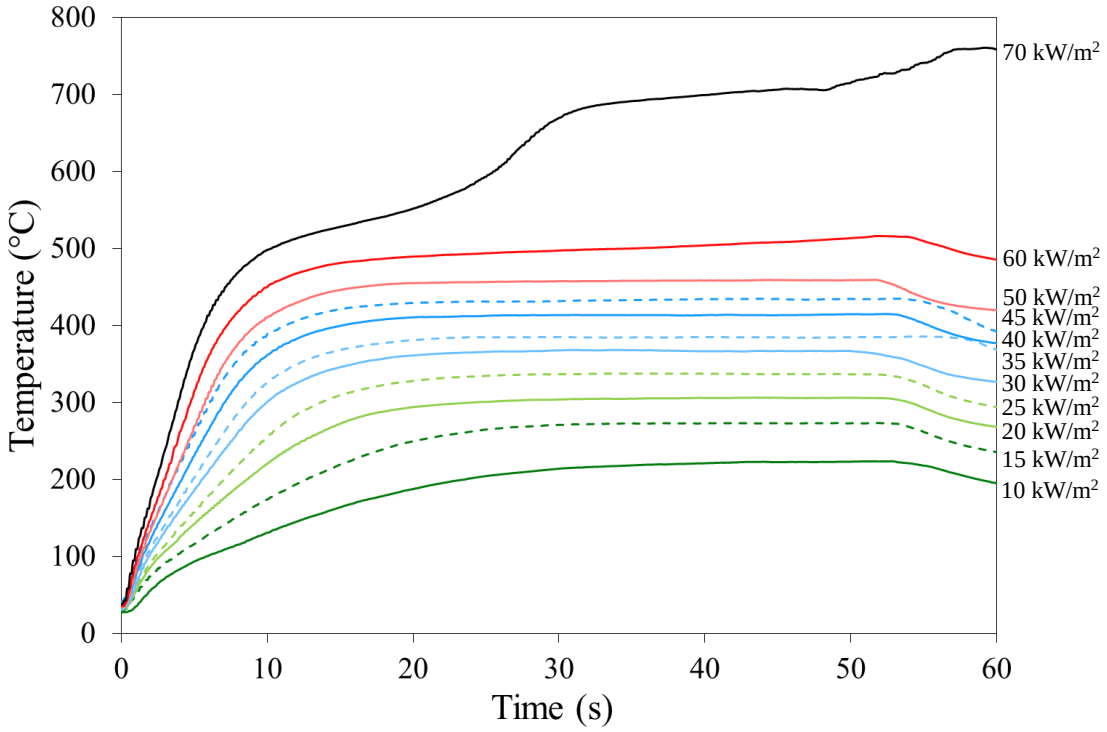


(b)

*Figure 3.4 RS Natural temperature measurements taken on the back of the fabric using an infrared thermometer showing (a) repeatability for 10 kW/m$^2$ exposure and (b) for all exposures*

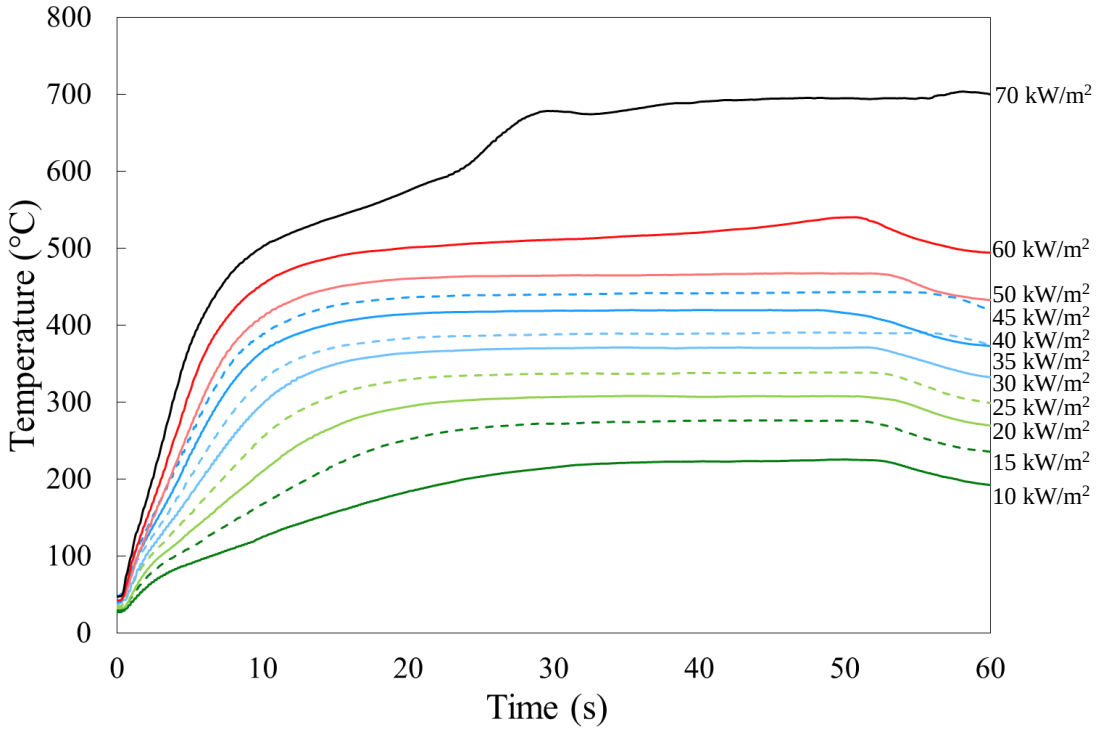


*Figure 3.5 RS Black temperature measurements taken on the back of the fabric using an IR thermometer during exposure to heat fluxes from 10 – 70 kW/m²*

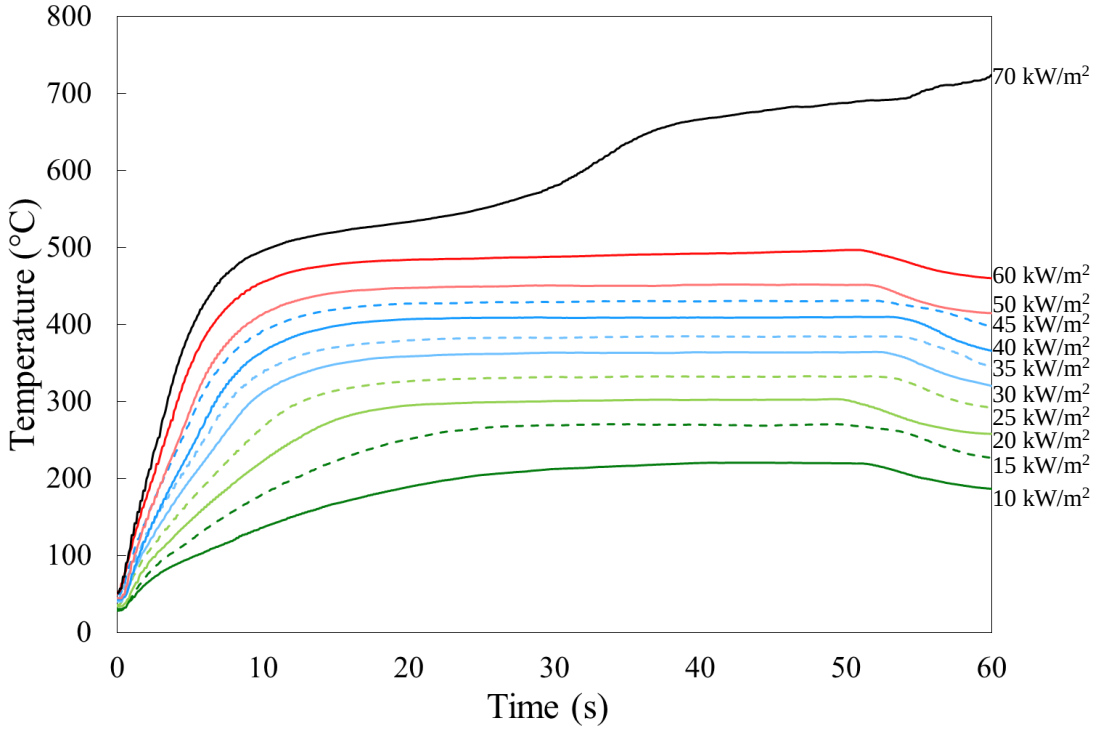


*Figure 3.6 SCI PBI Max temperature measurements taken on the back of the fabric using an infrared thermometer during exposure to heat fluxes from 10 – 70 kW/m²*

*Table 3.1 Averages and standard deviations in temperature increases for all fabric types during thermal ageing*

| Fabric Type | Temperature Increase, ΔT (°C) | | | | | |
|---|---|---|---|---|---|---|
| | RS Natural | | RS Black | | SCI PBI Max | |
| Heat Flux ($kW/m^2$) | Ave | Std Dev | Ave | Std Dev | Ave | Std Dev |
| 10 | 196 | 1.2 | 199 | 0.4 | 193 | 1.5 |
| 15 | 246 | 1.6 | 248 | 0.4 | 241 | 0.9 |
| 20 | 275 | 1.0 | 276 | 1.4 | 269 | 0.4 |
| 25 | 306 | 2.2 | 306 | 1.3 | 298 | 0.9 |
| 30 | 333 | 1.7 | 334 | 1.3 | 324 | 0.9 |
| 35 | 355 | 5.1 | 354 | 0.3 | 344 | 0.3 |
| 40 | 377 | 3.7 | 381 | 0.2 | 368 | 1.5 |
| 45 | 394 | 3.3 | 398 | 1.7 | 382 | 0.5 |
| 50 | 425 | 4.2 | 426 | 1.3 | 408 | 2.3 |
| 60 | 484 | 4.4 | 500 | 6.5 | 447 | 3.1 |
| 70 | 726 | 6.6 | 657 | 8.9 | 691 | 28.8 |

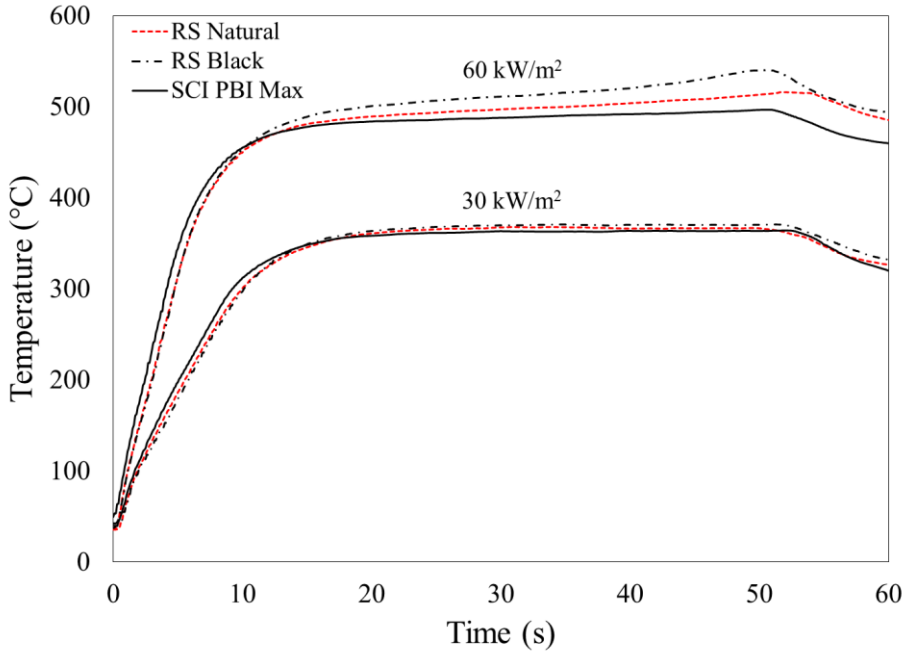


*Figure 3.7 Comparison of steady-state temperatures reached for 30 and 60 $kW/m^2$ exposures*

For thermal exposures which produced temperatures of 250°C (e.g. up to 15 kW/m$^2$) the fabrics appeared to retain original characteristics (i.e. aged specimens looked and felt the same as unaged specimens). Exposures which produced temperatures of at least 300°C (e.g. greater than 20 kW/m$^2$) caused significant off-gassing and subsequent colour change and charring. Fabric material structures also become increasingly brittle with increasing temperature. This increasing degradation trend continued until the 60 kW/m$^2$ (i.e. temperature of 500°C) exposures. After this point specimens began to experience a significant loss of material around the upper section of the exposed window along with the development of a noticeable sheen near this area. This appearance of a sheen may be due to the hot gas layers rolling up the front of the fabric and depositing material on the fabric surface. At the highest incident heat flux considered of 70 kW/m$^2$ open flames began to appear on the front of the fabric around 600°C of all trials (Figure 3.8). These open flames were responsible for the sudden and large temperature increase at this point in time for the 70 kW/m$^2$ exposure (Figure 3.4 – 3.6). The time to reach this 600°C temperature ranged from 30 s for the RS Black trials to 45 s for both the RS Natural and SCI PBI Max trials. These highest exposure levels left all specimens very charred and physically weak. Basic handling of these specimens occasionally resulted in material failure prior to mounting procedures conducted in the tensile testing portion of this study (Section 3.5).

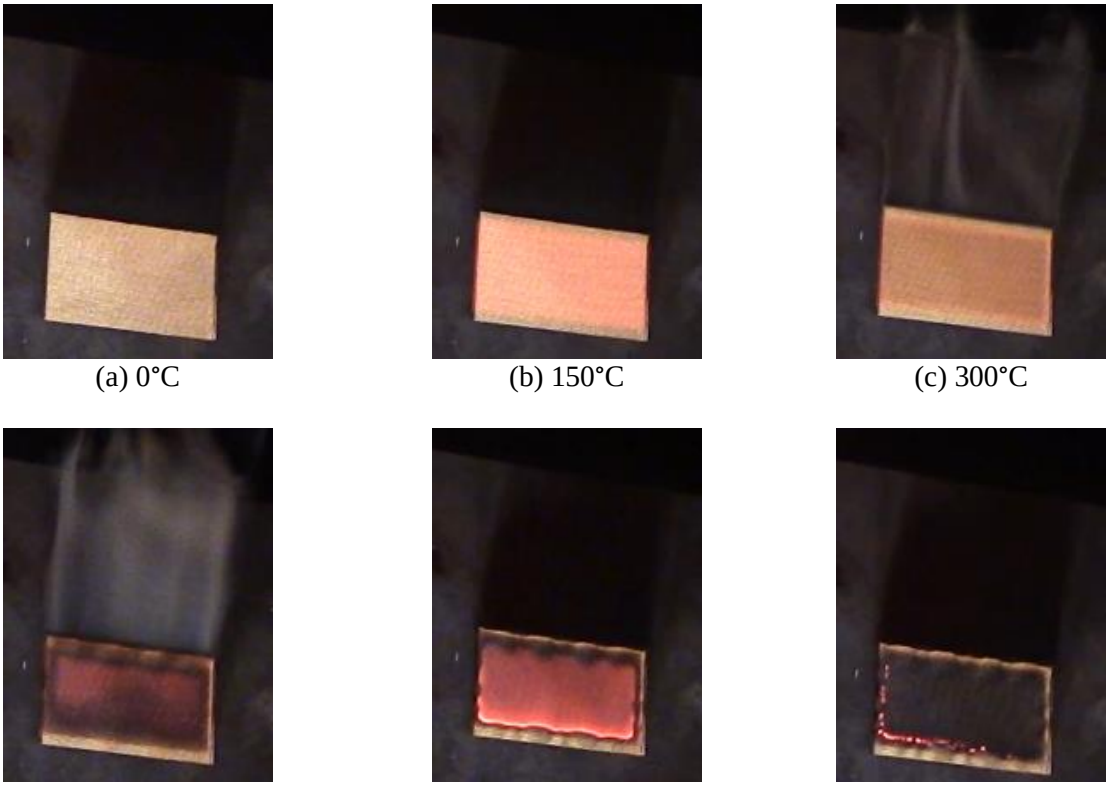

(a) 0°C (b) 150°C (c) 300°C

(d) 550°C (e) 700°C (f)

*Figure 3.8 RS Natural 70 kW/m$^2$ heat flux exposure showcasing approximate temperature increase and damage of (a) specimens prior to exposure, (b) immediately following shutter removal, (c-d) off gassing and colour change, (e) opening flaming on front, and (f) immediately following shutter insertion at end of exposure*

The relationship between incident heat flux and resultant temperatures may be non-intuitive. Figure 3.9 shows the relationship between incident heat flux and steady-state temperatures reached on the back of the fabric for the RS Natural fabric. RS Black and SCI PBI max specimens also reached similar temperatures when subjected to the same heat flux levels in the cone calorimeter (Table 3.1). Steady-state temperatures were reached and maintained between 20 – 50 seconds of the thermal ageing for all trials except for the 70 kW/m$^2$ exposure. The steady-state temperature for these final heat flux exposures (70 kW/m$^2$) were reached between 10 – 30 seconds.

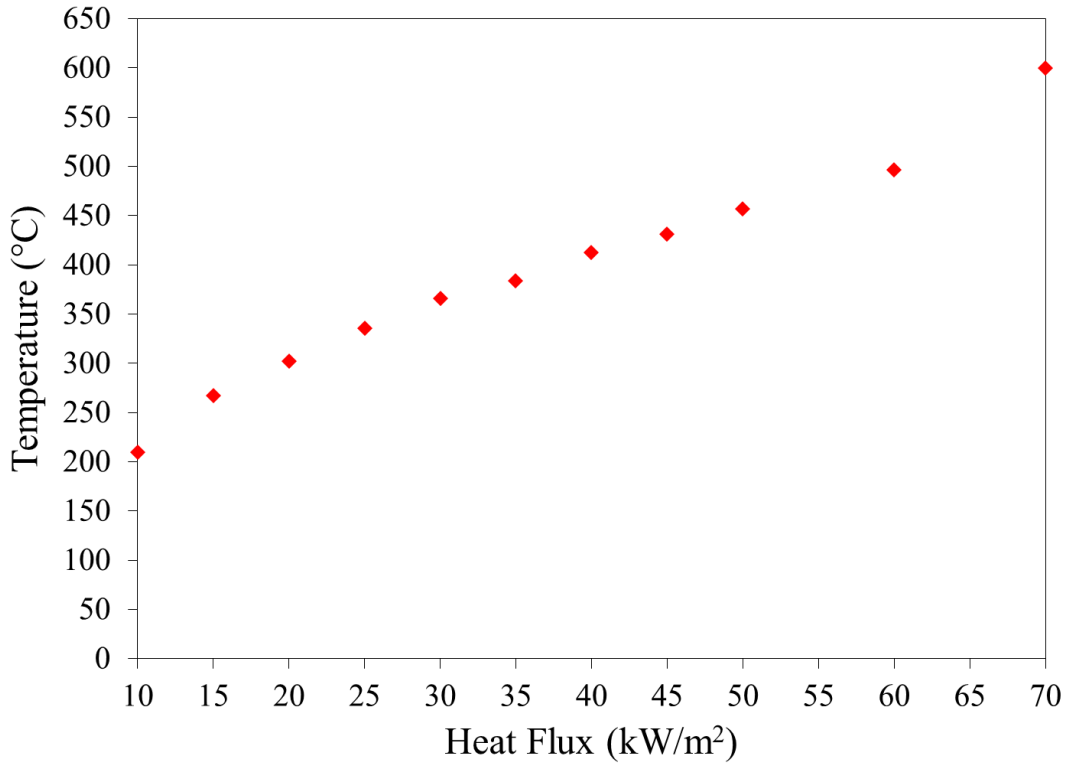


*Figure 3.9 Steady-state temperatures recorded on the back of the fabric resultant from heat flux exposure for the RS Natural fabric*

## 3.3. UV Ageing

The Weatherometer device at the University of Alberta has been described previously in Section 2.6. The Weatherometer has the ability to record accumulated UV irradiance values (Table 3.2) and numerous chamber conditions (Table 3.3). However, the internal chamber air temperature device was non-operational so the true chamber temperature was somewhere between the black panel temperature and cooling water temperature readings. The suggested test conditions in Table 3.3 are automatically generated by the Weatherometer control system. Additionally, the total irradiance values in Table 3.2 are a cumulative total for the entire active service life of the Weatherometer. Actual exposure irradiance is calculated in the data systems by subtracting the start-of-test irradiance value from the end-of-test irradiance value.

*Table 3.2 Irradiance values recorded during test*

| Date | Test Interval (SFH) | Total Irradiance (kJ/m$^2$/nm) |
|---|---|---|
| START | 0 | 59041.2 |
| 25-Oct-16 | 21.3 | 59126.3 |
| 26-Oct-16 | 20.0 | 59205.1 |
| 27-Oct-16 | 1.6 | 59211.3 |
| Fabric Removed | **40** | **170.1** |
| 29-Oct-16 | 20.0 | 59298.7 |
| 1-Nov-16 | 20.0 | 59378.2 |
| 2-Nov-16 | 1.4 | 59383.6 |
| Fabric Removed | **80** | **342.4** |
| 2-Nov-16 | 20.0 | 59463.1 |
| 3-Nov-16 | 20.0 | 59542.7 |
| 4-Nov-16 | 20.0 | 59622.3 |
| 7-Nov-16 | 20.0 | 59701.9 |
| Fabric Removed | **160** | **660.7** |
| Cumulative values | **164.3** | **660.7** |

*Table 3.3 Weatherometer chamber conditions during UV ageing testing*

| | suggested test conditions | 25-Oct-16 | 26-Oct-16 | 27-Oct-16 | 29-Oct-16 |
|---|---|---|---|---|---|
| | | actual | actual | actual | actual |
| Black panel (°C) | 63 | 70.0 | 70.9 | 70.9 | 70.5 |
| Chamber air (°C) | 43 ± 2 | not recorded | not recorded | not recorded | not recorded |
| Conditioning $H_2O$ (°C) | 45 | 44.0 | 43.1 | 43.4 | 45.5 |
| Dry bulb (°C) | 32 - 33 | 34.6 | 34.3 | 34.6 | 33.7 |
| Wet bulb (°C) | 19 - 20 | 21.2 | 22.1 | 21.7 | 20.9 |
| RH (%) | 30 ± 5 | 29 - 30 | 34 | 31 - 32 | 30 - 31 |

| | suggested test conditions | 1-Nov-16 | 2-Nov-16 | 4-Nov-16 | 7-Nov-16 |
|---|---|---|---|---|---|
| | | actual | actual | actual | actual |
| Black panel (°C) | 63 | 66.0 | 66.9 | 67.0 | 66.8 |
| Chamber air (°C) | 43 ± 2 | not recorded | not recorded | not recorded | not recorded |
| Conditioning $H_2O$ (°C) | 45 | 45.5 | 45.2 | 45.3 | 45.3 |
| Dry bulb (°C) | 32 - 33 | 33.9 | 32.9 | 34.0 | 33.0 |
| Wet bulb (°C) | 19 - 20 | 21.2 | 20.5 | 21.1 | 19.9 |
| RH (%) | 30 ± 5 | 31 - 32 | 31 - 32 | 31 | 29 |

## 3.4. Aged Fabric Images

A visual record of the thermal and UV aged RS Natural (Figure 3.10), RS Black (Figure 3.11), and SCI PBI Max (Figure 3.12) specimens can be found in this section. Photographs were taken using a Sony Alpha (ILCE) A3000 (Pathum Thani, TW) camera with an SEL-1855 lens.

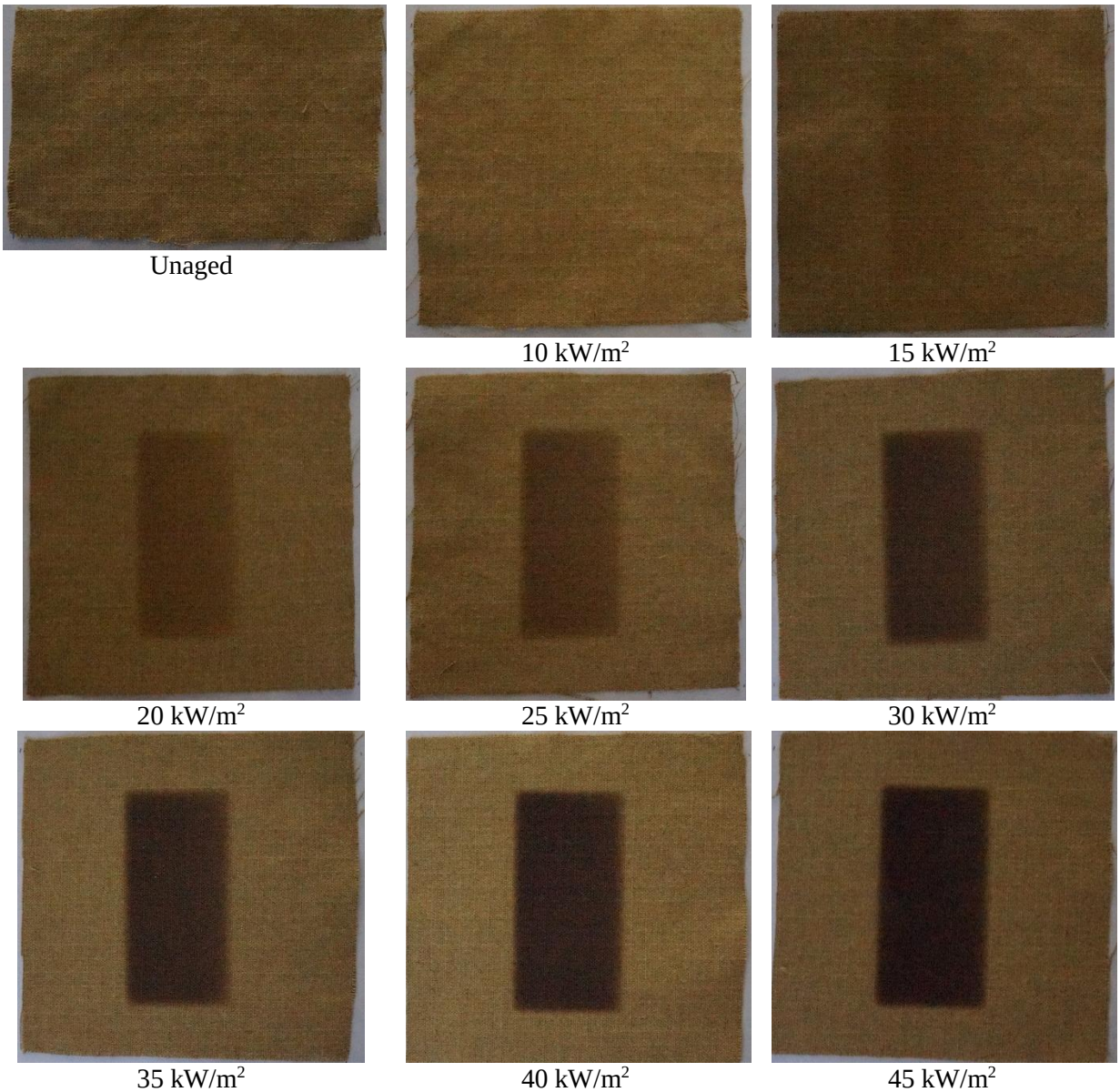


*Figure 3.10 Photographs of unaged and aged RS Natural specimens*

50 kW/m$^2$ 60 kW/m$^2$ 70 kW/m$^2$

40 SFH 80 SFH 160 SFH

*Figure 3.10 Continued*

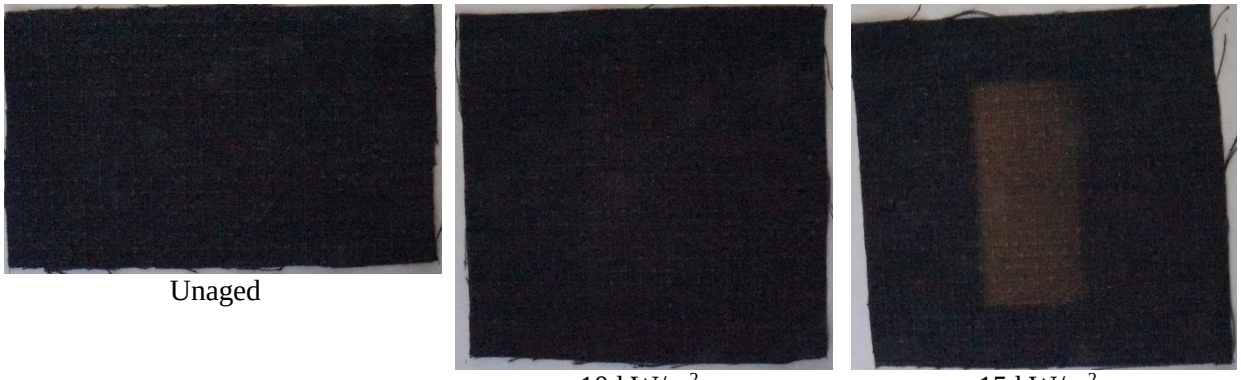

Unaged



10 kW/m$^2$ 15 kW/m$^2$

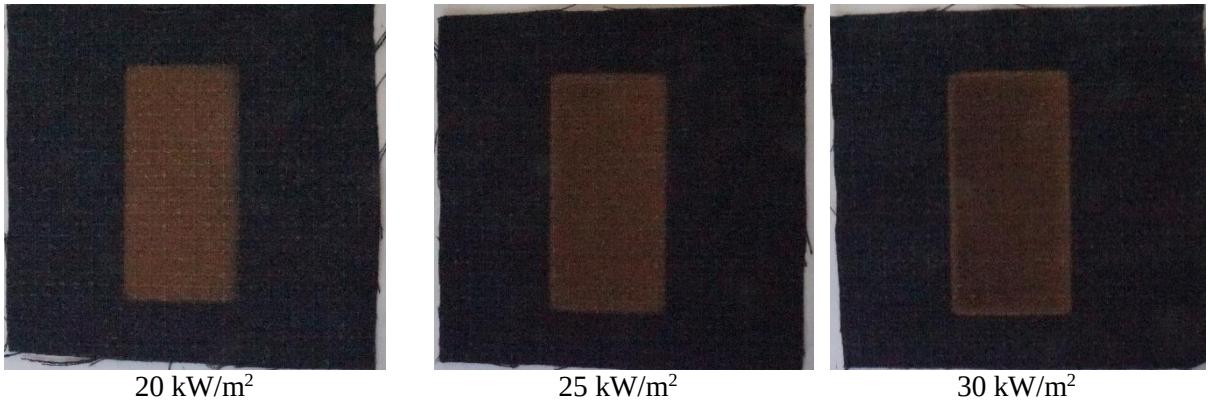

20 kW/m$^2$ 25 kW/m$^2$ 30 kW/m$^2$

*Figure 3.11 Photographs of unaged and aged RS Black specimens*

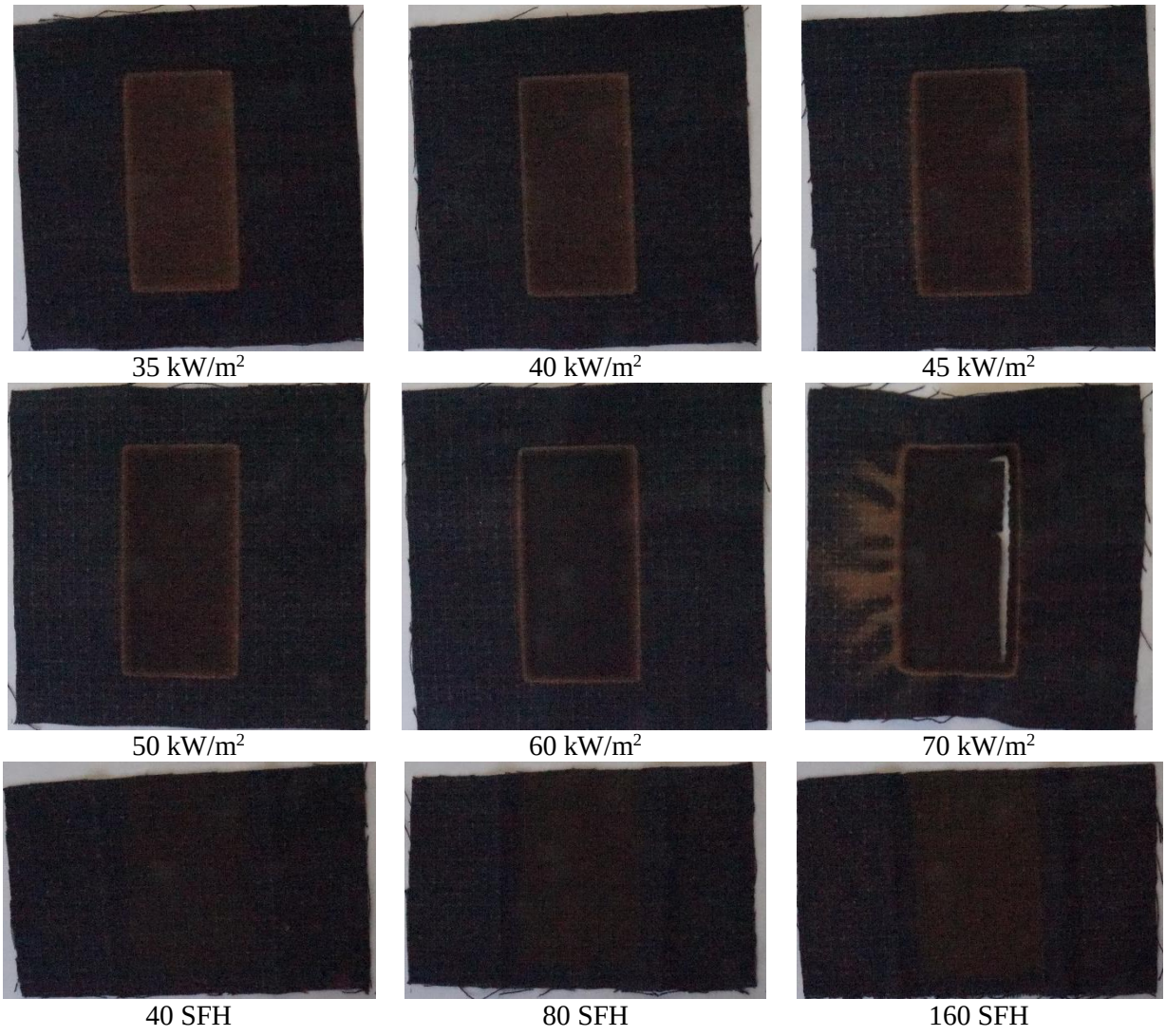


*Figure 3.11 Continued*


*Figure 3.12 Photographs of unaged and aged SCI PBI Max specimens*

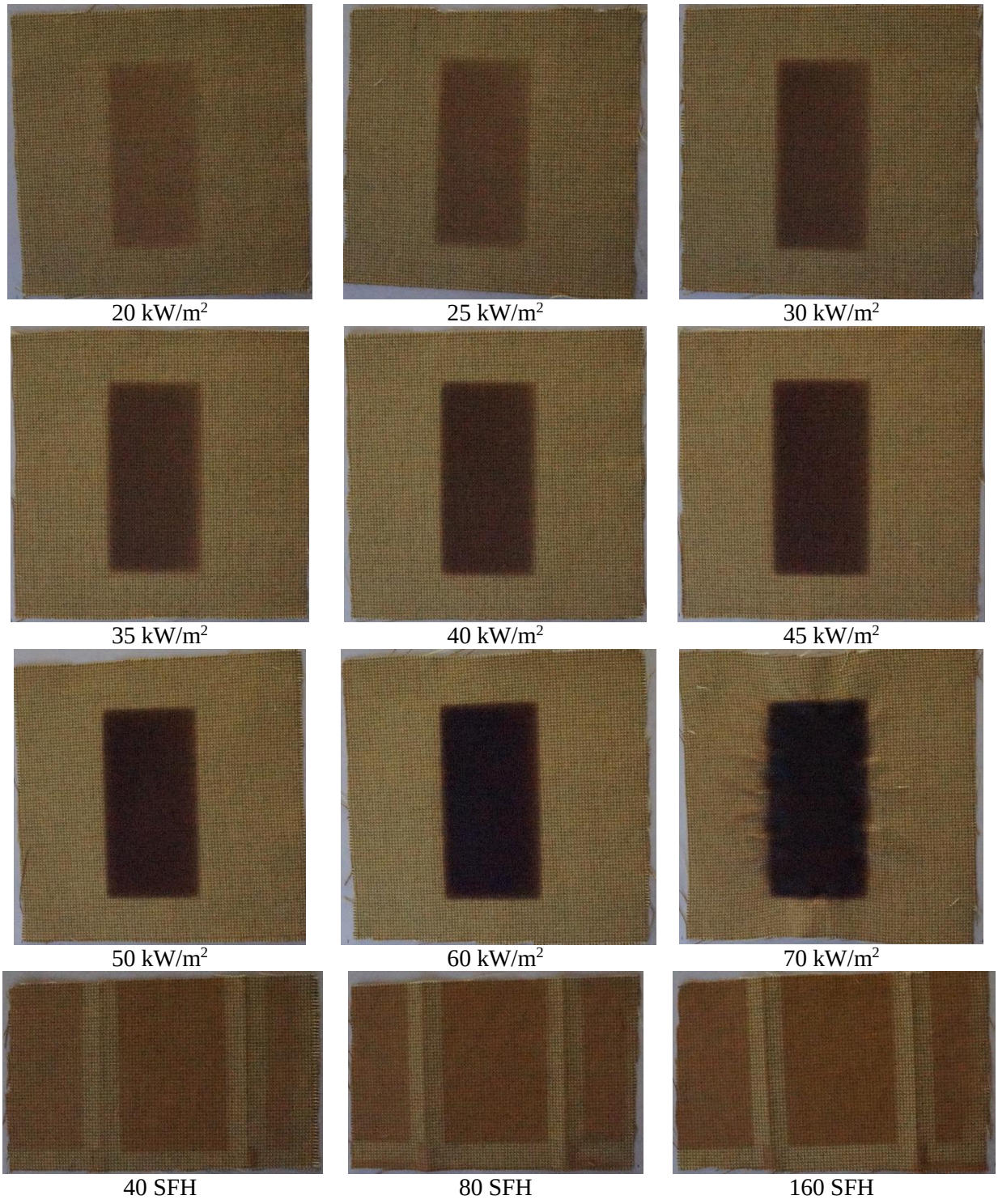


*Figure 3.12 Continued*

## 3.5. Tensile Testing

It was discussed in Section 1.7 that tensile strength is a key aspect of performance for firefighters' clothing. This section contains results of destructive tensile testing. Tensile testing was conducted on the Instron 5565 tensile testing device based on the ASTM D5035 (2015) standard with a modified 60 mm/min extension rate previously mentioned in Section 2.7. Load, extension, and time measurements were recorded up to three decimal places. For very high heat flux exposed specimens (e.g. 70 $kW/m^2$) a lack of tensile testing data indicated the specimen broke during either transport or preparation.

The 35 x 150 mm test strips were further pared down to 25 x 150 mm sizes in order to compare tensile strength results between the different fabric types (Figure 2.2). This final paring or ravelling down procedure involved counting individual fibers through the use of the Seiwa Optical microscope and ensuring the same fiber density between all trials. Since the different fabrics have different construction techniques that would lead to variability in tensile results great care was taken in this procedure. For the 25 mm allowable width the RS Natural fabric had 42 yarns (5 Ripstop ribs), the RS Black had 52 yarns (6 Ripstop ribs), and the SCI PBI Max had 47 yarns in the final pared down trial sizes cut from each specimen. All trials were mounted with the unexposed side of the fabric facing towards the user and tested in the warp-wise direction of the fabrics. Taking an average of five specimen trials for each measurement produced the tensile testing results in Figure 3.13 which also shows the NFPA 1971 (2013) strength requirement of 623 N. An investigation and detailed comments on the repeatability of each individual specimen tensile testing trial can be found in Appendix B. Numerical values for average tensile strength and standard deviations are in Table 3.4.

The original unaged breaking strengths appear around 900 N for both RS Black and SCI PBI Max fabrics and around 1070 N for the RS Natural fabric (Figure 3.13). However, SCI PBI Max may have a higher unaged tensile strength than indicated by this study. Use of pneumatic grips only allowed for 75 psi applied pressure and filament fibers in the structure remain undamaged. At failure, the non-filament fibers were pulled apart at the grip location, and therefore the results for SCI PBI Max may not represent the actual unaged strength of the fabric. Non-pared down

(i.e. full 35 mm strip width (Figure 2.2) instead of 25 mm) unaged trials of the SCI PBI Max achieved a tensile strength around 1200 N; this non-pared down strength value was much higher due to the strength differential between the two different fiber types in this PBI construction. Use of a manually adjusted clamping method may allow for higher applied pressure and a more accurate unaged tensile strength for this composite fiber construction in future studies.

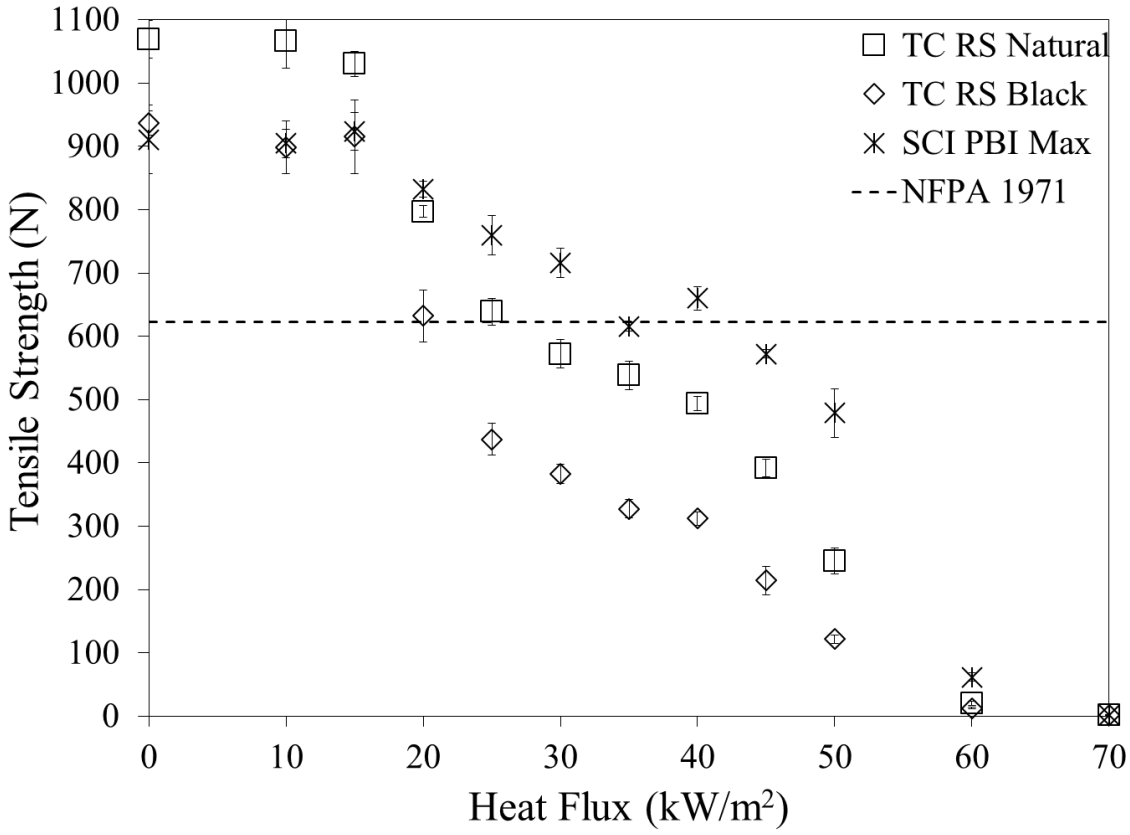


*Figure 3.13 Average tensile strength results following thermal ageing procedures performed in the cone calorimeter at indicated heat flux levels for 60 s*

No significant change (< 5% reduction) occurs during the first two levels (10 and 15 kW/m$^2$) of thermal exposure. However, at the 20 kW/m$^2$ trial all three fabrics see a significant reduction in mechanical strength (26% loss for Natural, 32% for Black, and 8% for PBI). A heat flux of 20 kW/m$^2$, which resulted in fabric temperatures reaching approximately 300°C, also corresponds to a slight increase in the derivative mass loss in the TGA results for all fabrics considered (Figure 3.1 – 3.3). This seems to indicate a material decomposition change occurring around this transition temperature that is within the upper limits of ordinary working conditions

for a firefighter (Thorpe 2004). Field fire testing conducted in Prince Albert, Saskatchewan also confirm these heat flux ranges to be within the working range of a firefighter (e.g. sustained 22 kW/m$^2$ thermal radiation levels in Section 1.4). The percent of original tensile strength remaining after thermal ageing can be found in Figure 3.14.

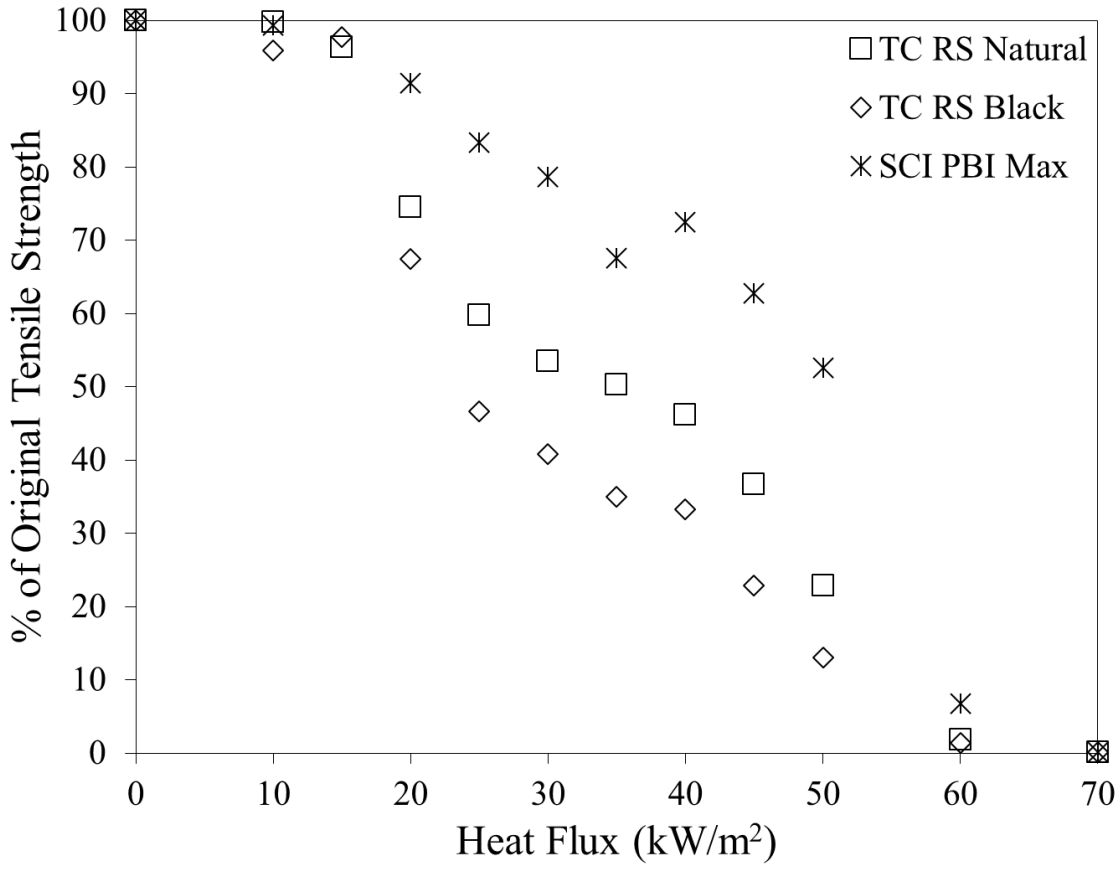


*Figure 3.14 Percent of original tensile strength in relation to thermal ageing heat flux levels*

Tensile strength continues to decrease between the 20 – 30 kW/m$^2$ heat flux exposures. At 25 kW/m$^2$ the tensile strength values of all three fabrics see significant reduction in strength (41% loss for RS Natural, 54% loss for RS Black, and 27% loss for SCI PBI Max from original tensile strength) followed by another decrease at 30 kW/m$^2$ (47% loss for RS Natural, 60% loss for RS Black, and 32% loss for SCI PBI Max from original tensile strength). By 35 kW/m$^2$ the Ripstop constructed fabrics have fallen below the NFPA 1971 (2013) strength requirement of 623 N (Figure 3.13). The SCI PBI Max fabric also falls below this value, but then appears to increase in strength when subjected to a higher heat flux of 40 kW/m$^2$. This increase in tensile strength is most likely due to a "tightening" of the fabric structure around the filament yarns in

this particular weave pattern. At the highest heat flux exposures considered (> 60 kW/m$^2$) all three fabrics become very fragile and approach a tensile strength of 0 N.

It can be seen that SCI PBI Max retains a much higher percentage of original tensile strength when compared to the Ripstop constructions across most thermal ageing conditions. For example, after exposure to a 40 kW/m$^2$ heat flux the SCI PBI Max retains 72% of its unaged tensile strength while the Ripstop constructions only retain 46% (RS Natural) and 33% (RS Black) of their unaged strength. This increased durability could be due to the high PBI content of the filament yarn or from the unique weave pattern (Section 2.1).

The percent of original tensile strength proceeds non-linearly with increased thermal ageing. These trends can be roughly summarized as:

- 10 – 15 kW/m$^2$: minor losses in tensile strength across all fabric types;
- 20 – 30 kW/m$^2$: significant losses in tensile strength,
- 35 kW/m$^2$: Ripstop fabrics fall below strength requirement for new fabrics;
- 45 kW/m$^2$: SCI PBI Max fabric falls below strength requirement for new fabrics;
- 60 kW/m$^2$: complete loss of strength (> 90% loss of strength for all fabric types).

The loss of tensile strength in response to increased UV ageing exposure conditions appears to be linear, but this is difficult to justify using only three experimental data points. Exposure to 40 SFH caused a significant initial decrease in strength values (percent of original tensile strength of 81% for RS Natural, 91% for RS Black, and 90.5% for SCI PBI Max) and these percentage decreases continue for both the 80 SFH and 160 SFH exposures. Over the UV ageing trials the SCI PBI Max retains the highest percentage of its original tensile strength (71% of original tensile strength) when compared to the loss of strength in RS Natural and Black constructions (51% and 60% of original tensile strength, respectively). These fabrics are known to experience significant loss of mechanical properties following UV irradiation (H. Zhang, et al. 2006; Zhu, et al. 2014) and these results (Figure 3.15 – 3.16) confirm this phenomenon. Examination of SEM and NIR results will be used to help explain this intense photodegradation trend in Chapter 4.

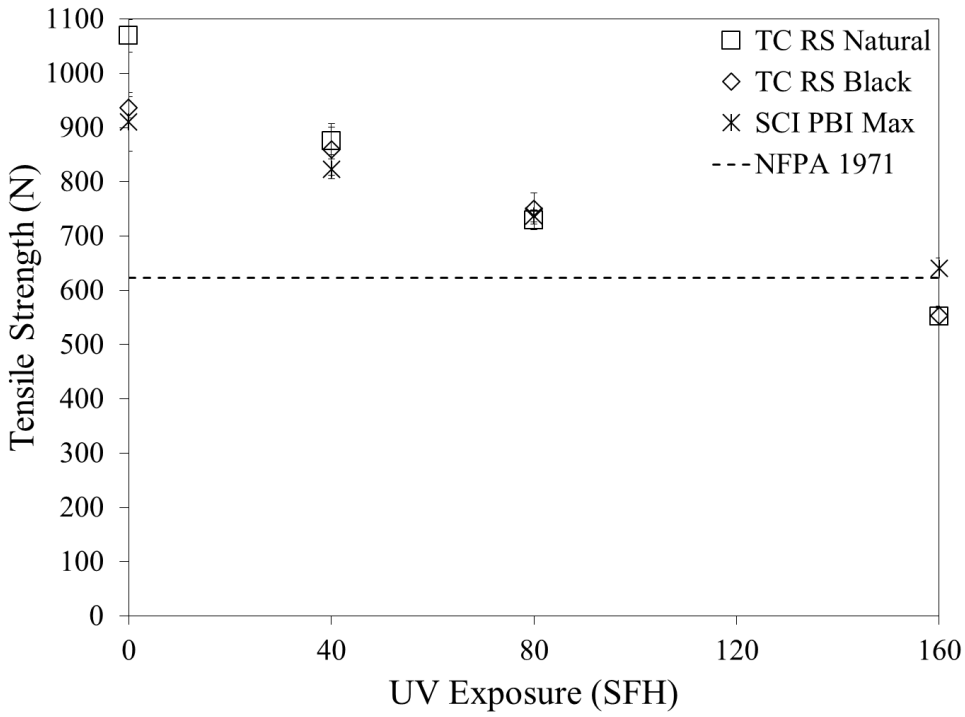


*Figure 3.15 Average tensile strength results following UV ageing procedures*

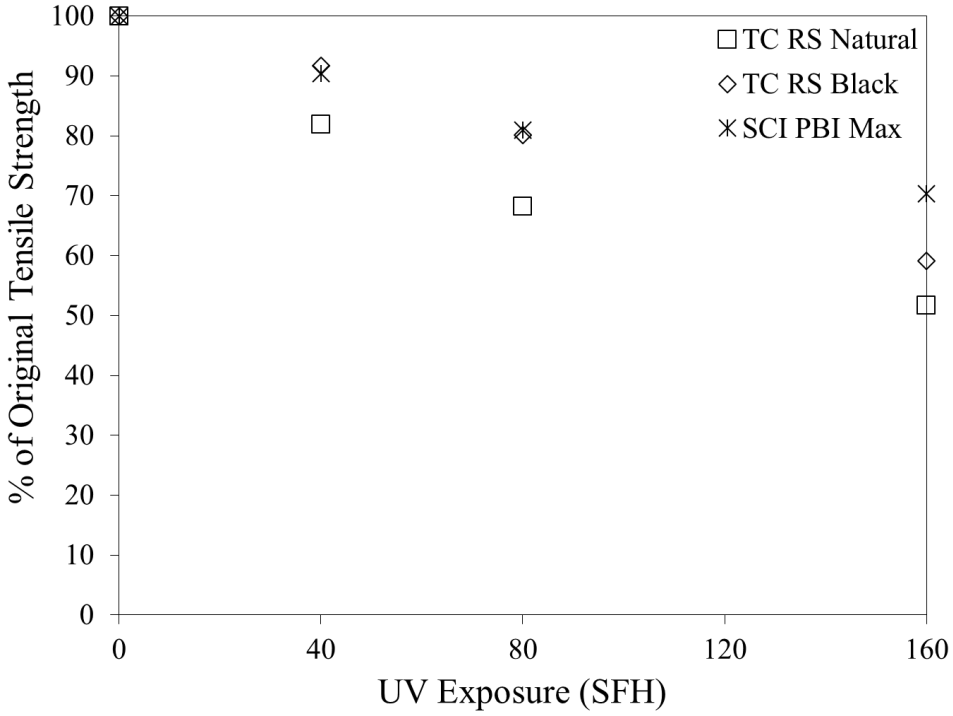


*Figure 3.16 Percent of original tensile strength in relation to UV exposure*

*Table 3.4 Averages and standard deviation of tensile strength for all fabrics*

| | Tensile Strength (N) | | | | | |
|---|---|---|---|---|---|---|
| Fabric Type | RS Natural | | RS Black | | SCI PBI Max | |
| Heat Flux ($kW/m^2$) | Ave | Std Dev | Ave | Std Dev | Ave | Std Dev |
| 0 | 1069.0 | 29.6 | 936.9 | 19.6 | 910.9 | 54.1 |
| 10 | 1066.2 | 42.8 | 898.3 | 41.2 | 904.6 | 22.5 |
| 15 | 1030.3 | 19.7 | 915.1 | 57.9 | 923.7 | 29.4 |
| 20 | 796.7 | 9.2 | 632.0 | 40.7 | 832.5 | 12.9 |
| 25 | 638.6 | 21.7 | 437.1 | 25.0 | 759.2 | 31.2 |
| 30 | 572.3 | 22.5 | 382.6 | 15.7 | 716.1 | 23.4 |
| 35 | 538.2 | 22.2 | 327.5 | 14.4 | 615.1 | 7.6 |
| 40 | 494.0 | 11.4 | 312.0 | 10.4 | 659.7 | 18.9 |
| 45 | 391.7 | 13.7 | 214.1 | 22.8 | 571.8 | 6.6 |
| 50 | 244.8 | 20.4 | 121.6 | 6.3 | 478.7 | 38.7 |
| 60 | 20.1 | 2.9 | 13.0 | 0.8 | 61.6 | 6.9 |
| 70 | 1.4 | 0.6 | 1.5 | 1.1 | 1.2 | 0.0 |
| UV Exposure (SFH) | | | | | | |
| 40 | 875.2 | 25.8 | 859.7 | 47.8 | 823.8 | 17.9 |
| 80 | 729.6 | 18.2 | 750.8 | 28.6 | 737.4 | 11.0 |
| 160 | 552.3 | 14.8 | 554.0 | 17.2 | 641.0 | 18.3 |

## 3.6. Scanning Electron Microscopy

Background on the JEOL JSM 6010 (Akishima, JA) SEM device was covered in Section 2.9. Branching, charring, and carbonization are evident in specimens subjected to increasing heat exposure conditions. The images in this section indicate that increased exposure conditions (e.g. higher heat flux, longer UV exposure) produced increased damage in the fiber structure. A full ageing history of the RS Natural specimens can be found below (Figure 6.4) from 350x low magnification (left), 1000x medium magnification (middle), and 3000x high magnification (right) while the RS Black and SCI PBI Max images are located in Figure 3.18 and 3.19. Many of the degradation and microstructure change indicators are similar between the fabrics examined in this SEM study.

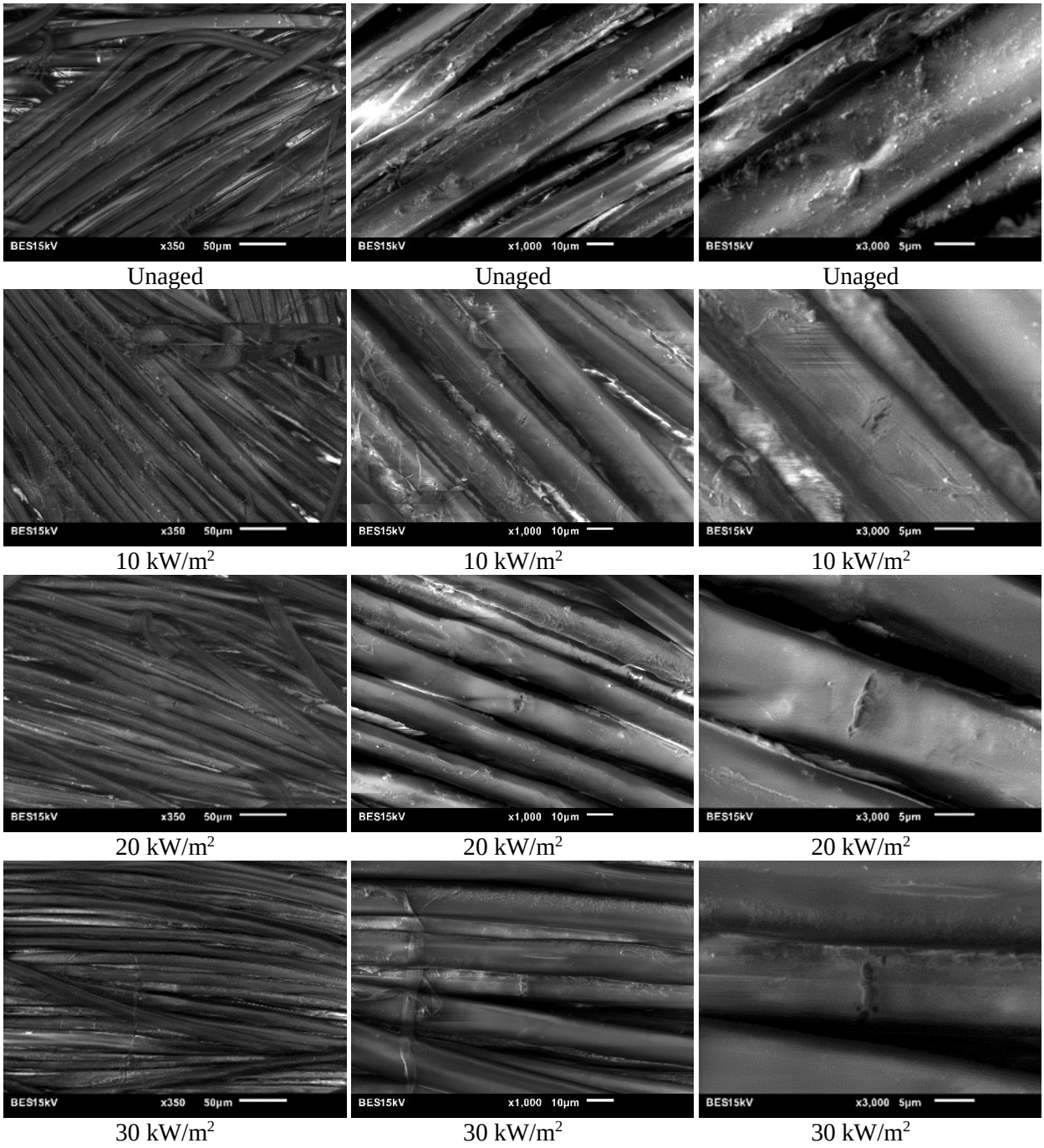


*Figure 3.17 RS Natural fibers under 350x (left), 1000x (middle), and 3000x (right) magnifications using BES at 15 kV under low-vacuum conditions for unaged to 70 kW/m$^2$ heat flux exposures*

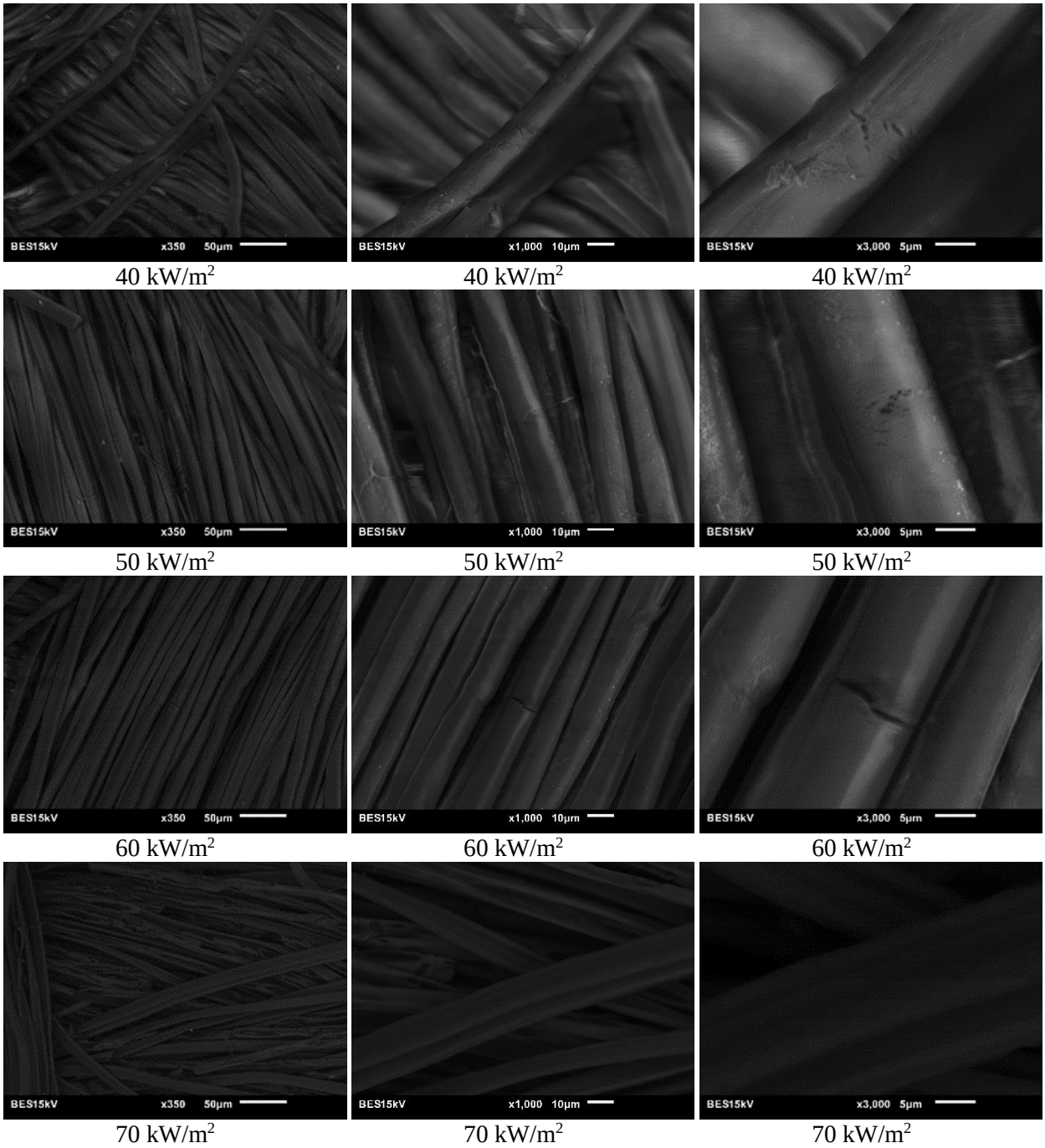


*Figure 3.17 Continued*

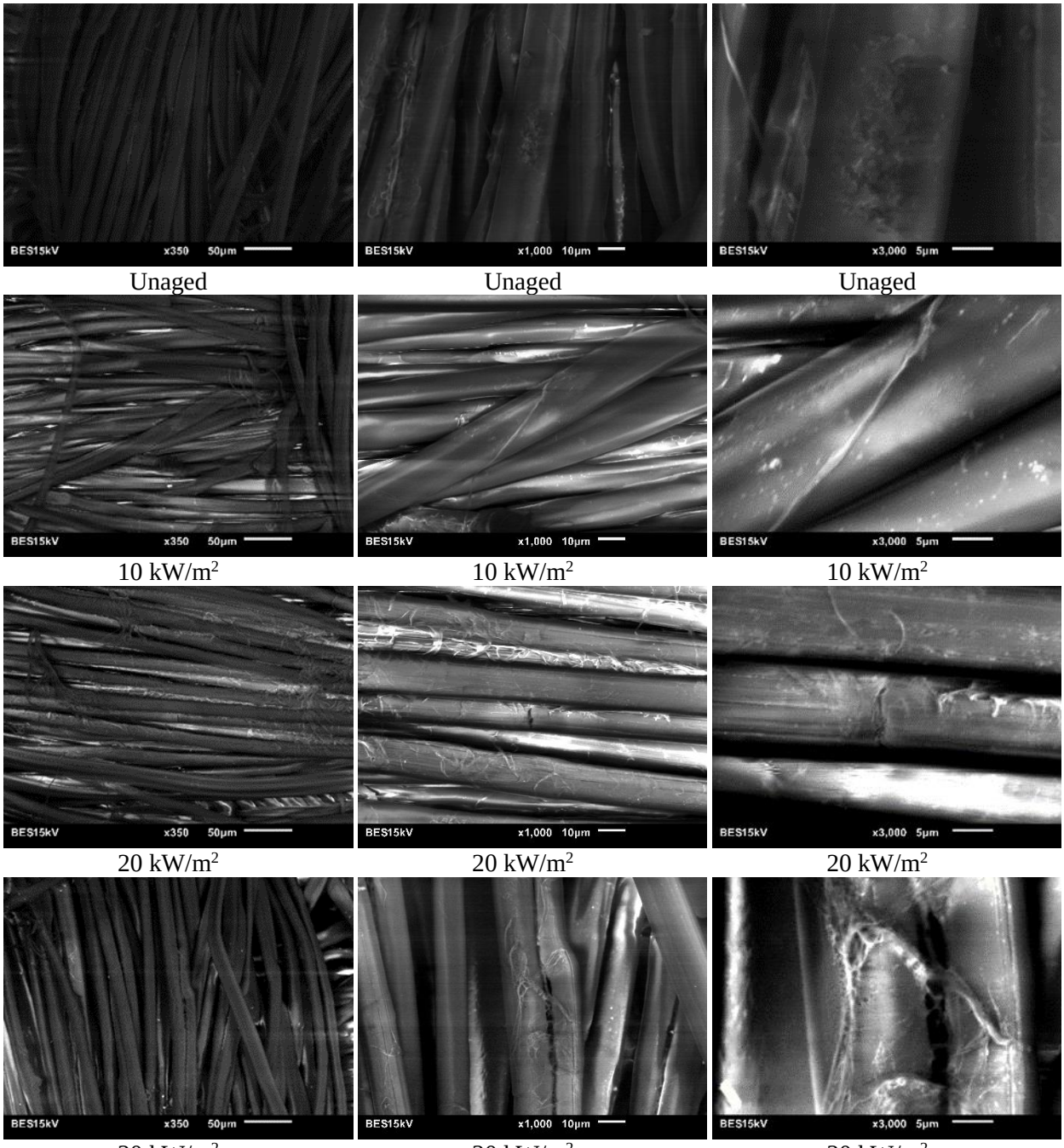


*Figure 3.18 RS Black fibers under 350x (left), 1000x (middle), and 3000x (right) magnifications using BES at 15 kV under low-vacuum conditions for unaged to 70 kW/m$^2$ heat flux exposures*

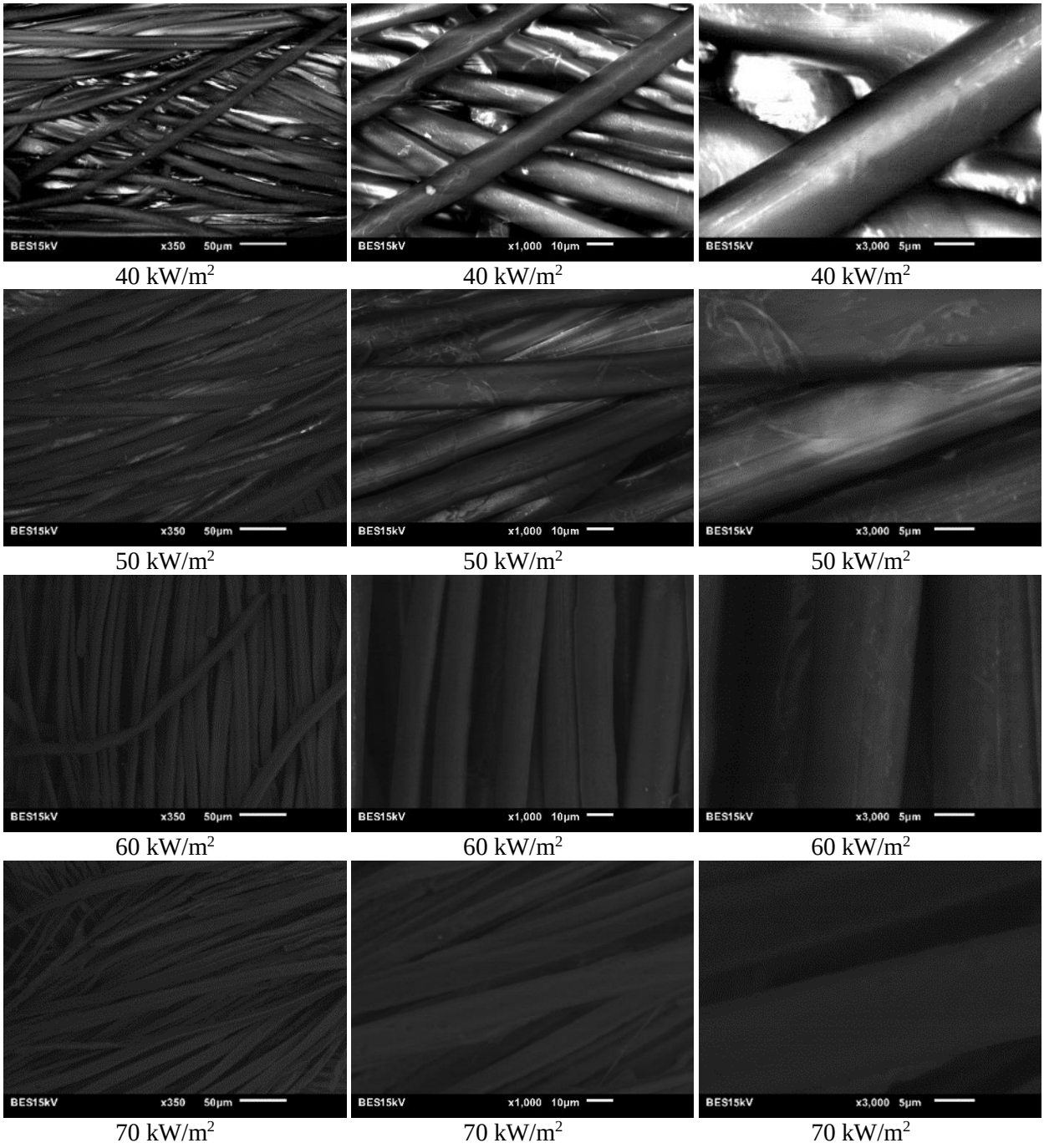


*Figure 3.18 Continued*

The following images (Figure 3.19) are similar to those shown previously, but for the SCI PBI Max fabric. The spun yarn was kept in focus for these images since the filament yarn held up very well under ageing exposures and did not contain notable surface feature changes. These

filament yarns also seemed to cause a “washing out” of the brightness/contrast when they were kept as the main focus using this particular SEM device.

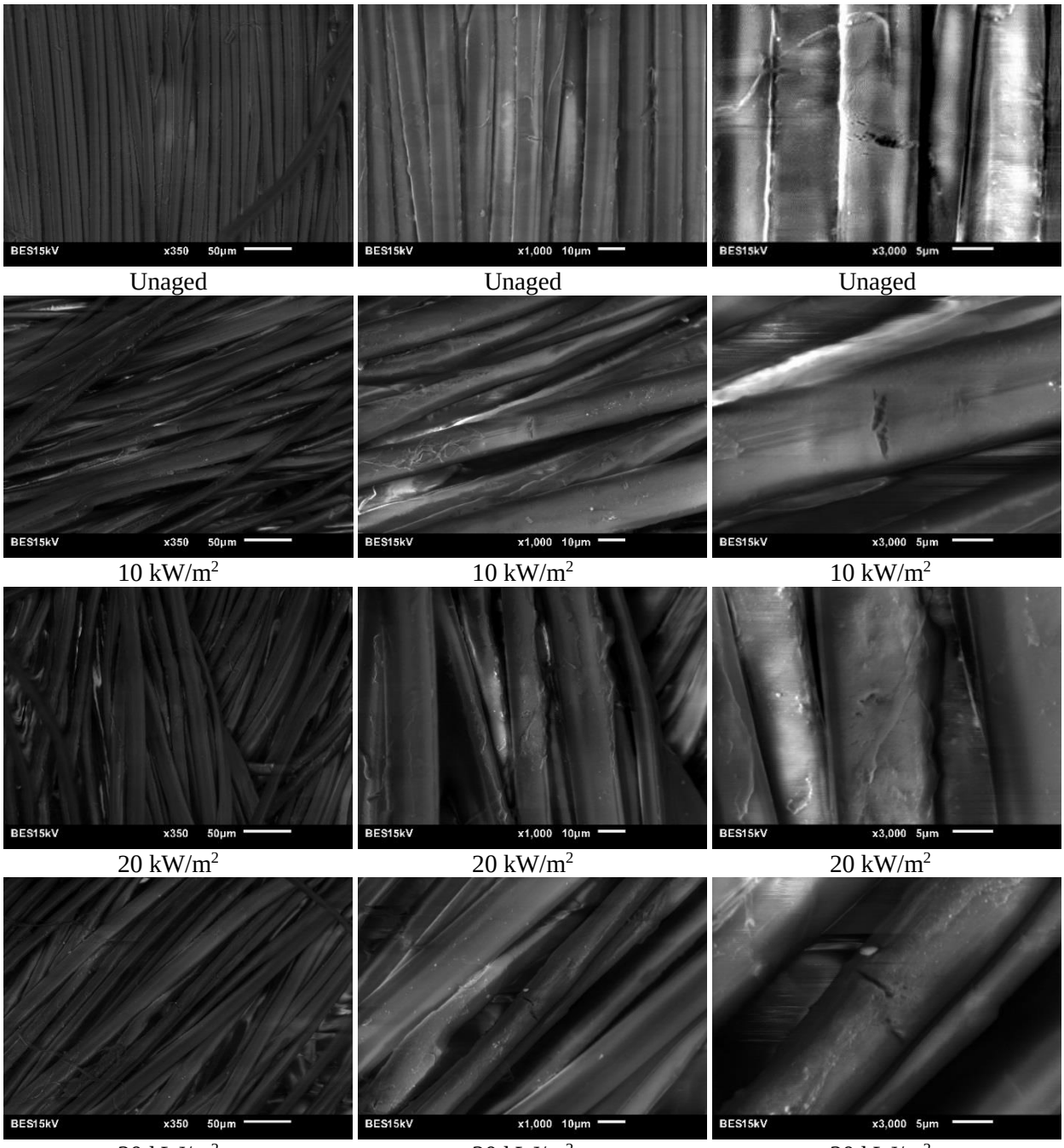


*Figure 3.19 SCI PBI Max fibers under 350x (left), 1000x (middle), and 3000x (right) magnifications using BES at 15 kV under low-vacuum conditions for unaged to 70 kW/m$^2$ heat flux exposures*

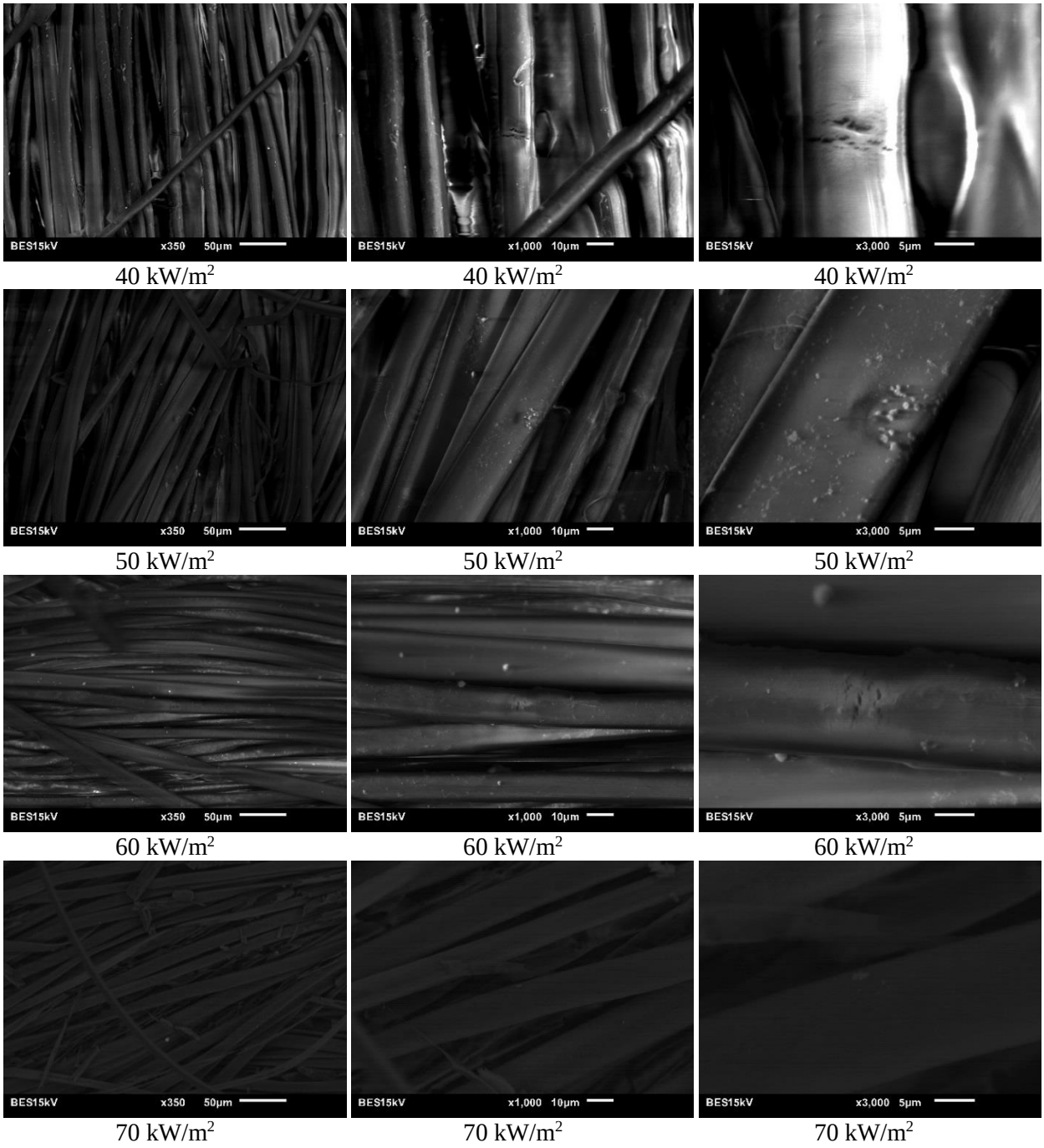


*Figure 3.19 Continued*

These images were used to investigate the influence of thermal (Figure 3.17 – 3.19) and UV ageing (Figure 3.22 – 3.24) on surface microstructure features at 350x, 1000x and 3000x magnifications. All specimens were focused at a magnification level of 6000x. However, some issues arise when using this increased magnification on textile structures. Initially the "as

received" materials from the factory conditions are supposed to be undamaged. In the production of these polyaramid fibers some microstructure damage may be unavoidable due to the chemical spinning, fabric rolling, and transportation/shipping (i.e. UV exposure through car window when traveling between laboratories, Section 1.5.1.) processes. This initial damage is evident from the appearance of holes in the original unaged specimen pictured in Figure 3.17 – 3.19. Additionally, the undulating over/under weave pattern of the fabrics causes the individual yarns to be parabolic in shape. This means that obtaining a focus-point on one fiber location will not translate into bringing the entire fiber structure into focus. Moreover, the varying heights and orientations of the individual adjacent fibers means these neighbouring structures may also remain out of focus when magnification levels are decreased. Both of these textile structure features lead to a large uncertainty in the actual surface feature conditions. For example Figure 3.20a shows a 3000x magnified view of a RS Natural fiber that has experienced 20 $kW/m^2$ ageing. It appears relatively undamaged. With increased focusing and image adjustments a U-shaped crack appears on the fiber surface (e.g. Figure 3.20b). This process of zooming in, focusing, and finding a seemingly "hidden" surface crack or even a large material hole could be repeated an infinite amount of times over the fabric surface. The continuing curvature and height variation across both the individual and grouped fibers makes determination and examination of the surface microstructure features a difficult task using this particular device and its limited manual point-focusing method. In order to improve the quality of future SEM images for fabric structures a software package capable of auto-focusing across discrete microstructure areas and compiling the focused images could be used. If this type of SEM software package is not currently available it should be constructed for future use. Additionally, future studies should consider the use of synchrotron-based studies, atomic-force microscopy, and laser scanning confocal microscopy (Davis, et al. 2010) to obtain more information on these surface features.

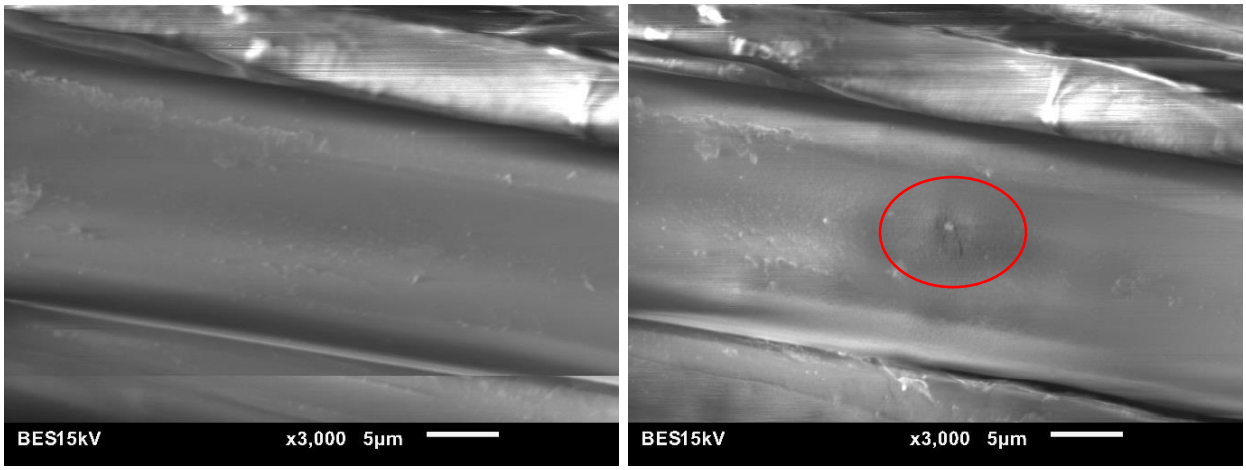


*Figure 3.20 Textile fiber-focusing uncertainty with (left) unfocused and (right) focused locations containing a surface crack of a 20 kW/m$^2$ aged RS Natural fiber*

The impact of thermal ageing is evident when comparing even the lowest applied heat flux level specimen to the unaged specimen (e.g. Figure 3.17 – 3.19, Unaged compared to 10 kW/m$^2$). At just 10 kW/m$^2$ applied heat flux for 60 s the microstructure begins to show branching and foreign material deposits on the surface of the fibers. However, tensile strength results do not indicate significant damage at heat flux levels below 15 kW/m$^2$. This may indicate that initial low-level heat flux exposures only cause surface microstructure damage and leave the body of the fiber relatively intact. The surface features following the 20 kW/m$^2$ exposure show increased crack development into the depth of the fiber (Figure 3.17 – 3.19, 20 kW/m$^2$) when compared to the 10 kW/m$^2$ exposure (Figure 3.17 – 3.19, 10kW/m$^2$) at the 3000x magnification. Therefore, heat flux exposures below 20 kW/m$^2$ could be said to exhibit surface cracking while exposures after this level experience partial-thickness cracking. At the 30 kW/m$^2$ exposure this cracking continues to increase in severity and surface striations appear around this point (Figure 3.17 – 3.19, 30kW/m$^2$). The combined impact of crack depth propagation into the individual fibers and overall higher percentage of microstructure damage could contribute to the significant loss of mechanical properties following 20 – 30kW/m$^2$ exposure levels. This result also compares well to the initial spike in TGA results for 300 – 400°C temperature ranges (Figures 3.1 – 3.4).

At the 40 and 50 kW/m$^2$ trials the microstructure continues to develop partial-thickness cracks (Figure 3.17, 40 – 50 kW/m$^2$) in addition to the build-up of charred and other deposited

material on the fiber surface. Throughout the thermal ageing trials the brittleness of the microstructure appears to increase with increased ageing temperatures. This is made evident by the increasing brittle nature of the microstructure and the increased frequency of crack and fracture development across the low and medium magnification images (350x and 1000x). When the 60 kW/m$^2$ exposed fabric is examined evidence of full-thickness cracking (Figure 3.17 – 3.19, 60kW/m$^2$) appears along with the loss of surface features. This surface feature loss (viewed at low magnifications in Figure 3.17, 60 – 70 kW/m$^2$) could be the result of burning and pyrolysis of the fabric structure. The fibers at the highest flux exposures also appear noticeably thinner at high magnifications (Figure 3.17, 60 – 70 kW/m$^2$) indicating a significant loss of the original fiber diameter. At the 70 kW/m$^2$ trial most of the structure has been reduced to ash. These thin, extremely damaged fibers also appear very brittle and have a jagged, broken appearance (Figure 3.17, 70kW/m$^2$). Additionally, open flaming on the exposure-side of the fabric was observed during thermal ageing procedures and this seemed to result in a further loss of defined surface characteristics when compared to the 60 kW/m$^2$ microstructure.

These thermal microstructure degradation trends are evident in the other two fabric types (Figure 3.18 – 3.19). The filament fibers in the SCI PBI Max appear to sustain less damage with increased thermal ageing. The Black Ripstop fibers seem to develop a higher amount of foreign material deposition in the form of microstructure material-strands that are not evident in the other two fabrics. This increased amount of foreign material could be resultant from the presence of material dye in the RS Black fabric.

The thermal ageing process appears to cause significant material change within these high performance fibers. One major component contributing to the significant loss of mechanical strength is the development of microfiber cracks within the fiber structure. This process appears to start with surface crack initiation (Figure 3.17 – 3.19, 10 – 15kW/m$^2$), and at higher heat fluxes is followed by surface crack development (Figure 3.17 – 3.19, 20 – 30 kW/m$^2$), increased severity of partial-thickness cracks with additional build-up of char and other deposits on the microstructure surface (Figure 3.17 – 3.19, 40 – 50 kW/m$^2$), and ends with full thickness cracks that may cause separation of individual fiber strands, along with a significant loss of fiber diameter material (Figure 3.17 – 3.19, 60 – 70 kW/m$^2$). The process of microstructure crack-

development, propagation, and loss of material could also explain why some studies note decreased TPP results of thermally aged fabrics once they experience irreversible chemical changes and charring resultant from pyrolysis (Udayraj, et al. 2016). Increasing the size and depth of these microstructure cracks would increase the porosity of the overall fabric as well as increase the amount of radiative heat transfer through the microstructure. These factors could combine to decrease the thermal protective performance of a severely thermally aged fabric.

These stages of crack growth can be visualized in Figure 3.21. This microstructure degradation process is proposed based on the SEM images obtained in this study and could be confirmed in future studies through the use of atomic force microscopy (AFM), laser scanning confocal microscopy (LSCM), or some similar measurement technique that is capable of defining the depth of these microstructure defects on individual fibers.

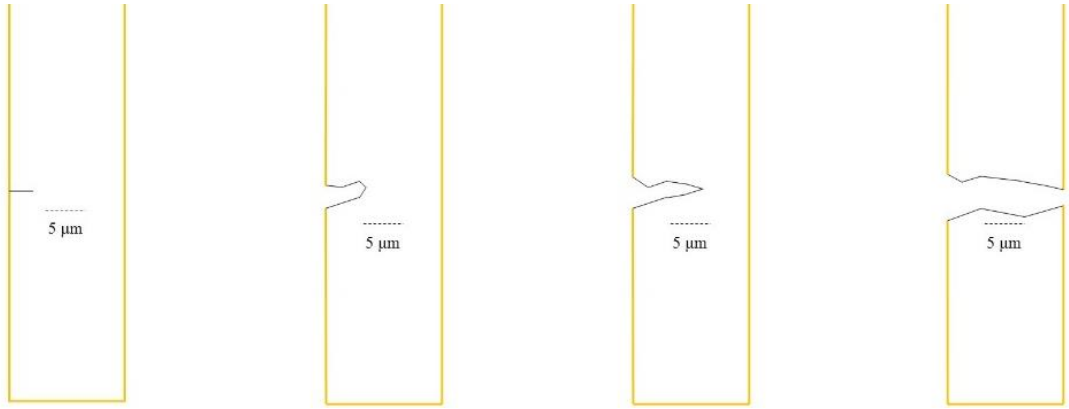


*Figure 3.21 Visualization of the development of microstructure cracks from (a) crack initiation, (b,c) partial thickness crack propagation, and (d) full thickness cracks resultant from increasing thermal ageing exposure conditions*

The microstructure degradation trends for the UV ageing trials (Figure 3.22 – 3.24) differ slightly from the thermally ageing, but remain consistent across the three fabric types considered. The UV ageing microstructure damage process also appears to degrade steadily in relation to increased exposure time when compared to the thermally aged images. The lowest 40 SFH UV ageing causes a loss of material that is made evident from the significant development of holes and elongated striations in the fabric microstructure (Figure 3.22 – 3.24, 40 SFH). This damage increases in both appearance and severity as the duration of UV light exposure is increased.

Additional pitting and foreign material evolution also occur with an increase in UV light exposure to 80 SFH (Figure 3.22 – 3.24, 80 SFH). The charring and burning phenomena observed in the thermally aged specimens is not present following UV exposure (e.g. high UV exposures still have defined microstructure features), but a significant transition to a brittle structure appears to occur. This is evident from the increased fracture sites observed in the SEM images and the increased brittleness of the surface structure and material deposits. Following the 160 SFH UV exposure level the material deposits and surface cracks are severe (Figure 3.22 – 3.24, 160 SFH). Additionally, obtaining a reliable focus at high magnifications (e.g. 6000x) became difficult at the highest UV ageing exposure of 160 SFH for all fabric types. High magnifications of these fibers appeared to cause a "washing out" of the colour contrast and an extreme brightening effect of the image; this phenomena was present even when focusing was attempted by another operator possessing a more significant background in SEM procedures. This change was most evident in the RS Natural fabric type (Figure 3.22), but was also present in both RS Black and SCI PBI Max fabrics (Figure 3.23 – 3.24). It could be possible the material deposits on the fabric surface following UV ageing have some impact on the electron measurement settings in this particular study because this phenomena has not been mentioned in previous UV ageing studies. Future analysis of the material formed on the microstructure following UV ageing (e.g. ATR-FTIR analysis of components) could be used to confirm previous photo-oxidative reaction processes for Kevlar®/PBI suggested by researchers (Arrieta, et al. 2011b).

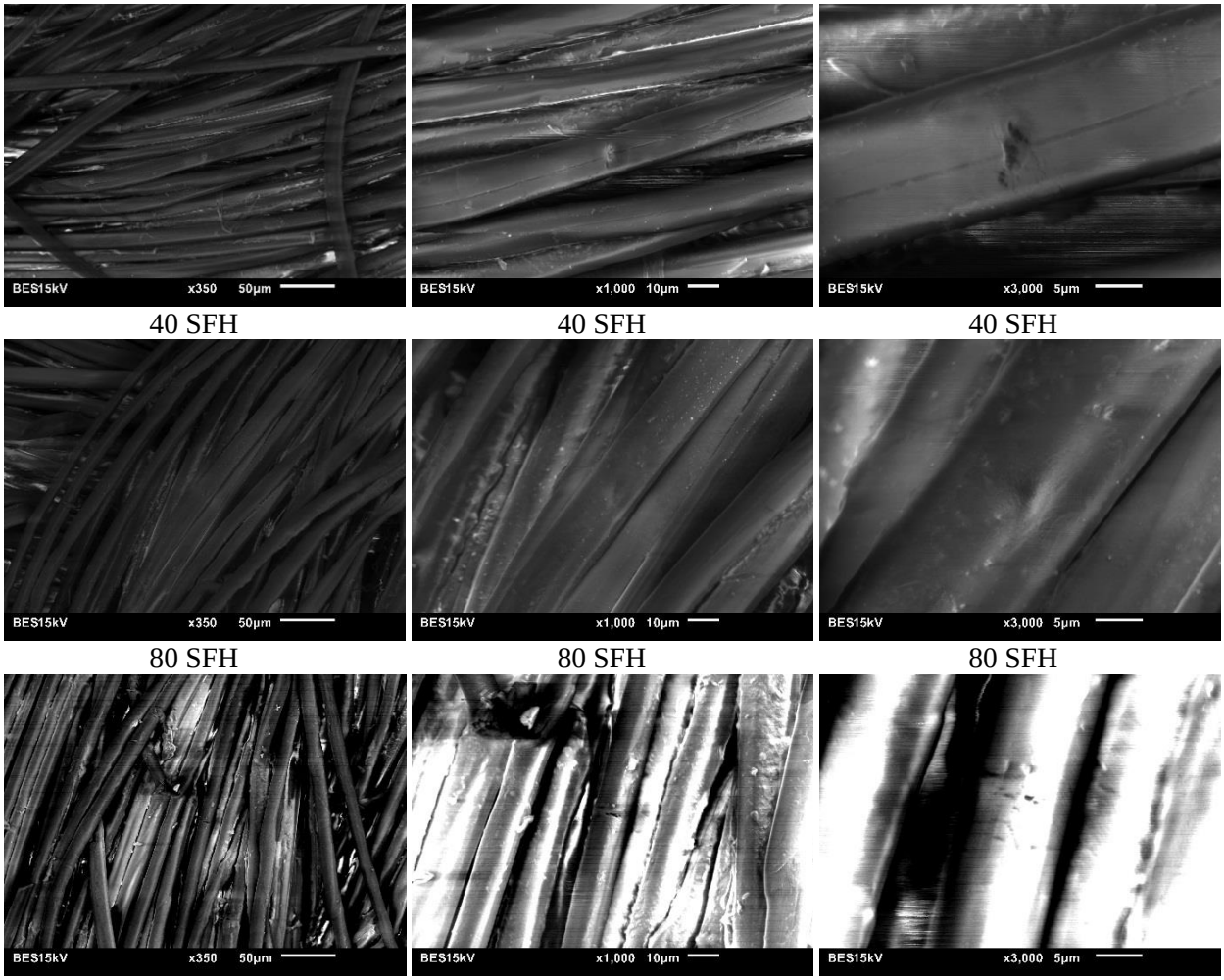


*Figure 3.22 Surface imaging investigation of RS Natural fibers under 350x (left), 1000x (middle), and 3000x (right) magnifications using BES at 15 kV under low-vacuum conditions for 40 – 160 SFH UV exposures*

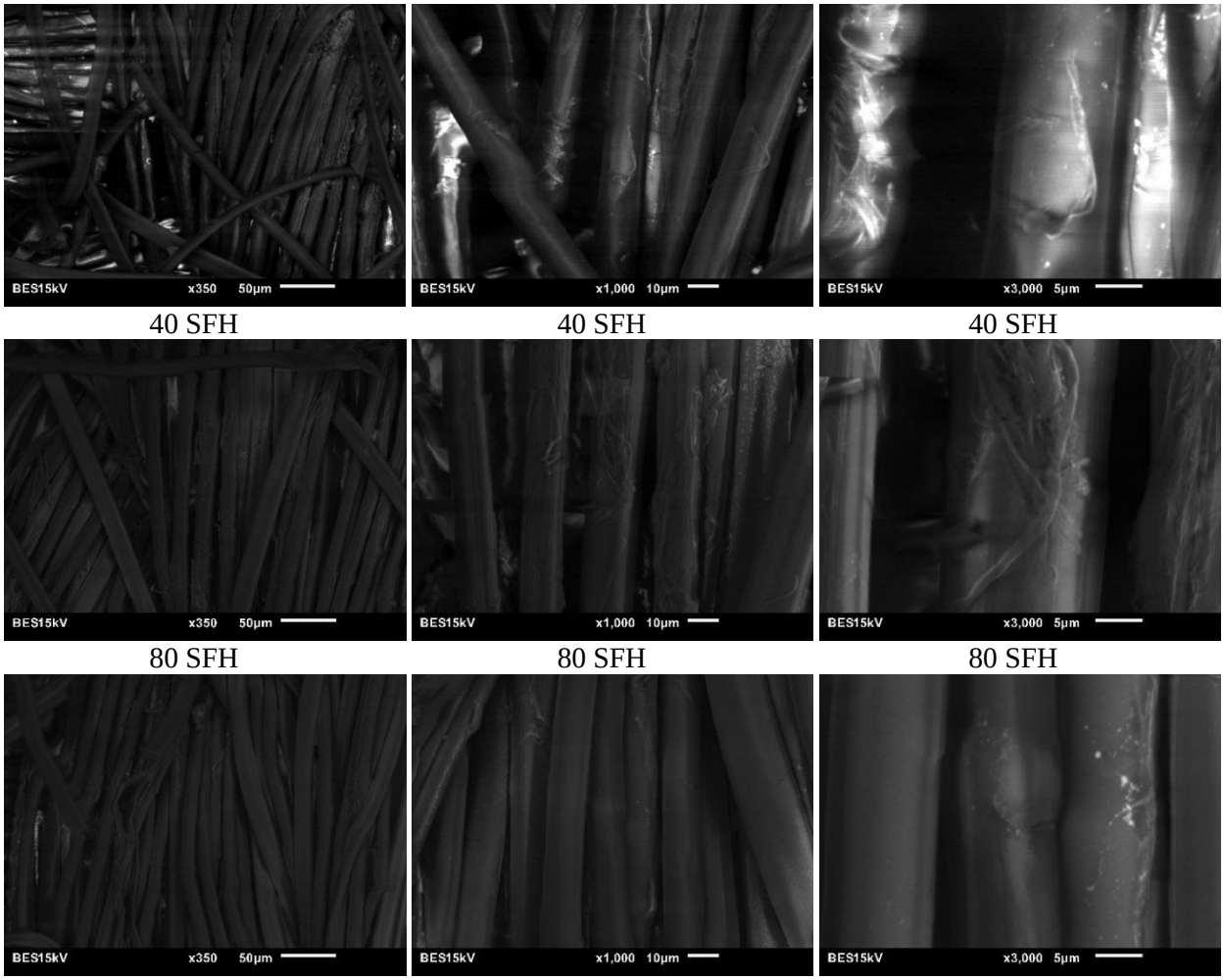


*Figure 3.23 Surface imaging investigation of RS Black fibers under 350x (left), 1000x (middle), and 3000x (right) magnifications using BES at 15 kV under low-vacuum conditions for 40 – 160 SFH UV exposures*

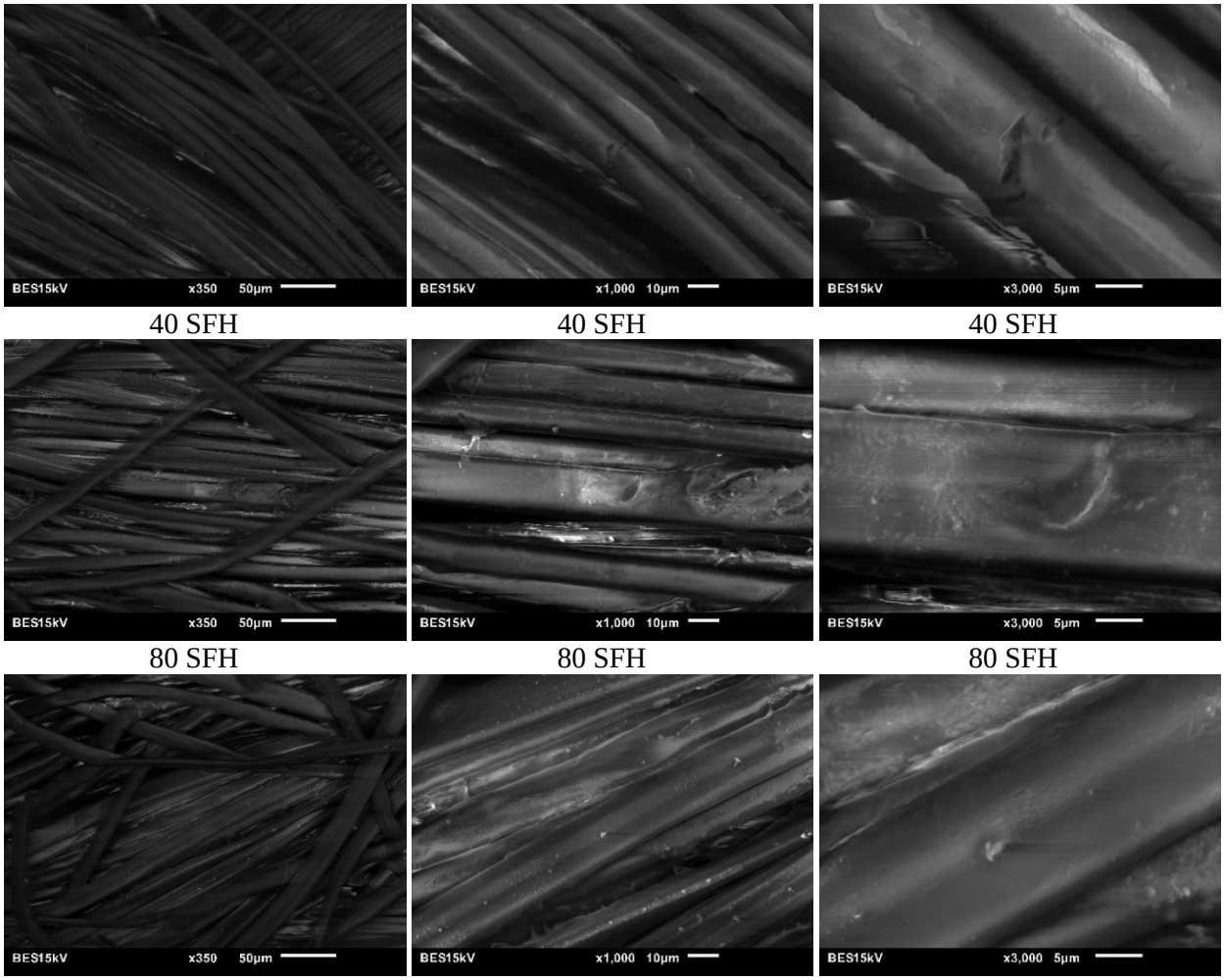


*Figure 3.24 Surface imaging investigation of SCI PBI Max fibers under 350x (left), 1000x (middle), and 3000x (right) magnifications using BES at 15 kV under low-vacuum conditions for 40 – 160 SFH UV exposures*

The following points in Table 3.5 summarize the important information obtained from this section of the SEM investigation.

*Table 3.5 SEM investigation summary*

| Exposure/Event | Comment |
|---|---|
| Unaged | Initial "as received" unaged fabrics shown to have minor surface imperfections |
| SEM acquisition | Parabolic shape and weave pattern of textiles makes SEM focusing difficult, other methods of determining surface characteristics should be used in future studies |

*Table 3.5 Continued*

| Exposure/Event | Comment |
|---|---|
| Microstructure cracking | The following microstructure crack development process was proposed: initial surface crack development; partial-thickness crack development and surface striations; partial-thickness crack propagation; and full-thickness cracking that separates individual fibers entirely |
| 10 kW/m$^2$ | Branching and material deposits evident on fabric microstructures without significant loss of tensile strength at these levels |
| < 15 kW/m$^2$ | May cause microstructure surface damage, but leave body of fiber relatively intact. This is made evident from a lack of significant decrease in tensile strength combined with the evidence of damage found in SEM imaging |
| > 20 kW/m$^2$ | Increased crack development into the fiber structure possibly indicating partial-thickness cracking when compared to previous surface cracking at lower heat flux exposures |
| 30 kW/m$^2$ | Continued crack development and introduced development of micro-surface striations. Significant loss of tensile strength at this point (e.g. 20 – 30 kW/m$^2$) is possibly explained by combined impact of deeper microstructure cracks in individual fibers and higher percentage of microstructure damage |
| 40 – 50 kW/m$^2$ | Exposures increase severity of partial-thickness cracks and additional build-up of charred and other material deposits on microstructure surface |
| 60 – 70 kW/m$^2$ | Exposures show evidence of full-thickness cracks and significant loss of individual fiber material (e.g. loss of individual fiber diameters) |
| Crack development | Progressive development of microstructure cracks and holes could be the cause of decreased TPP ratings following thermal ageing (e.g. increased porosity and lost material in fabric structures causes increased radiative heat transfer) noted in previous studies (Cui, Ma and Lv 2015) |
| NIR reflectance shifting (Chapter 4) | Overall shifting behaviour of NIR reflectance results (to be discussed in Section 4.2) would be explained by increased absorbance due to the crack and hole development in the individual fibers |
| Brittleness | Increased thermal ageing caused increasing brittle nature of individual textile fibers that was made evident from proposed crack/fracture development process |
| SCI PBI Max Fabric | Fabrics appear to retain microstructure features and resist microstructure cracking/damage under increasing ageing conditions |

*Table 3.5 Continued*

| Exposure/Event | Comment |
|---|---|
| RS Black Fabric | Fabrics develop a higher amount of foreign material deposits with increased ageing that could be explained by the additional material dyes |
| UV exposure | UV ageing exposure causes “washing out” of SEM colour contrast and brightening that is difficult to manage at the highest exposure (160 SFH) |
| UV exposure | Causes increased pitting and hole development in fabric microstructures |
| UV exposure | Fabrics still appear to become more brittle with increased exposure durations |

# 4. Near Infrared Evaluation

This chapter covers near-infrared results (both diffuse reflectance and absorbance) that were related to degradation trends of the aged fabrics (Sections 4.1 – 4.2). Results from unaged, heat flux exposure at 10 – 70 kW/m$^2$, and UV exposure at 40, 80, and 160 SFH specimens are examined.

## 4.1. Near Infrared Evaluation – Reflectance and Absorbance

In the near infrared (NIR) evaluation the damaged side of specimens was subjected to a near-infrared light source. In reflectance spectroscopy if the frequency of the incident light is equal to the vibrational modes of the chemical bonds of the mounted sample the light will be absorbed in varying intensity (Clark and Roush 1984). For rough surfaces (e.g. textiles) diffuse reflectance NIR spectroscopy is often utilized (Frank 1997). Therefore, diffuse reflectance is utilized in this current study. Any reference to reflectance is to be taken as diffuse reflectance. The reflectance value gives the ratio of the intensity of the reflected light from the specimen to the intensity of the light reflected from a reference material. Similarly, the absorbance value can be derived from reflectance values to give the ratio of the intensity of the absorbed light. This reflected spectrum can be acquired through the variation of the incident wavelength of the beam. More detailed background information can be found in previous research (Rezazadeh 2014). Background on the Cary-UV-Vis spectrophotometer is contained in Section 2.8.

These diffuse reflectance results correlate with the proposed microstructure crack development process taking place in the aged fibers. The overall shifting behaviour of the reflectance results would be explained through a physical change in the fabric structure in addition to carbonization. As the microstructure cracks elongate, deepen, and become more severe with increased exposure conditions the reflectance values experience an overall downward shift. Conversely, the overall absorbance values should increase. This overall shifting behaviour could be due to the larger amount of NIR light being absorbed or scattered in these developing microstructure cracks and subsequent increased porosity in the fabric structure. Both of these factors would decrease the amount of light being reflected back at the integrating sphere of the spectrophotometer. Figures 4.1 – 4.3 show reflectance spectrum following thermal exposure to 10 – 70 kW/m$^2$ for a duration of 60 seconds.

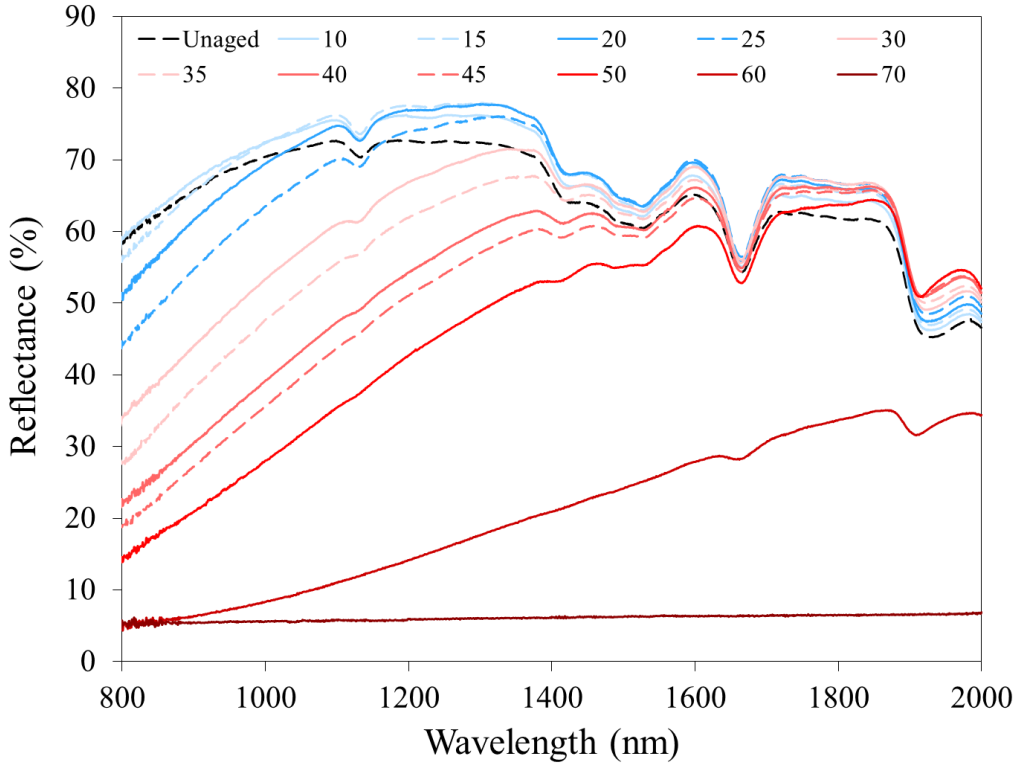


*Figure 4.1 Reflectance spectrum for RS Natural specimens after heat flux exposure (kW/m$^2$) for 60 s*

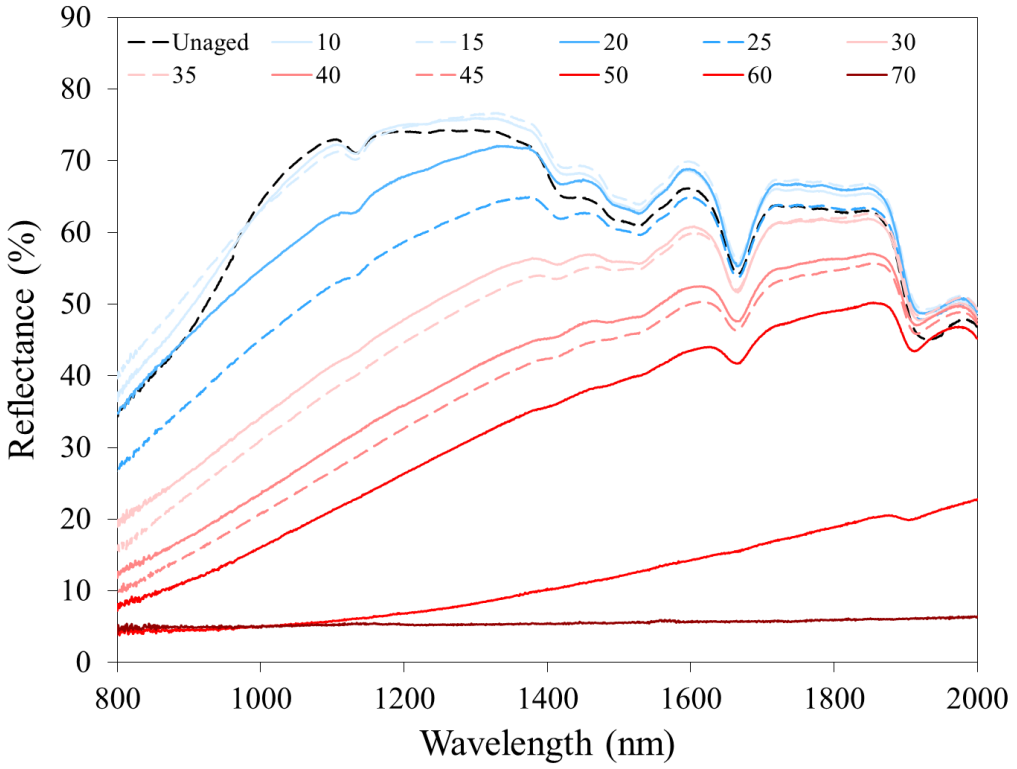


*Figure 4.2 Reflectance spectrum for RS Black specimens after heat flux exposure (kW/m$^2$) for 60 s*

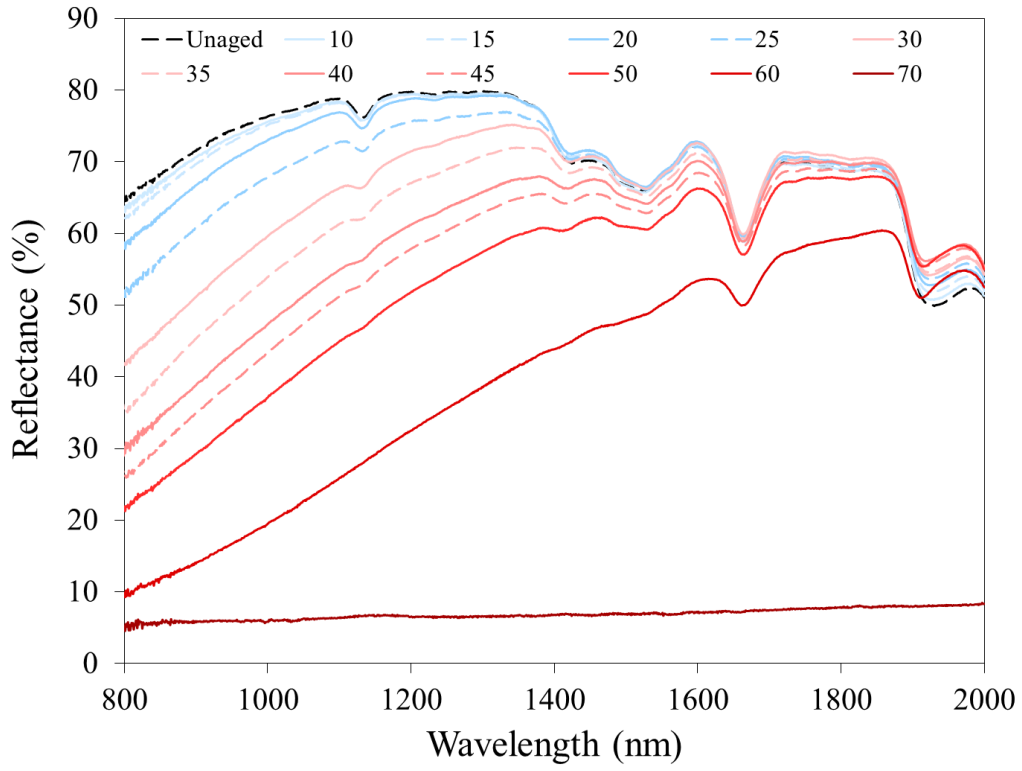


*Figure 4.3 Reflectance spectrum for SCI PBI Max specimens after heat flux exposure (kW/m$^2$) for 60 s*

The change in reflectance spectrum with increased thermal ageing intensity is indicative of chemical and microstructural changes occurring within the textile. Initial low-level heat flux exposures (up to 15 kW/m$^2$) cause a reflectance change less than 5% in magnitude across all three fabric types. Moreover, tensile strength values decrease by less than 5% in this thermal ageing region (Section 3.5). Incident thermal radiation exposures below 15 kW/m$^2$ produce fabric temperatures below 300°C (e.g. Table 3.1; Figure 3.4 – 3.6). This varies greatly from the maximum reflectance change that occurs at the highest heat flux exposures of 70 kW/m$^2$ (producing temperatures > 700°C) that can change up to 95% from the unaged readings. Reflectance changes between these minimum and maximum values will be the most useful for further analysis with regards to thermochemical fabric changes.

The difference in reflectance or absorbance results is important, but false interpretation of these results is common without a background knowledge of the base chemical components and structure of the specimen (Westad, Schmidt and Kermit 2008). Thermochemical changes can also be related to slope changes in these NIR results (Gau 1996). A number of changes are

evident with increasing thermal ageing conditions in the RS Natural fabric (Figure 4.1). After the 20 – 30 kW/m$^2$ heat flux exposures (fabric temperatures of 300 – 350°C) a number of changes take place in the reflectance results. Reflectance peaks between 1200 – 1400 nm experience a reduction in prominence and a downward shift in reflectance values. This region (e.g. 1200 – 1400 nm) corresponds to a chemical bond in the Kevlar/PBI® structure (Arrieta, et al. 2010). With increasing incident heat flux (e.g. fabric temperatures of 400 – 700°C), the peak in this reflectance region (1380 – 1400 nm) continues to flatten and appears to signify increasing stretching and damage of the chemical bond in the fabric. This measurable change in reflectance could be correlated to the reduction in tensile strength of all fabrics that occurs near these ageing condition. For example, after the 20 kW/m$^2$ exposure tensile strength decreases by up to 33% of the original value while still remaining above the NFPA 1971 (2013) 623 N strength requirement (Figure 3.13). However, after exposure to 30 kW/m$^2$ tensile strength values drop by up to 60% (e.g. RS Black in Figure 3.13). This reflectance trend appears to be less significant in the SCI PBI Max fabric (Figure 4.3) and this may correlate to the higher strength retention of this fabric following thermal ageing. Tensile strength values for SCI PBI Max after a 30 kW/m$^2$ exposure only drop by 22%. This is significantly less than the RS Black strength loss at this exposure and this is also evident when comparing the magnitude of reflectance value decreases between the two fabrics (Figure 4.1 and 4.2 following 30 kW/m$^2$ exposure).

Wavelength regions between 1150 – 1300 nm experience a change in reflectance values with increased thermal ageing across all fabric types. The spectra for the unaged specimens appear relatively flat in this region. However, thermal ageing conditions greater than 20 kW/m$^2$ cause a slope change of the reflectance results. The decreasing slope trend becomes more pronounced at higher heat flux conditions (e.g. exposures > 30 kW/m$^2$). This wavelength region corresponds with multiple chemical bonds (Arrieta, et al. 2010) making it difficult to decisively say which base chemical structure could relate to reflectance changes in this wavelength region. However, since the C-N bond corresponds to lower wavelengths (e.g. 1240 nm) the majority of the reflectance change in this region might be attributed to N-H and C-C damage. The reflectance feature at 1130 nm decreases in intensity and eventually disappears with increased incident heat flux (e.g. 40 kW/m$^2$). This feature change at 1130 nm could possibly be used as an indicator and

related to mechanical property changes. These two trends between 1130 – 1300 nm are evident across all three fabric types considered.

The wavelength region between 1640 – 1650 nm is associated with chemical bonds in the hydrogen linked amide of these fibers (Arrieta, et al. 2010). A local feature in reflectance values does appear to decrease in severity with increased thermal ageing exposure across all three fabrics. However, this region does not appear to show any large change in reflectance readings until higher heat flux exposures (e.g. > 30 kW/m$^2$). Wavelength regions between 1900 – 1960 nm show interesting trends, but the literature currently has no link to any chemical bonds in these fabric types. The changes in this highest wavelength region could also be the result of a nearby water-band that is investigated in Section 4.1.1.

These NIR results can also be related to the absorbance of the damaged fabrics. Absorbance is obtained by taking the inverse logarithm of the reflectance readings:

$$A = Log\left(\frac{1}{\rho}\right) \qquad (4.1)$$

It naturally follows that spectral features sensitive to damage identified in this research (e.g. 1150 – 1300 nm, 1380 – 1400 nm, 1640 – 1650 nm) also appear in these absorbance trends pictured below for all three fabric types. The highest heat flux exposure of 70 kW/m$^2$ is not pictured due to the very low reflectance readings.

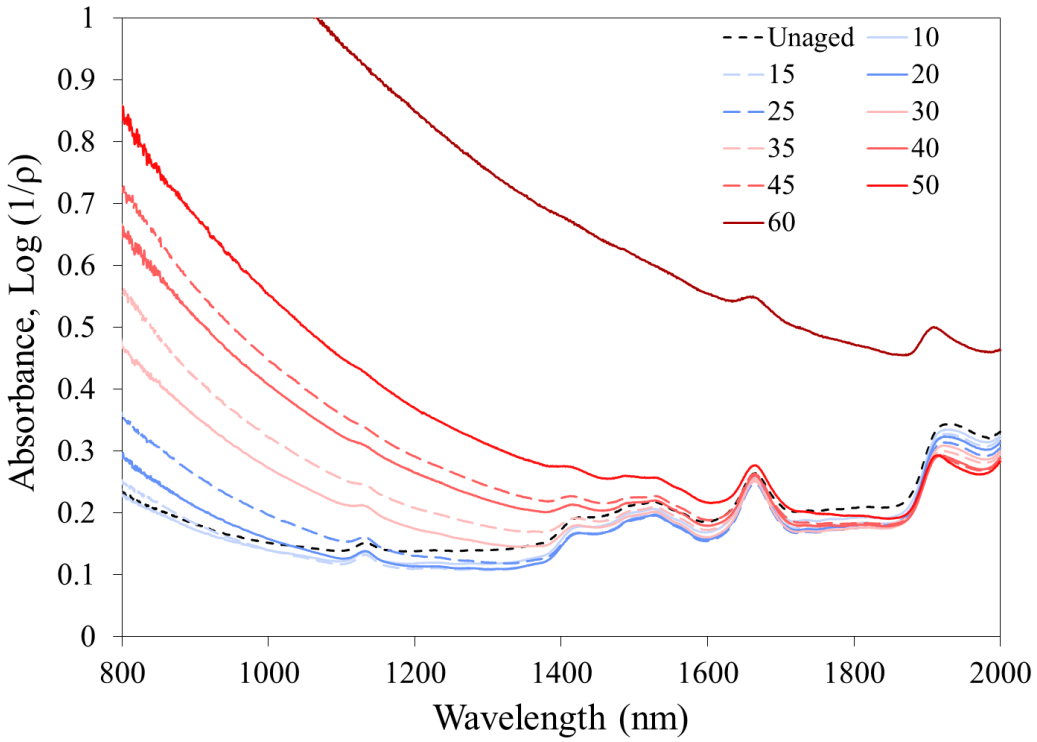


*Figure 4.4 Absorbance spectrum for RS Natural specimens after heat flux exposure (kW/m$^2$) for 60 s*

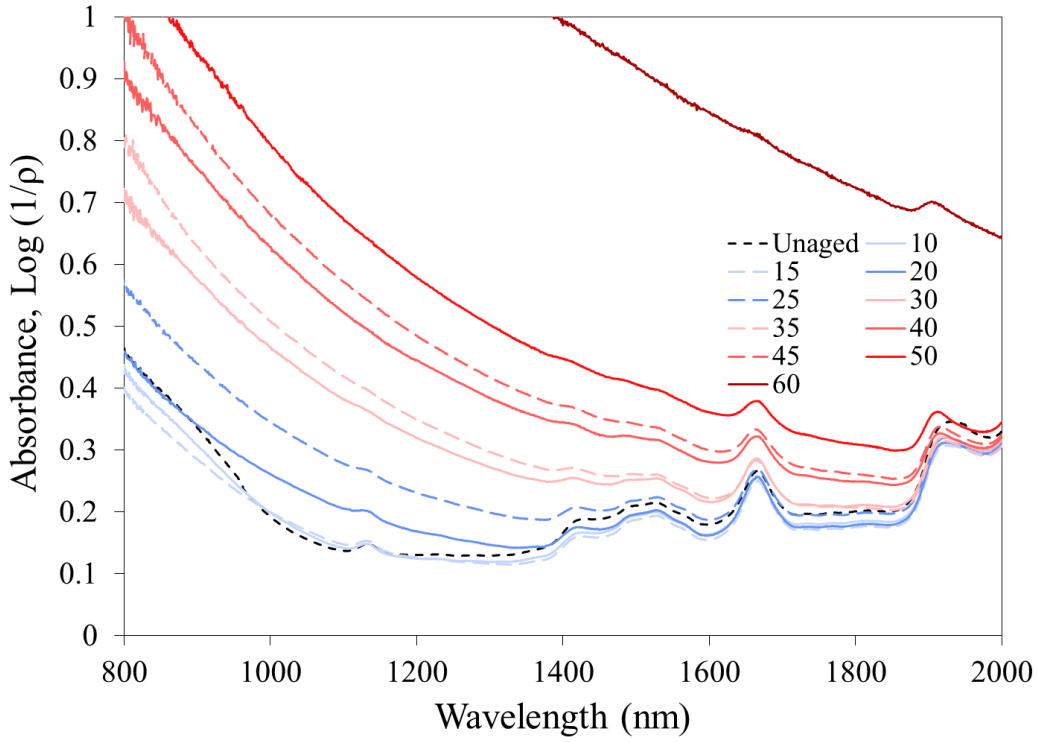


*Figure 4.5 Absorbance spectrum for RS Black specimens after heat flux exposure (kW/m$^2$) for 60 s*

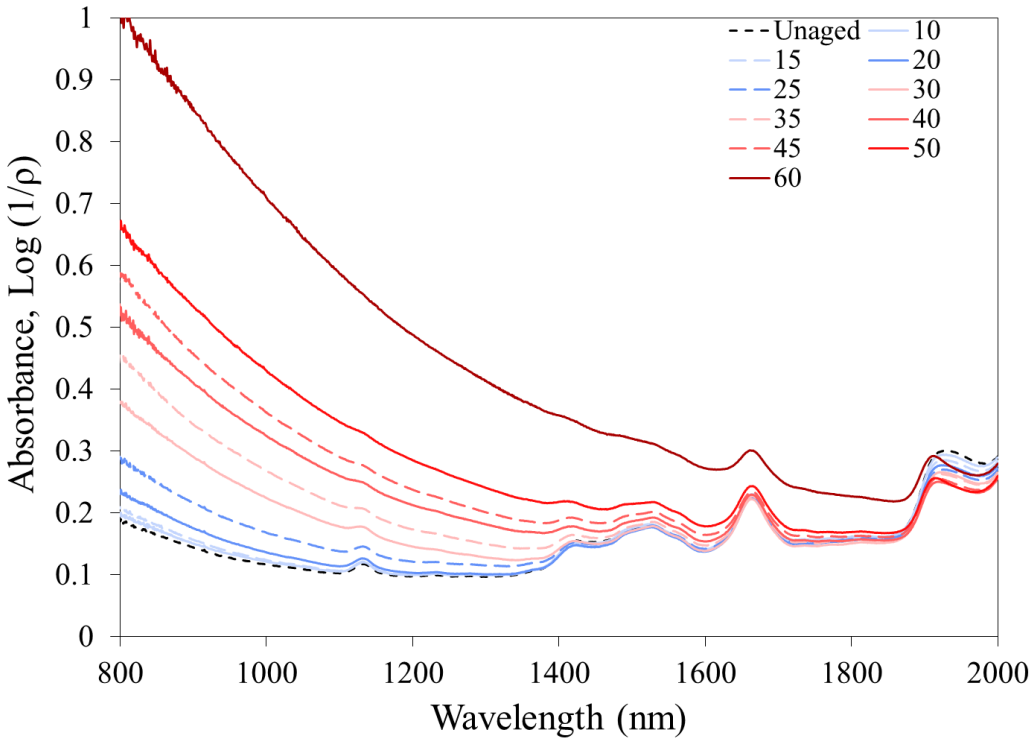


*Figure 4.6 Absorbance spectrum for SCI PBI Max specimens after heat flux exposure (kW/m$^2$) for 60 s*

NIR results were also obtained for the UV aged specimens. With the reduction in tensile strength properties after just 40 SFH of exposure (e.g. Figure 3.16, 10 – 20% tensile strength reduction in all fabrics) one would expect to see some change in NIR results pictured in Figure 4.7 – 4.9. The reflectance values increase following UV exposure for both Ripstop constructed fabrics, but decrease for the SCI PBI Max fabric. However, the UV exposure conditions do not appear to cause any great change in the characteristic wavelength regions previously noted in the thermal ageing results. In fact, the shape changes of the peaks and valleys in the UV aged NIR reflectance results (Figure 4.7 – 4.9) are very small. The lack of change in distinguishing NIR curve characteristics suggests reflectance may not be the best method for predicting the remaining tensile strength of UV aged Kevlar®/PBI fabrics considered in this study. UV NIR reflectance results are within ± 10% of the unaged fabric's NIR signature even though tensile strength may decrease significantly (e.g. 50% loss of mechanical properties) after 160 SFH of UV exposure. Graphing the absorbance of the UV aged specimens (Figure 4.10 – 4.12) does not improve visualization of these small changes in the NIR results.

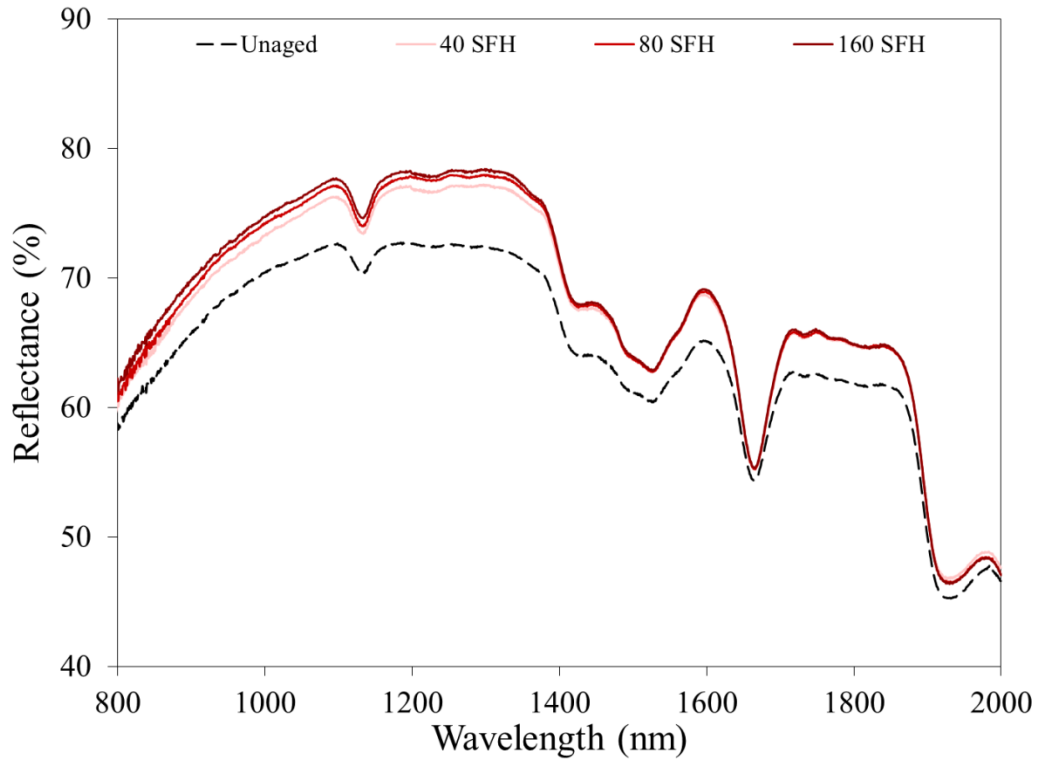


*Figure 4.7 Reflectance spectrum for RS Natural specimens after UV exposure*

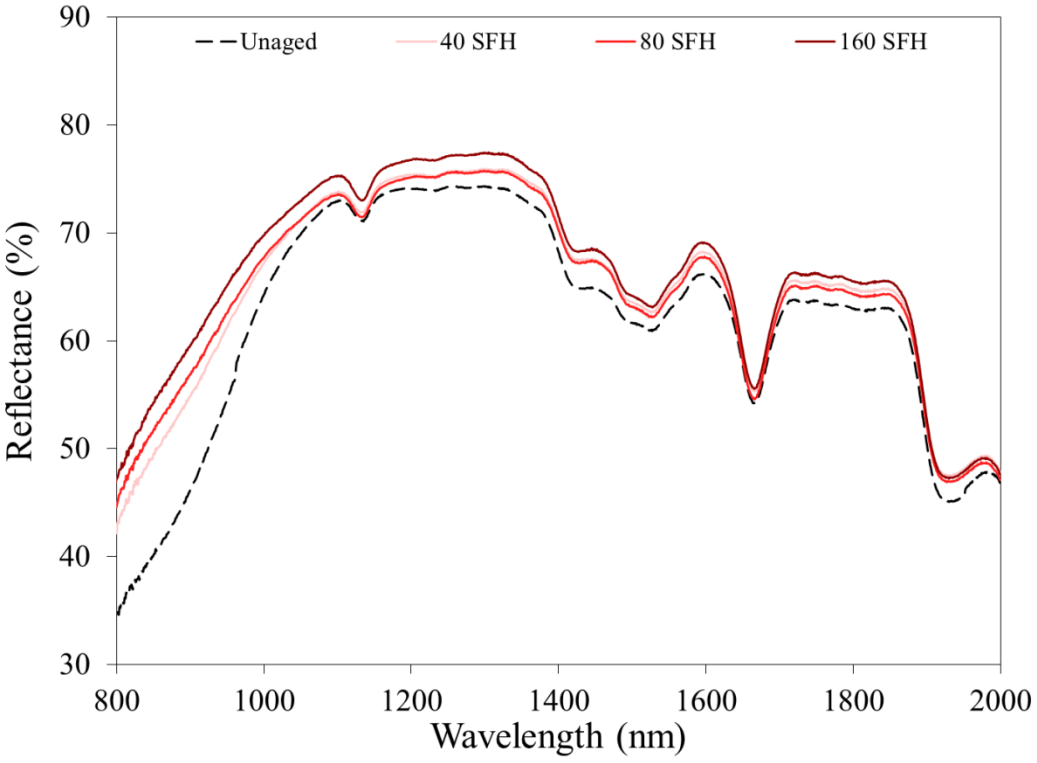


*Figure 4.8 Reflectance spectrum for RS Black specimens after UV exposure*

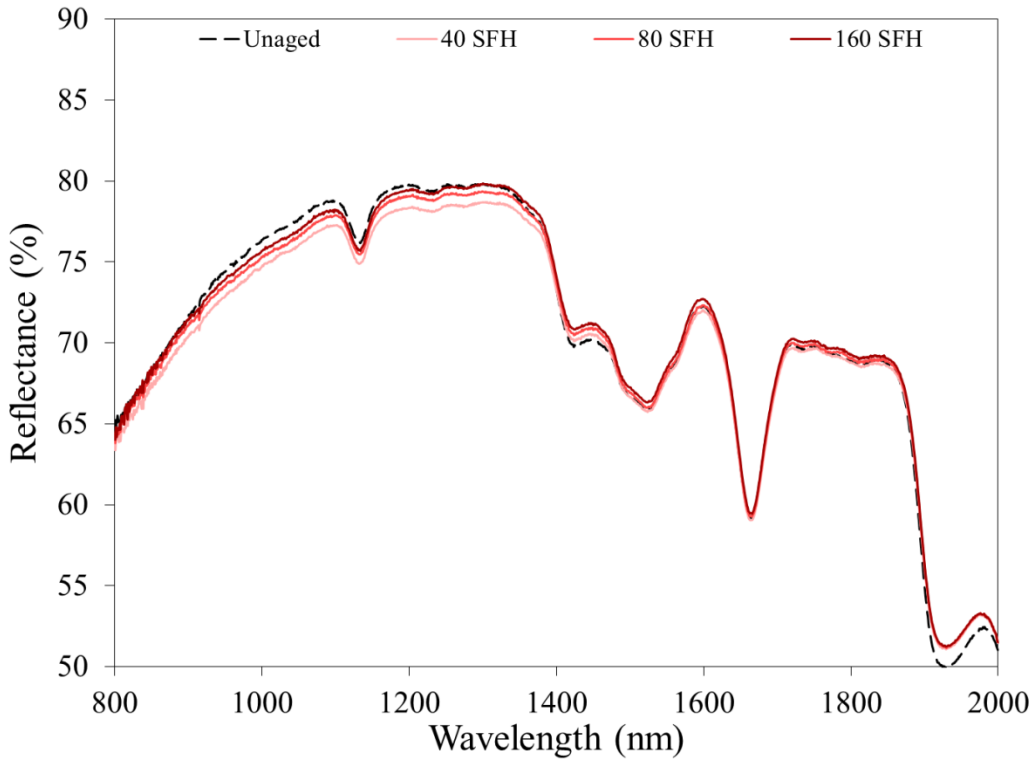


*Figure 4.9 Reflectance spectrum for SCI PBI Max specimens after UV exposure*

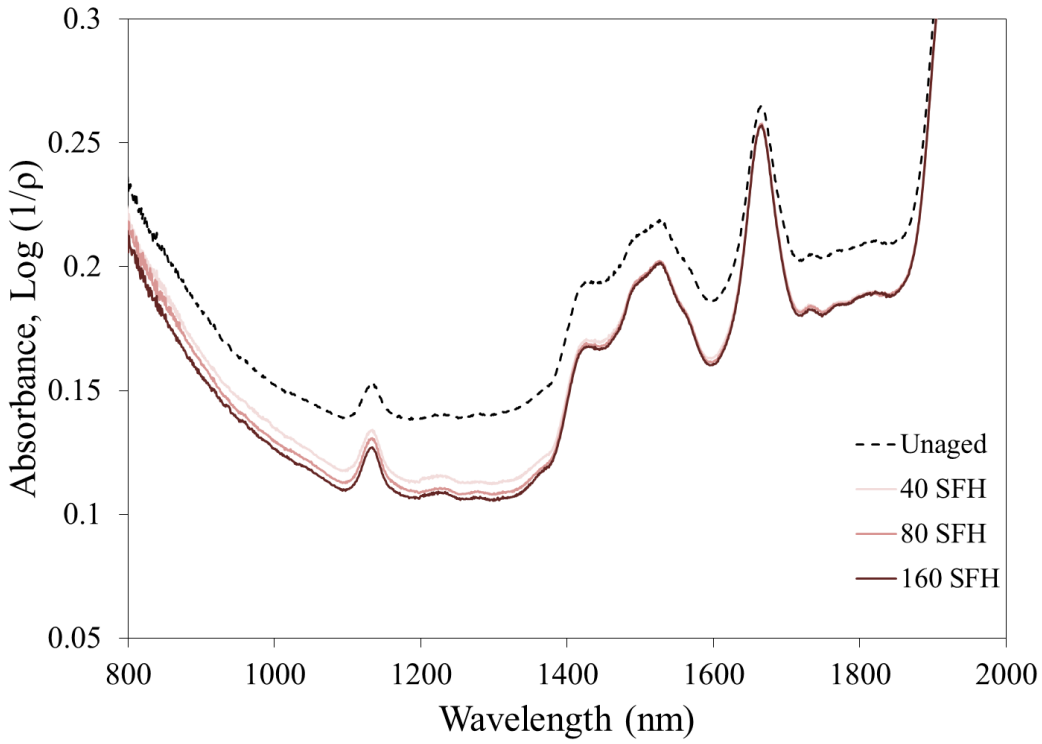


*Figure 4.10 Absorbance spectrum for RS Natural specimens after UV exposure*

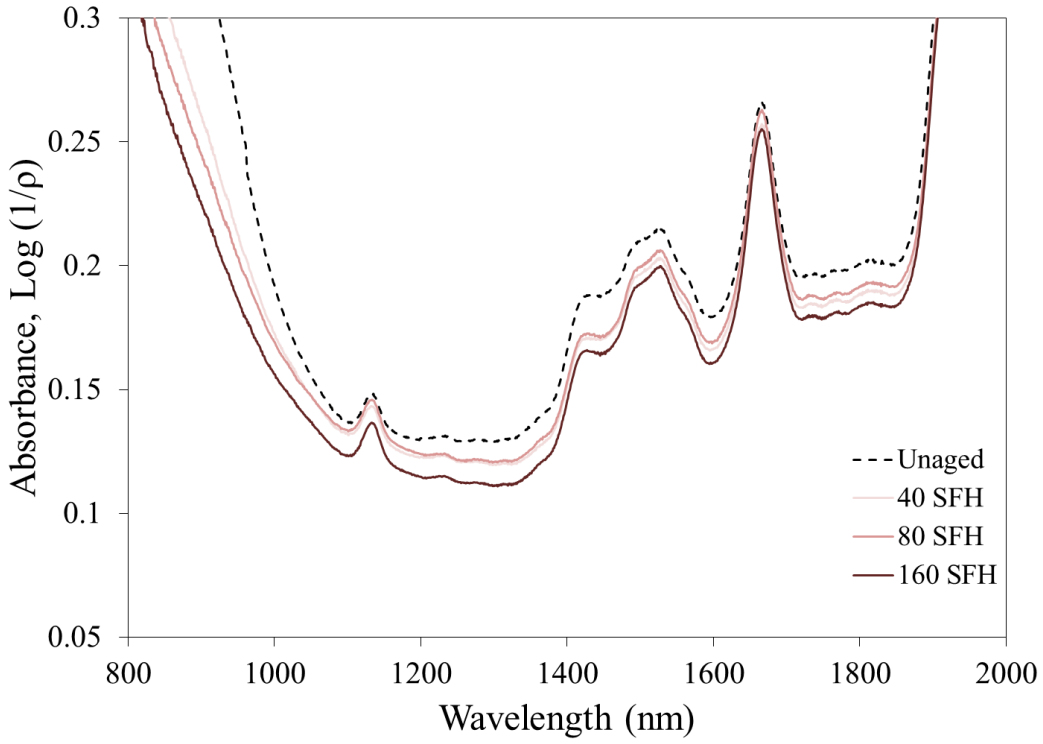


*Figure 4.11 Absorbance spectrum for RS Black specimens after UV exposure*

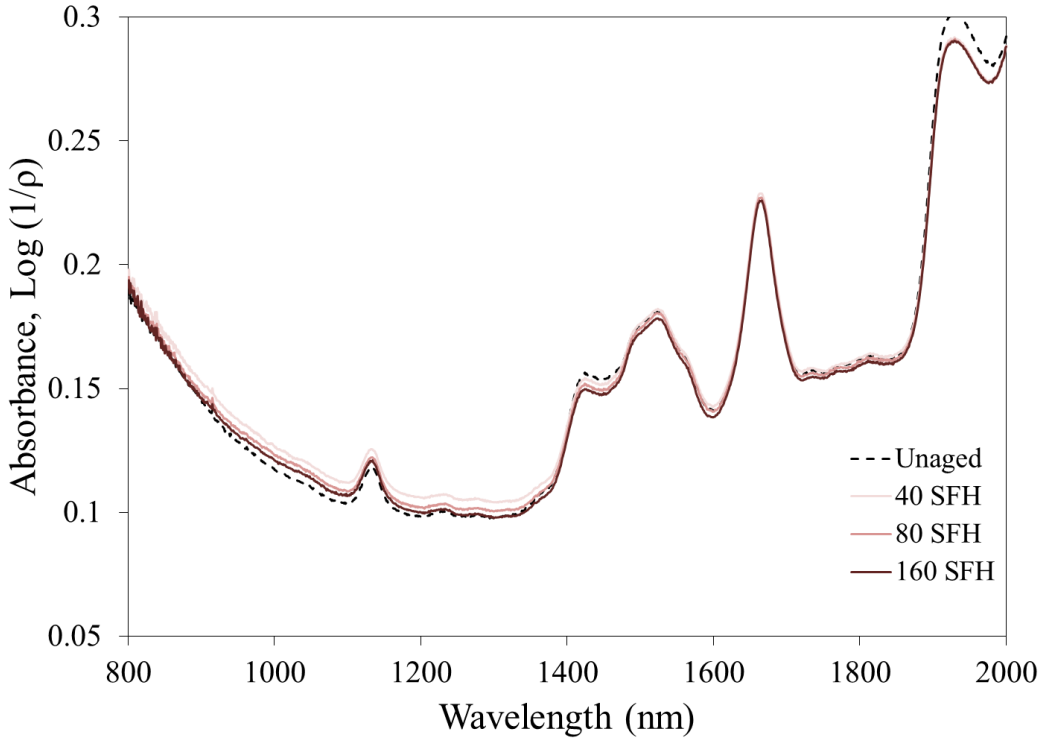


*Figure 4.12 Absorbance spectrum for SCI PBI Max specimens after UV exposure*

The lack of change in UV aged NIR results can be highlighted by comparison to the changes in NIR results for the thermally aged results (Figure 4.13). This comparison looks at the RS Natural fabric and the other two fabrics (RS Black and SCI PBI Max) have similar trends. A 50% reduction in tensile strength is achieved through thermal ageing exposure at 30 kW/m$^2$ and there are significant changes in the reflectance data. On the other hand, the RS Natural fabric takes 160 SFH of UV exposure to reach the same reduction in tensile strength while there is little change in NIR reflectance (Figure 4.13). The UV aged reflectance values do experience an overall shift from the unaged specimen, but there does not appear to be any great change in slope or feature shape.

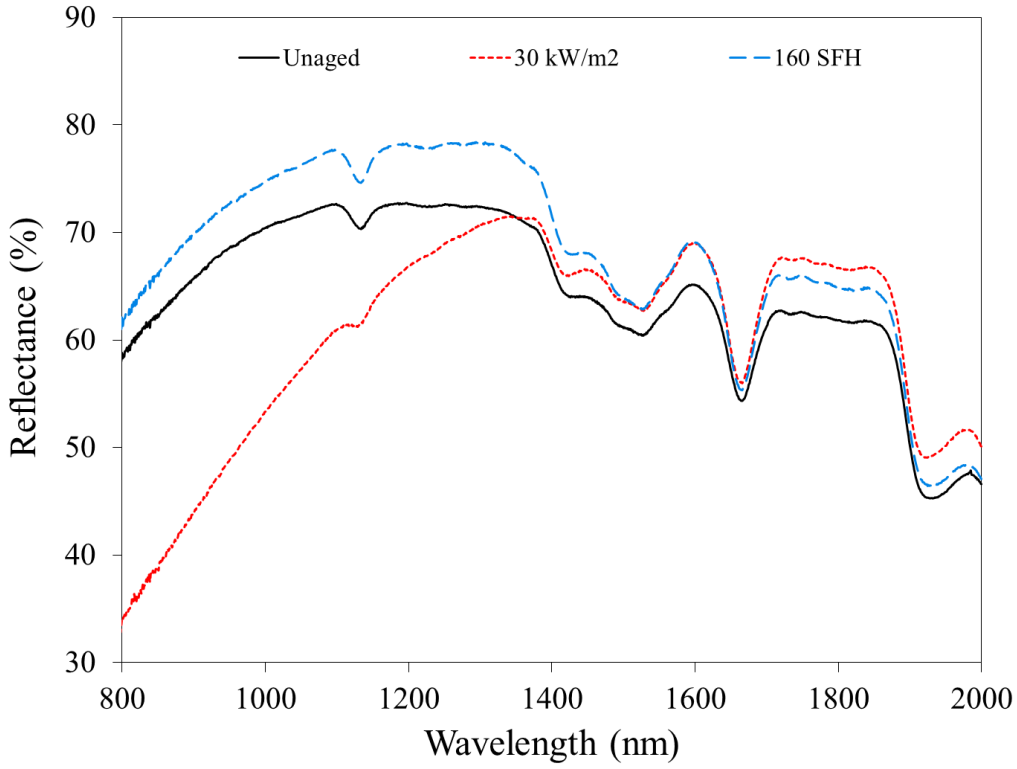


*Figure 4.13 NIR reflectance comparison of thermally and UV aged RS Natural specimens that experience a 50% reduction in tensile strength*

### 4.1.1. Water content NIR investigation

During the interpretation of NIR results it was suggested that water absorbance bands could be playing a background role in some of the infrared results. NIR scans were performed on a pipette filled with liquid water. These NIR results lacked significant overlap in key regions examined in this study. To examine the influence of entrained moisture on NIR readings fabric specimens were preconditioned at 60% RH and 50% RH (both at 22°C). These were compared to NIR results of fabric specimens dried at temperatures between 112 - 115°C using a Blue M Stabil-Therm D-2631-Q (Riverside, MI) oven for a duration of approximately thirty minutes and then scanned in the spectrophotometer previously described. Figure 4.14 shows the impact of these changes in humidity levels of the fabrics. Small discrepancies in the 1400 – 1480 nm and 1880 – 2000 nm wavelength regions are evident when comparing the oven dried specimens to the preconditioned specimens. The 1400 nm regions was not examined in-depth in this current study, but the region around 1930 nm contained a feature that was related to ageing. The dependence on entrained moisture content in this 1880 – 2000 nm region most likely means this NIR region is located around a strong water absorbance band. Drawing meaningful conclusions about changes in fabric structure from this region (e.g. 1930 nm) would be difficult due to this strong dependence on entrained moisture.

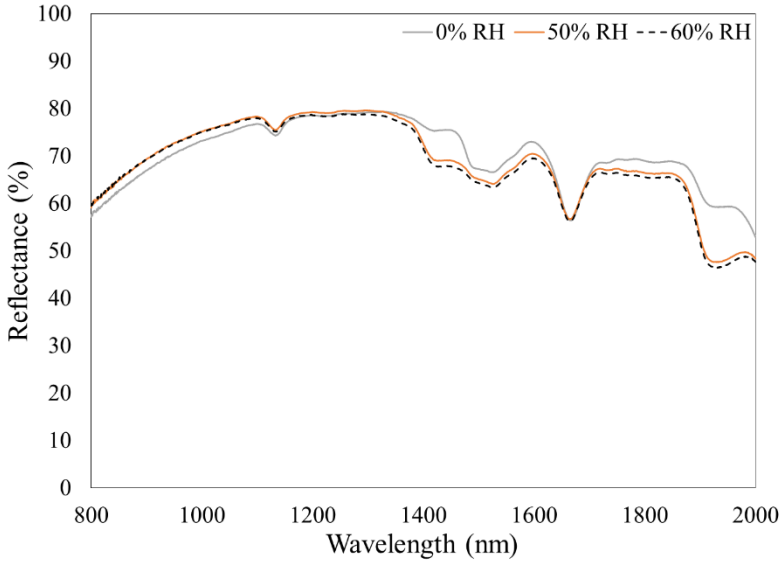


(a)

*Figure 4.14 Impact of varied preconditioning humidity levels from 0-60% Relative Humidity (RH) for (a) RS Natural, (b) RS Black, and (c) SCI PBI Max fabrics*

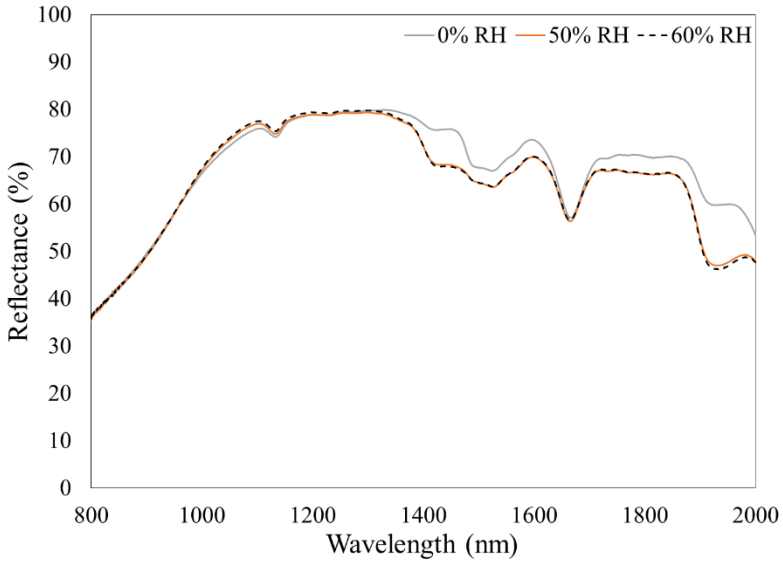


(b)

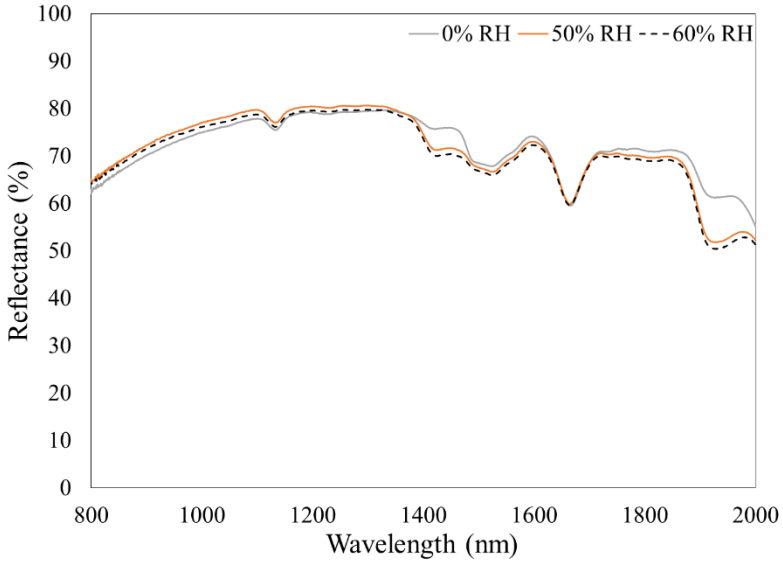


(c)

*Figure 4.14 Continued*

## 4.2. Near Infrared Evaluation – Tensile Strength Correlations

The main goal of this particular study is to relate results of non-destructive methods (e.g. NIR reflectance and absorbance) to the performance of firefighters' outer shell materials. The characteristic shifts in NIR reflectance and absorbance readings can be related to the material tensile strength shown in this section. Additionally, the Gaussian peak and trough features (e.g. amplitude/width of an absorbance or reflectance feature) could also be used to evaluate thermochemical and photooxidative changes resultant from exposure conditions. Methods of

analysis for the NIR results will be explored in Section 4.2 that include percentage shifts in reflectance results, continuum removed absorbance feature area changes, absorbance feature prominence changes, and a normalized-difference index evaluation of NIR reflectance slope changes (Figure 4.15).

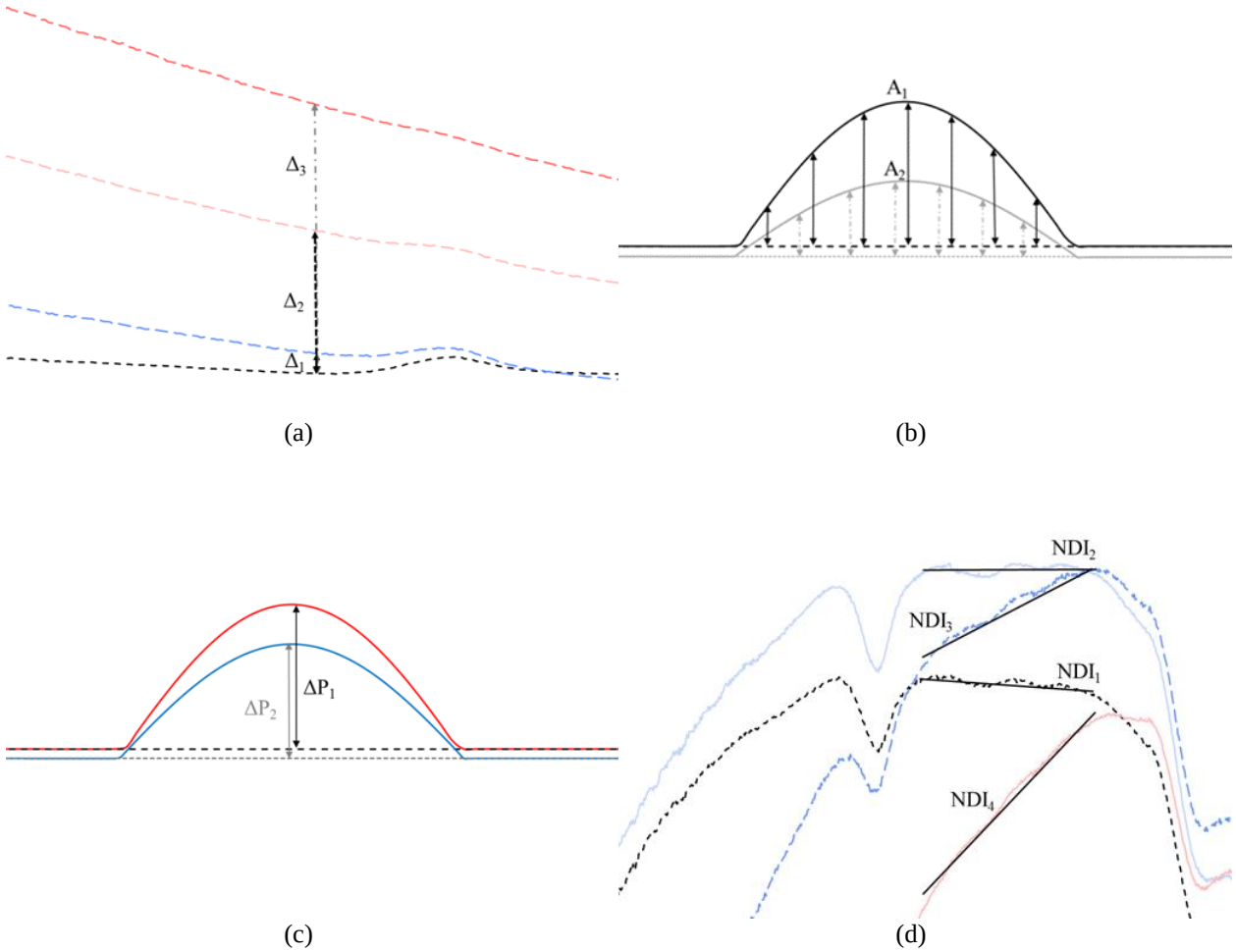


*Figure 4.15 Sketches representing (a) percentage shifts in reflectance results, (b) continuum removed absorbance feature area changes, (c) absorbance feature prominence changes, and (d) a normalized-difference index evaluation of NIR reflectance slope changes*

### 4.2.1. Percentage Shifts in Absorbance

Selection of an individual wavelength region allows for consistent comparison of percentage change in reflectance or absorbance results across all three fabric types. Additionally, the cost of developing a future NIR sensor would be significantly reduced if a narrow wavelength region could be identified. For this initial investigation the wavelength of 1100 nm was selected. This specific wavelength is near the band assignment for the in-plane chemical bond and also near the Gaussian feature that occurs at 1130 – 1140 nm.

Shifts in the absorbance spectrum differ slightly depending on the type of fabric exposed to thermal ageing (Figure 4.4 – 4.6). The RS Natural fabric has a reduction in absorbance spectrum until thermal exposures reach the 20 $kW/m^2$ level (Figure 4.4). After this point the absorbance results increase with increases in heat flux. Conversely, the Black and PBI specimens only see a gradual increase in absorbance with an increase in thermal ageing heat flux. As previously mentioned, the UV aged trials do not appear to show any strong relationship to absorbance spectrum shifts. The relation between the remaining tensile strength, the percent change in absorbance wavelength, and the ageing conditions is a complex trend that can be viewed in Figures 4.16 and 4.17. This initial manipulation of the NIR results (Figures 4.16 and 4.17) shows there is a relation between change in material tensile strength and the percentage change in NIR results for this selected 1100 nm wavelength.

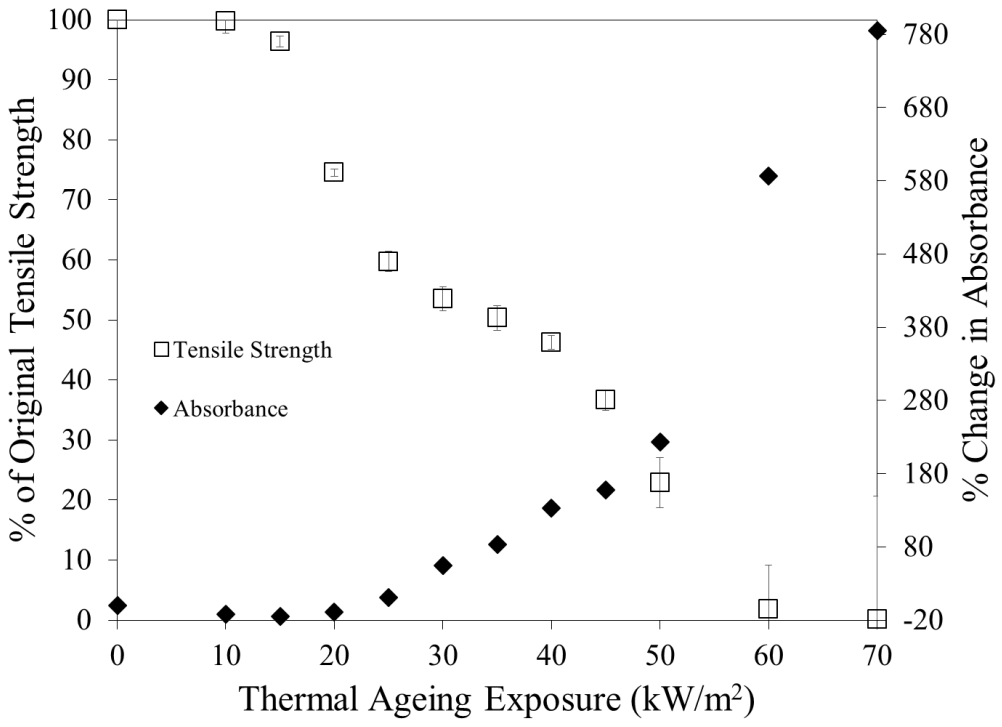


(a)

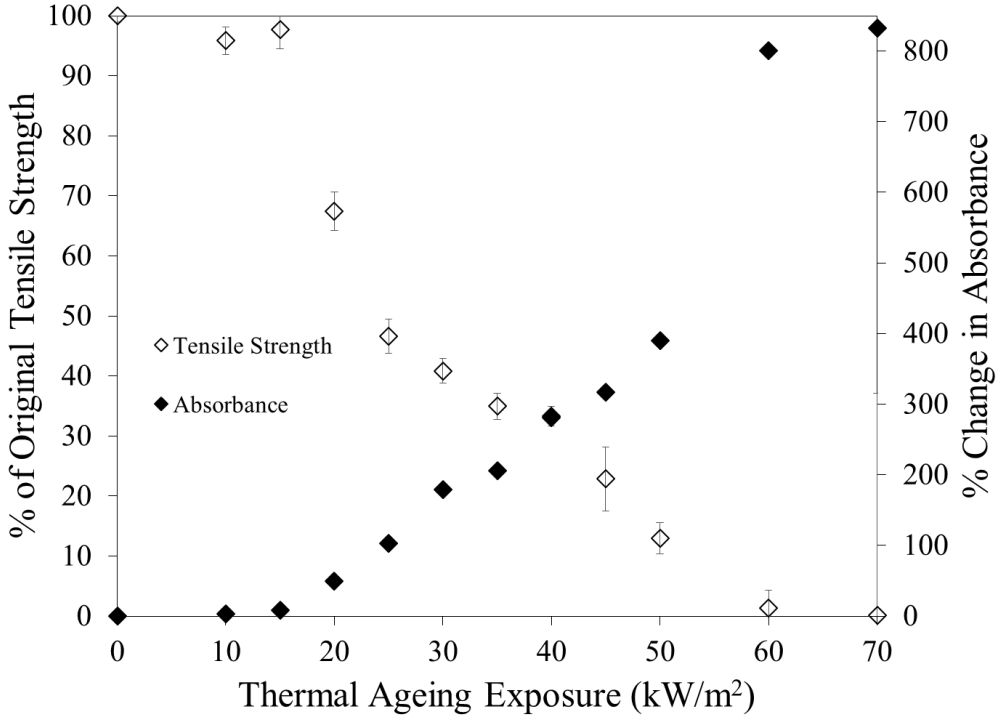


(b)

*Figure 4.16 Percent change from original tensile strength and percent change in NIR absorbance from thermal exposure (0 – 70 kW/m$^2$) for 1100 nm of (a) RS Natural, (b) RS Black, and (c) SCI PBI Max fabrics*

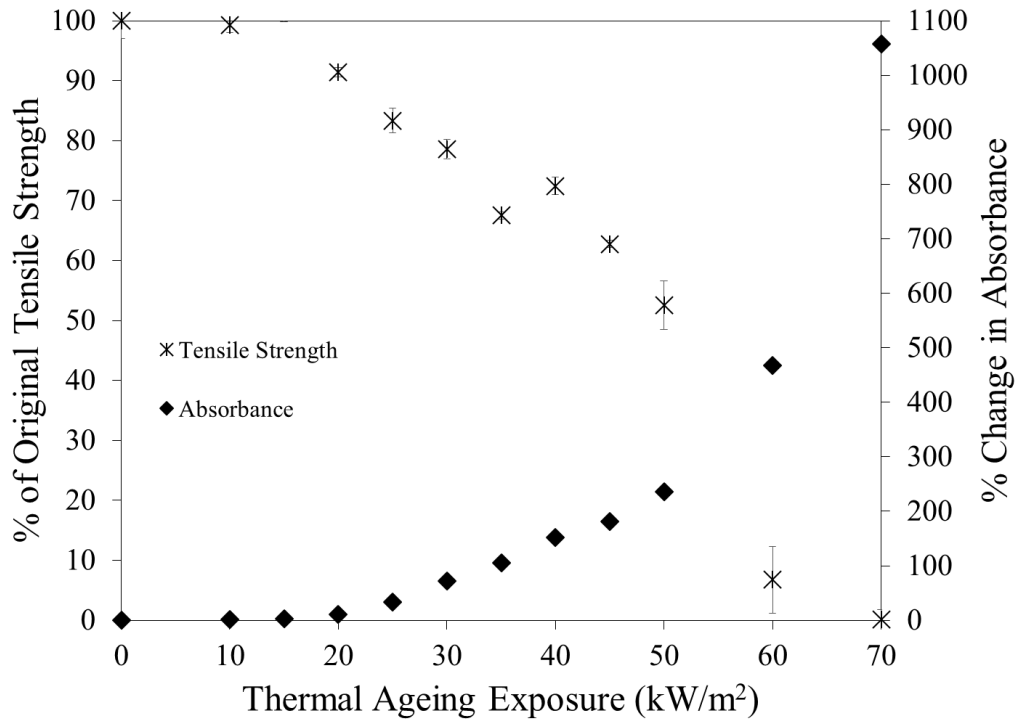


(c)

*Figure 4.16 Continued*

These initial results (e.g. thermal ageing impact on percent change in tensile strength, and percent change in absorbance) can also be shown for UV aged specimens at the 1100 nm wavelength, but do not reveal the same level of correlation as the thermally aged specimens pictured above. As previously mentioned in Section 4.1 (Figure 4.13) the UV aged specimens do not show the same level of change in NIR results as for fabric with a similar reduction in tensile strength after thermal ageing.

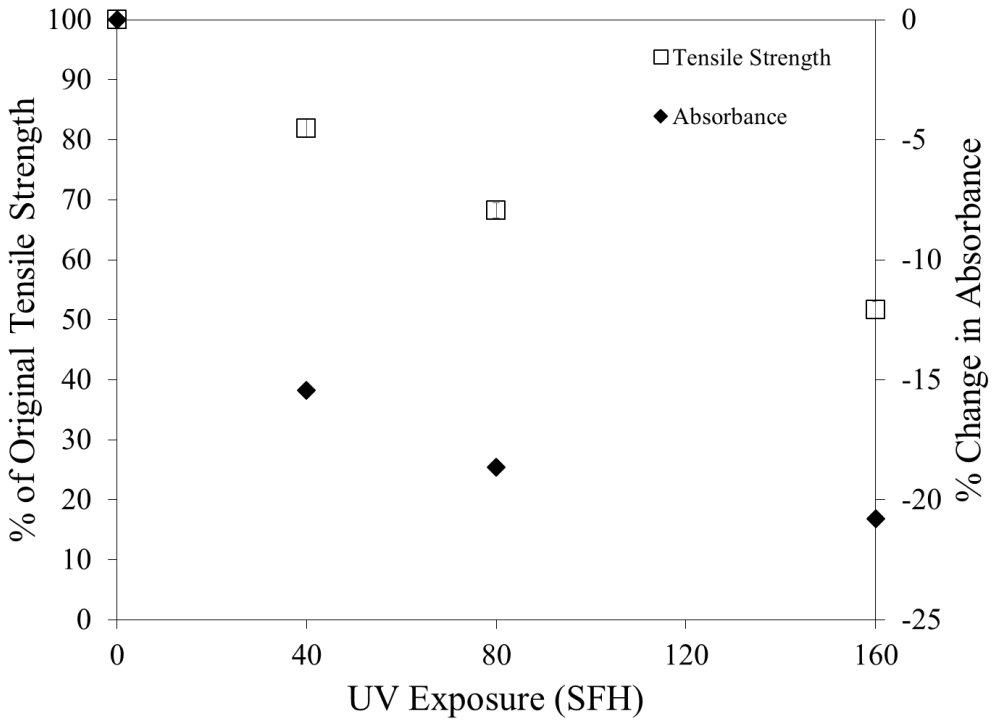


(a)

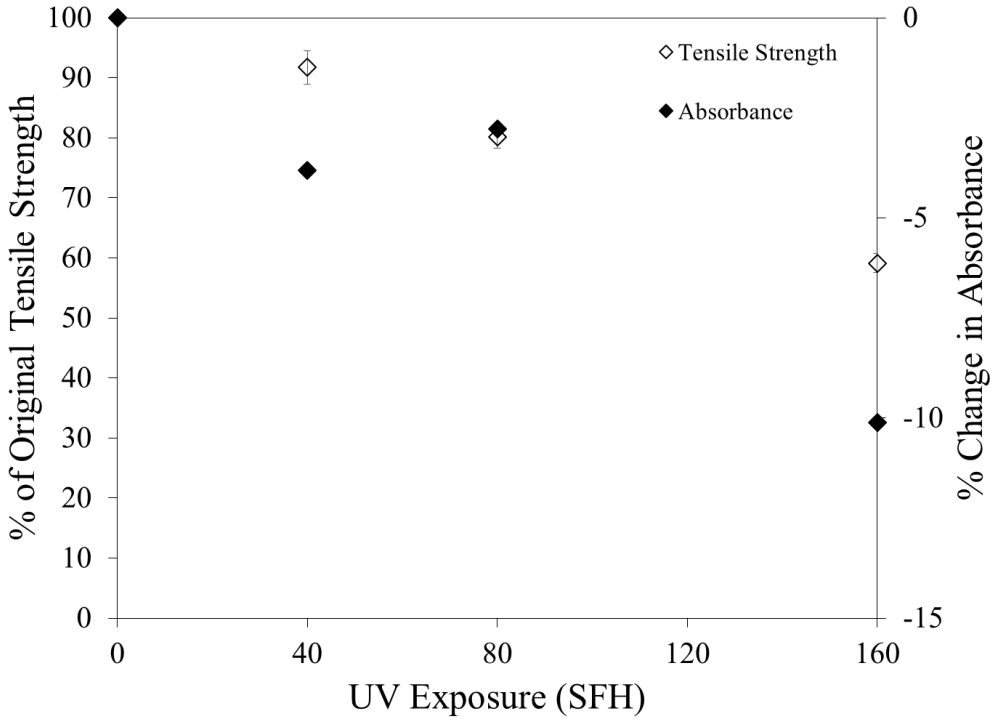


(b)

*Figure 4.17 Percent change from original tensile strength and percent change in NIR absorbance from UV exposure (0 – 160 SFH) ) for 1100 nm of (a) RS Natural, (b) RS Black, and (c) SCI PBI Max fabrics*

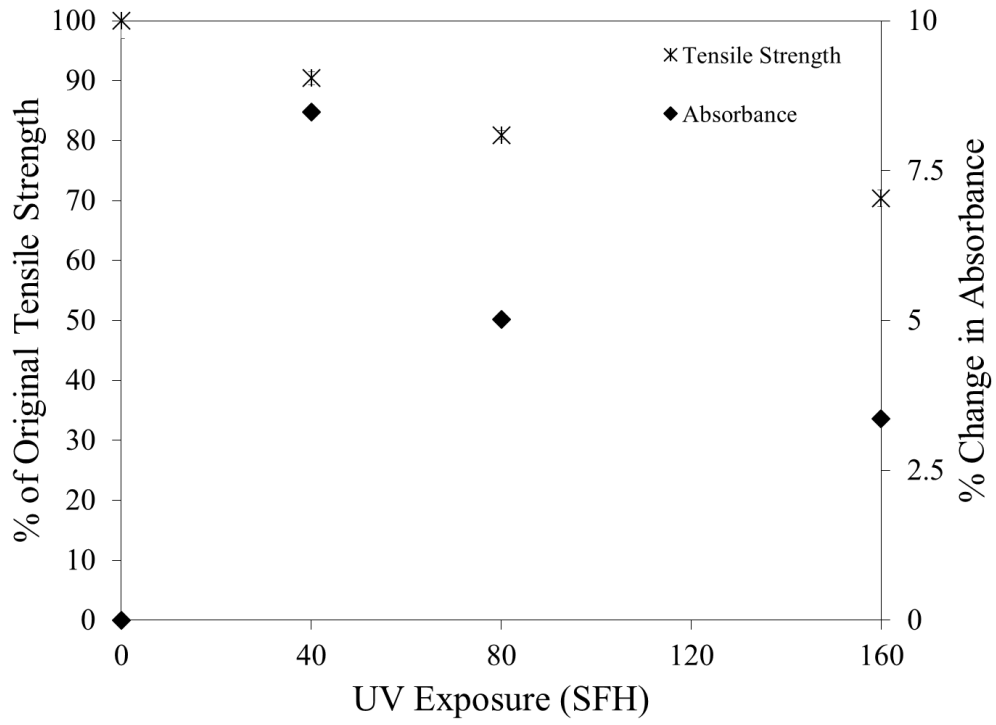


(c)

*Figure 4.17 Continued*

Direct comparison of the percent change from the original tensile strength to the percent change in wavelength for the 1100 nm region could be used to obtain a relation between the two variables. This absorbance region contains relatively smooth features across the different fabric trials and does not contain overlapping Gaussian features (e.g. interfering/overlapping features). This technique could also be used at other key absorbance regions (e.g. around 1380 nm, 1640 nm readings) to see how the fitted equations compare to one another. Polynomial relations were examined, but the ageing conditions at 60 and 70 kW/m$^2$ had a negative impact on obtained equations (e.g. no strength remains after highest exposures, but equations were influenced by large percent changes in absorbance) so these results are not featured. Therefore, exponential relations were considered without the inclusion of the 60 and 70 kW/m$^2$ data points. A few percent change in absorbance values less than zero were also driven to zero in order to improve the obtained relations (e.g. initial exposures for RS Natural have negative reflectance shifts in Figure 4.1). This explains why the curve-fit equations in Figure 4.18 do not always begin at 100% of the original tensile strength. These curve-fit equations using a log-log scale and a ratio

of unaged reflectance ($\rho_o$) to aged reflectance ($\rho_n$) can be found below for the thermally aged specimens across all three fabrics examined at the 1100 nm region.

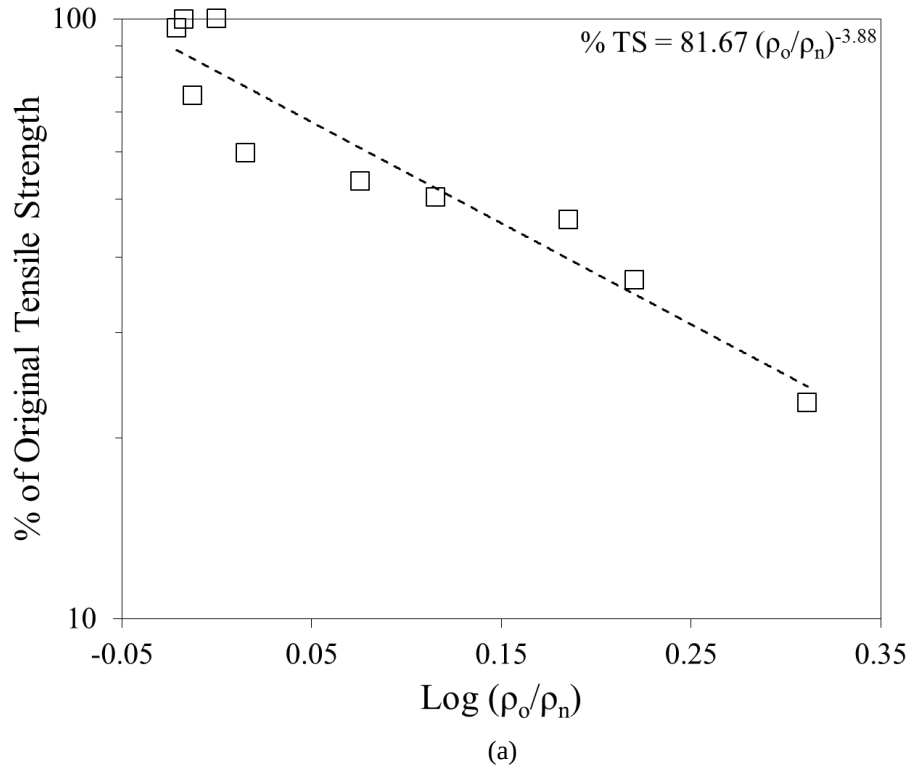


(a)

*Figure 4.18 Exponential relation between percentage of original tensile strength to the change in absorbance at 1100 nm of (a) RS Natural, (b) RS Black, and (c) SCI PBI Max fabrics*

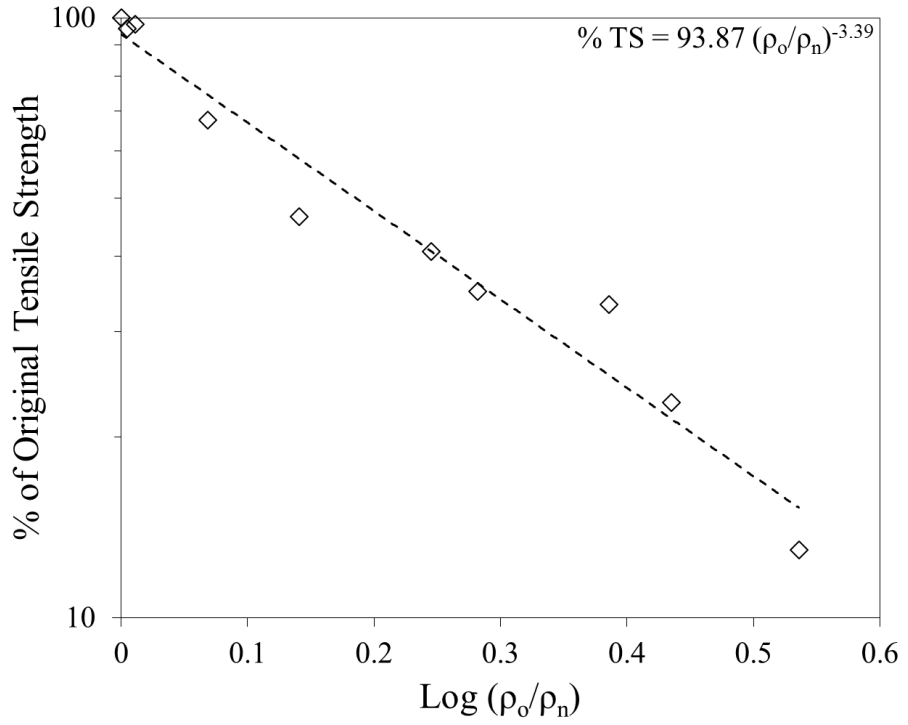


(b)

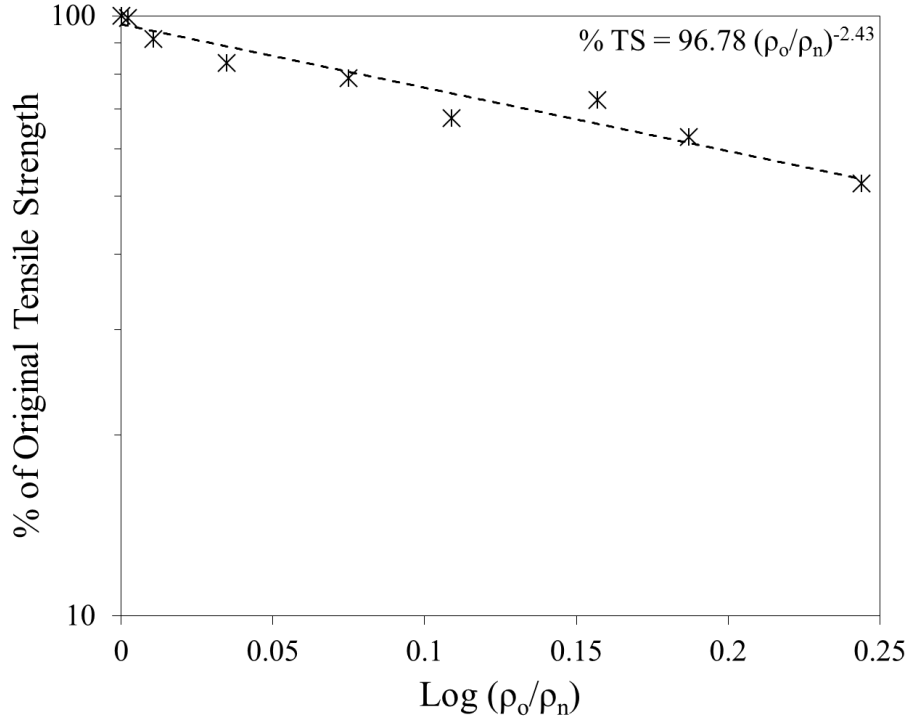


(c)

*Figure 4.18 Continued*

The same method of analysis can be made near the 1380 nm and 1600 nm regions. Table 4.1 contains the simplified exponential relations between the percent changes from the original tensile strength to the percent change in the absorbance readings.

*Table 4.1 Exponential relations between percent change in tensile strength to percent change in absorbance for selected wavelength locations without considering 60 and 70 kW/m$^2$ exposures*

| **Fabric** (% TS = ) | **1100nm** | **1380nm** | **1600nm** |
|---|---|---|---|
| RS Natural | $81.67\ (\rho_o/\rho_n)^{-3.88}$ | $65.44\ (\rho_o/\rho_n)^{-8.4}$ | $47.98\ (\rho_o/\rho_n)^{-16.64}$ |
| RS Black | $93.87\ (\rho_o/\rho_n)^{-3.39}$ | $79.86\ (\rho_o/\rho_n)^{-5.61}$ | $68.61\ (\rho_o/\rho_n)^{-9.20}$ |
| SCI PBI Max | $97.78\ (\rho_o/\rho_n)^{-2.43}$ | $93.48\ (\rho_o/\rho_n)^{-5.71}$ | $88.44\ (\rho_o/\rho_n)^{-14.56}$ |

## 4.2.2. Absorbance Feature Analysis – Area and Prominence

This section investigates attempts to correlate different NIR analysis techniques that are utilized in other research areas (such as planetary/astronomical spectroscopy) with the percentage change in tensile strength observed with increased ageing. As such, no specific mathematical relations (e.g. statistical methods and multiple linear regression) are developed, such as was the case in the previous studies (Rezazadeh 2014).

The percent change from original readings in absorbance or reflectance spectrum can be useful in many applications, but as previously noted they may also lead to false conclusions if the underlying chemical and structural changes are not well understood before interpretation (Clark and Roush 1984). However, examining the peak and trough features of the absorption (or reflectance) spectral results can be used to analyze complex materials (Clark 1983). This can be done by comparing the relative band depth and width of spectral features (e.g. local peaks and troughs in Figure 4.15). In this study the software package MatLab (R2015a) was utilized to compare the features located at 1120 – 1140 nm, 1400 – 1540 nm, 1620 – 1700 nm, and 1930 nm regions using an adaptation of the subroutine called “findpeaks”. These regions were judged to be the most well-defined absorbance peaks visible across all three fabric types (Figure 4.4 – 4.6). However, numerical results from MatLab did not match with observable feature changes for selected wavelength regions (e.g. areas/prominence values increasing when visually decreasing

in input data). The results obtained from this MatLab investigation are contained in Appendix D for completeness. It is possible the built-in subroutine for finding and analysing graph features could be modified further in the future to improve these results. For this current study Microsoft Excel® was used to calculate absorbance feature characteristics such as continuum removed feature area or local feature prominence (Figure 4.15b and 4.15c).

Manual manipulation of the absorbance data was used to calculate the continuum removed areas of the absorbance features (Figure 4.15b) using a straight-line segment between the local bounds (Appendix E) of the feature (Zhang, et al. 2012). These changes in feature area were then related to the incident heat flux exposure and the percentage change in original tensile strength for all three fabric types and are featured in Figure 4.19. The feature area was normalized to the unaged feature area for each wavelength region. An inverse of the normalized feature area ($A_n$) was related to the remaining tensile strength in order to improve readability of the data. The feature area experiences a large change during initial heat flux exposure levels while the tensile strength values experience a small change. The UV changes are not featured due to the lack of discernible trends in the limited trials considered in this study.

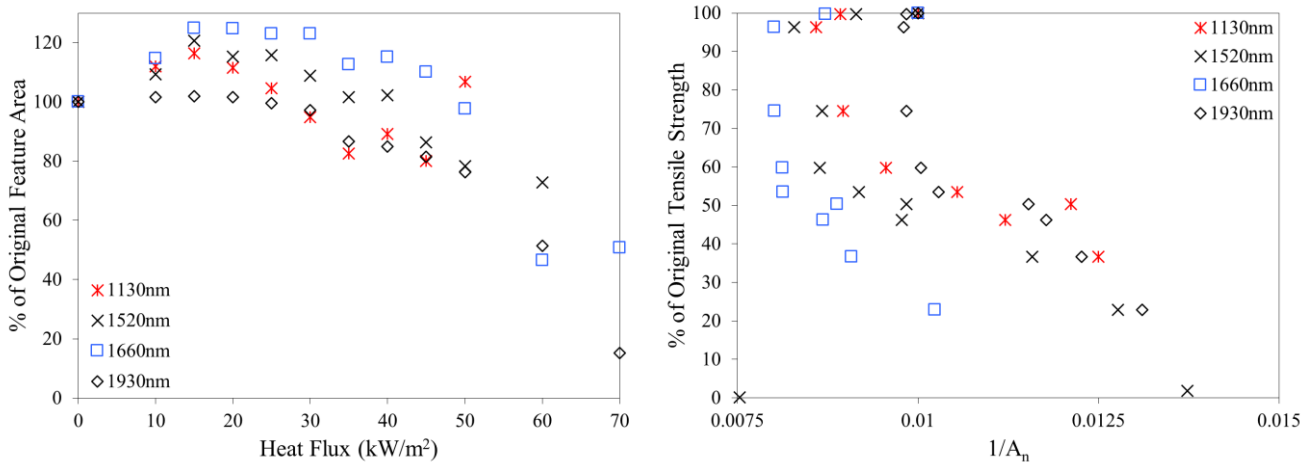


(a)

*Figure 4.19 Absorbance feature area changes in relation to (left) incident heat flux exposure and (right) percentage change from unaged tensile strength for the (a) RS Natural, (b) RS Black, and (c) SCI PBI Max fabrics at 1130, 1520, 1660, and 1930 nm regions*

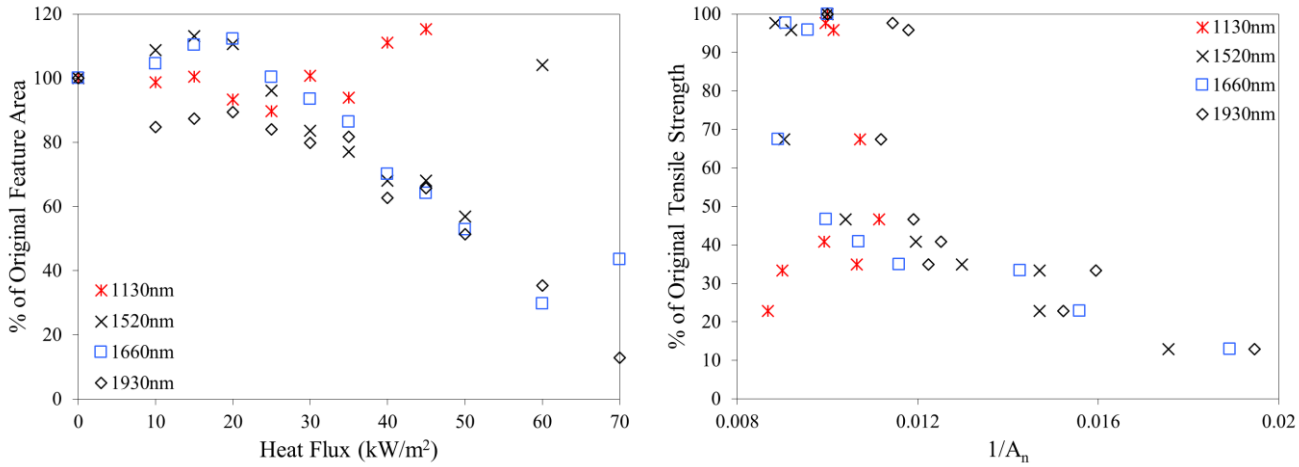


(b)

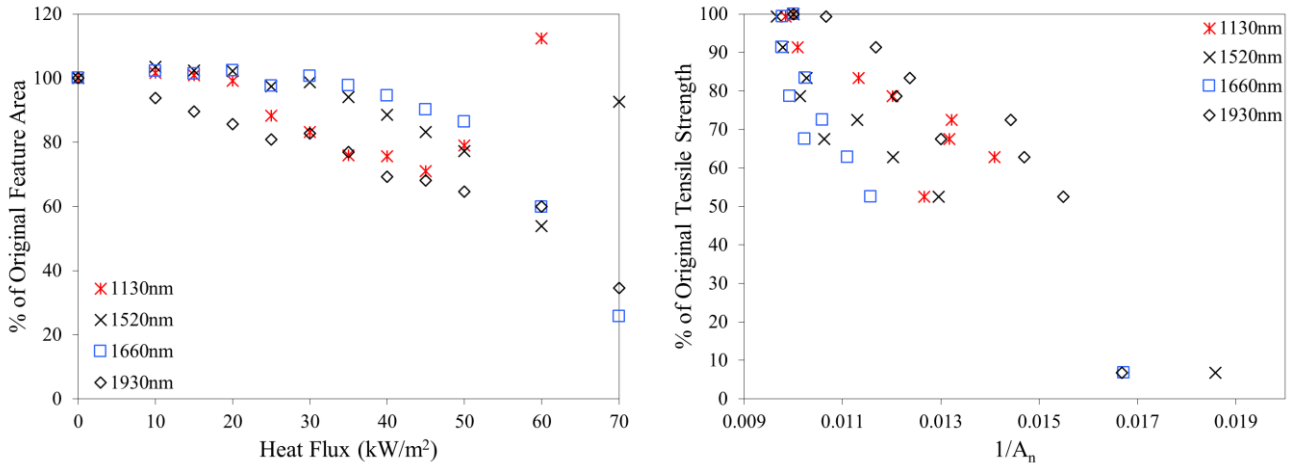


(c)

*Figure 4.19 Continued*

The changes in feature prominence (Figure 4.15c) was also examined across all fabric types. Again, the local feature prominence was normalized ($P_n$) to the unaged feature prominence. An inverse of this normalized prominence was related to the remaining tensile strength in order to increase readability in a similar fashion to the previous area changes. These results (Figure 4.20) show that prominence of an absorbance feature could be used to determine the remaining tensile strength of protective clothing considered in this study.

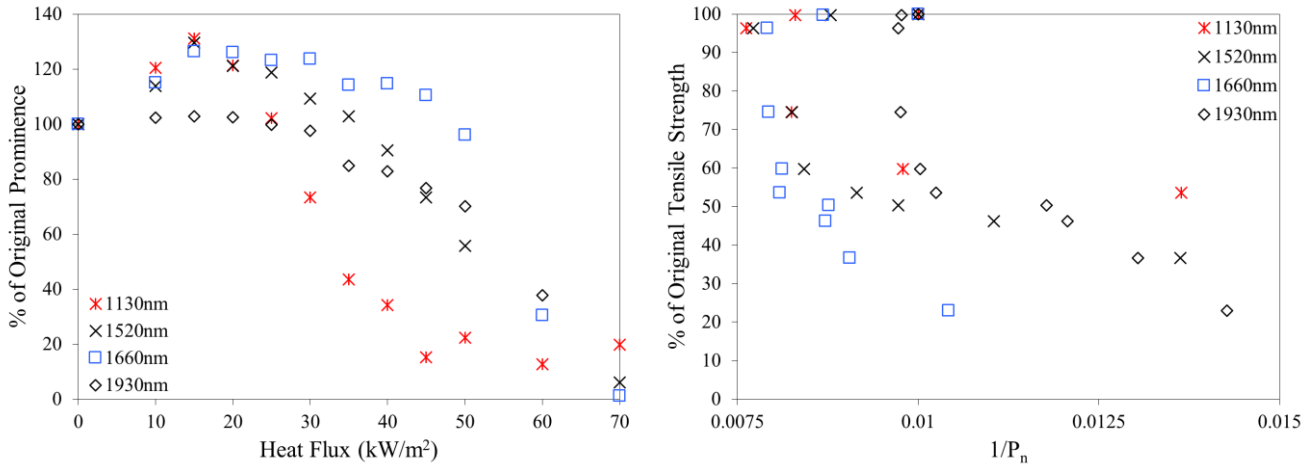


(a)

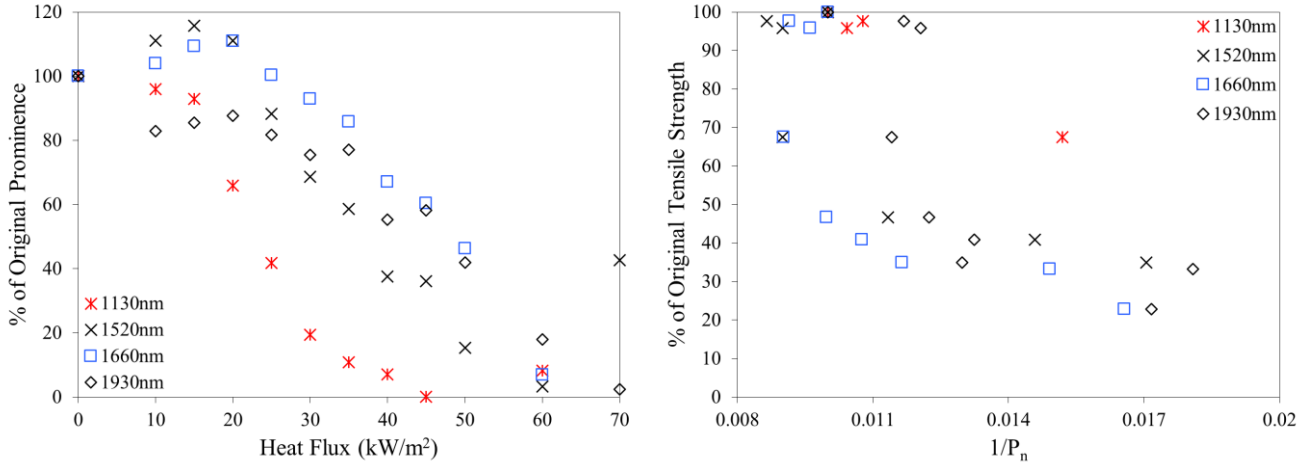


(b)

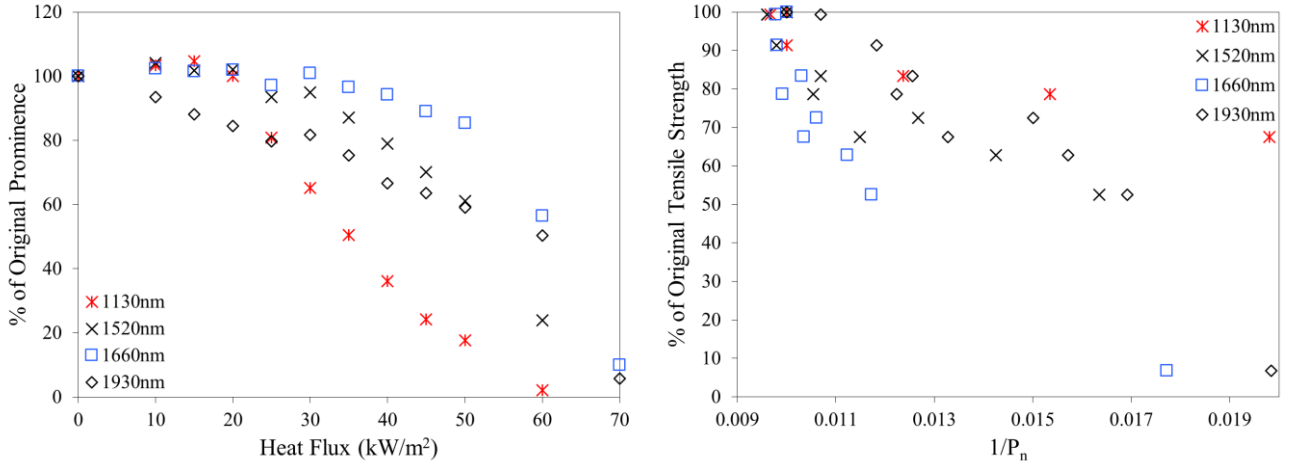


(c)

*Figure 4.20 Absorbance local prominence changes in relation to (left) incident heat flux exposure and (right) percentage change from unaged tensile strength for the (a) RS Natural, (b) RS Black, and (c) SCI PBI Max fabrics at 1130, 1520, 1660, and 1930 nm regions*

A number of general data trends emerge when peak prominence and area are plotted for these key 1130, 1520, 1660, and 1930 nm absorption features of all fabric types.

- **1130 nm:** this feature shows the largest sensitivity to thermal ageing exposure. This absorbance feature shows a 50% decline in local peak prominence and similar decreases in peak area. The feature also vanishes after 25 kW/m$^2$ exposure conditions across all fabrics. This could be evidence of the chemical bond's sensitivity to thermal damage (Arrieta, et al. 2010).
- **1520 nm:** This feature holds prominence and area longer than the 1130 nm absorbance features. It begins to show a drastic decrease (-75%) in both prominence and area after the 30 kW/m$^2$ exposure. The feature vanishes by the 40 kW/m$^2$ exposure for RS (both Natural and Black) constructions, but is still measureable at 50 kW/m$^2$ for the SCI PBI Max fabric. This could be evidence of chemical bond structure damage (Arrieta, et al. 2010).
- **1660 nm:** This feature shows an increasing trend in both prominence and area from unaged to 20 – 25 kW/m$^2$ exposures and then a decreasing trend after 30 kW/m$^2$ for both RS fabrics. Again the PBI Max fabric maintains features longer when subjected to a higher thermal exposure of 40 kW/m$^2$ before a decrease occurs. SCI PBI Max also appears more flat in both prominence and area features after lower thermal exposures when compared to the RS fabrics. This could be evidence the chemical bonds in hydrogen linked amide survive low heat flux exposure, but are sensitive to high temperatures (Arrieta, et al. 2010).
- **1930 nm:** It is difficult to draw any meaningful conclusions based on influence of the water absorbance band near this region (Section 4.1.1). The peak prominence of this feature declines with thermal exposures up to 20 kW/m$^2$ (17% loss for RS Natural and SCI PBI Max and about 40% loss for RS Black). This feature prominence then increases after 30 kW/m$^2$ remains measurable up to the 60 kW/m$^2$ exposure. The peak area remains flat with only significant change after the 35 kW/m$^2$ thermal exposure.

Unlike the absorbance feature changes resultant from thermal ageing the UV results do not demonstrate significant changes (Figure 4.13). Only the feature at 1660 nm appears to show any significant response to increased UV ageing exposure times and this response is not consistent

across all fabric types. However, only three UV ageing conditions are examined in this study and it is possible that a greater variety of exposure lengths and UV ageing trials could yield more potential results in future studies.

## 4.2.3. Normalized Difference Index

An investigation of slope change was performed between 1160 and 1360 nm regions of reflectance with the use of a normalized difference index (NDI) method (Figure 4.15d). A normalized difference index (Gau 1996) method was used to evaluate this slope change and relate this change to the percentage of remaining tensile strength (Figure 4.21). This normalized difference index was calculated through the equation:

$$NDI = \frac{\rho_{1360} - \rho_{1160}}{\rho_{1360} + \rho_{1160}} \qquad (4.2)$$

In this case $\rho_{1360}$ is equal to the reflectance value at 1360 nm and $\rho_{1160}$ is the reflectance value at the 1160 nm.

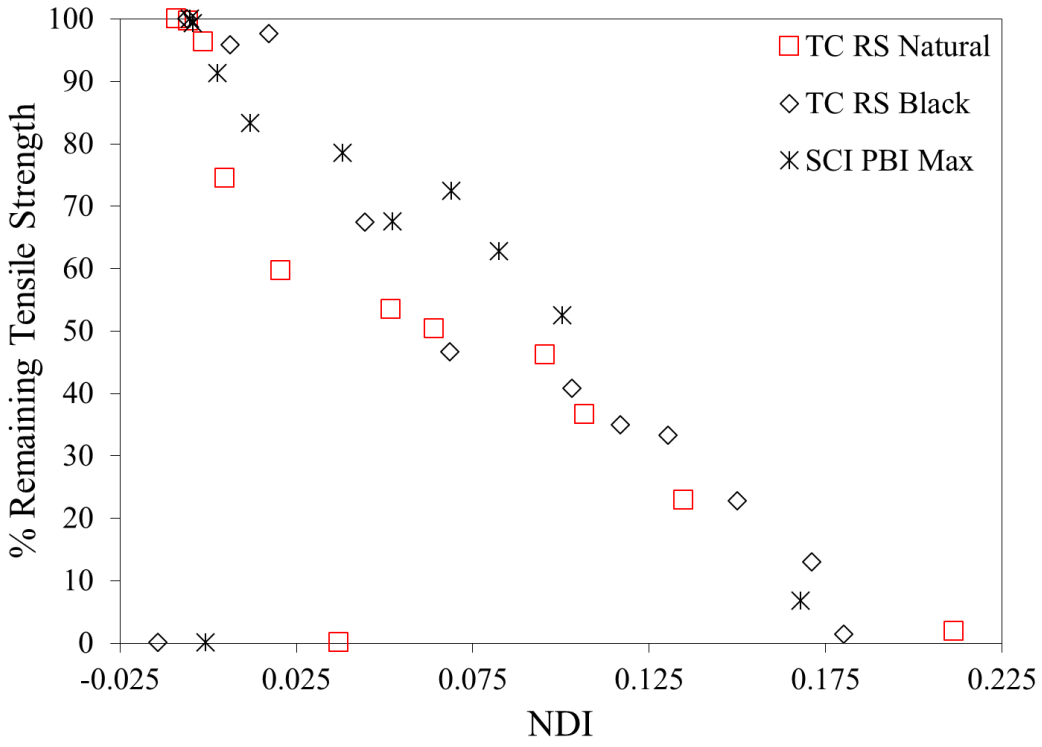


*Figure 4.21 Normalized difference index (NDI) of the reflectance slope change between 1160 and 1360 nm reflectance readings in relation to remaining tensile strength following thermal ageing*

The NDI method seems to show the best relation between NIR results and percentage changes in tensile strength due to thermal ageing. Initial slope changes seem varied across all fabric types after lower heat flux exposure (unaged to 30 kW/m$^2$), but have a much closer cross-fabric correlation when compared to previous methods of NIR analysis. Furthermore, the NDI of this selected slope region of the three fabrics obtained in this study appear to reach similar values (e.g. NDI of 0.1 – 0.175 in Figure 4.21) for thermally aged fabrics exposed to conditions greater than 40 kW/m$^2$. The 70 kW/m$^2$ exposures (bottom left three points in Figure 4.21) do not add much information to the overall trend due to their near-zero tensile strength values and have been removed from Figure 4.22 to showcase a cleaner comparison of the different NDI trends between the three fabric types.

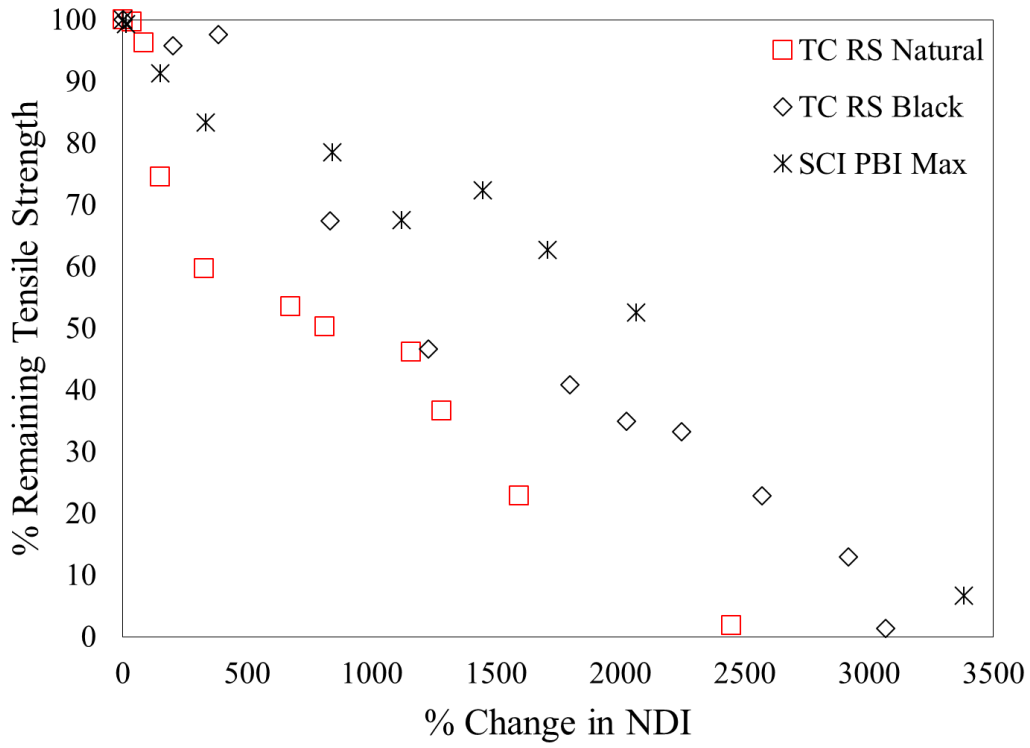


*Figure 4.22 Percentage change in the NDI between 1160 and 1360 nm reflectance readings in relation to the percentage decrease in tensile strength from thermal ageing exposure*

The NDI method of analysis also has benefits when considering the implementation of a commercial device. Utilizing a device that requires scanning a large range of wavelength values would be prohibitively expensive for many departments, but creating a device that measures and

compares two reflectance values from selected wavelength locations could prove economically viable. Additionally, the magnitude of percent change in the NDI between the 1160 and 1360 nm region is high when compared to the change in tensile strength (i.e. percentage change in NDI > 100% compared to < 30% decrease in tensile strength). This large change in NDI (Figure 4.22) could be useful for detecting small changes in fabric performance over the entire lifecycle of protective clothing.

## 4.3. Near Infrared Evaluation Summary

Each method of correlation to fabric tensile strength has a number of positive and negative qualities that are detailed in this section and summarized below.

- **Percentage change in reflectance at key wavelengths:**
    - Positives: quick, relatively easy to find flat reflectance/absorbance region.
    - Negatives: reflectance either increase or decrease depending on exposure, statistical analysis methods can give different results depending on the assumptions made (e.g. driving negative values to zero influences results, but improves readability), difficult to relate simple percentage changes to underlying chemical structure changes.
- **Absorbance feature area:**
    - Positives: relation to base chemical structures detailed in literature, trends show less deviation across fabric types, area change dependant on increased ageing conditions, data analysis can be performed using programming software (e.g. MatLab).
    - Negatives: trends in data may depend on selected wavelength (Figure 4.19), difficulty assigning feature area/width bounds, location of peak may change with ageing (e.g. 1920 nm region shifts), influence of foreign material on feature characteristics (e.g. dirt or ash).
- **Absorbance feature local prominence:**
    - Positives: relation to base chemical structures detailed in literature, does not depend on feature position, prominence change dependant on increased ageing

conditions, data analysis can be performed using programming software (e.g. MatLab).

  - Negatives: trends in data may depend on selected wavelength (Figure 4.20), ambiguity in some wavelength regions (e.g. multiple Gaussian features overlapping (Figure 4.1 – 4.3 1500 nm region), impact of entrained moisture (Section 4.1.1), less information on relation of absorbance prominence to chemical structure in literature, influence of foreign material on feature characteristics (e.g. dirt or ash).

- **Normalized Difference Index (NDI):**
  - Positives: best result convergence (e.g. trends appear similar regardless of fabric type), can be based on two wavelength readings (easily obtained), and reduced sensitivity to overall vertical shifts in reflectance or absorbance.
  - Negatives: does not give background chemical information, lack of information in literature on application to textile analysis.

# 5. Conclusions and Future Work

Firefighters' protective clothing must meet well-defined performance standards when new. However, similar quantitative metrics for in-use and aged clothing are not outlined by available standards. Current retirement guidelines rely on visual indicators, basic water penetration tests, and operator judgement. This leads to the possibility of continued use of firefighter clothing that may no longer meet performance requirements and stresses the need for increased information on the ageing of textiles used in firefighters' clothing.

A number of factors will influence the degradation process in an active field setting. Two factors, thermal and ultraviolet (UV) light exposure, were selected to age common outer shell fabrics used in the construction of firefighter's protective clothing. These exposure conditions will be experienced by a firefighter in the field and have been shown to induce both thermochemical and photooxidative changes in protective clothing textiles. Thermogravimetric analysis was carried out on the outer shell fabrics. Thermal ageing was accomplished using a primarily radiative exposure from the conical heater of a cone calorimeter and UV ageing was completed using a xenon-arc Weatherometer. Temperature profiles were recorded on the back of fabrics during thermal exposure to help explain performance and thermochemical changes. Following a detailed review of the current literature tensile strength was selected as a key material indicator of remaining fabric performance and evaluation of ageing exposure. Textile fibre microstructure degradation was examined using a scanning electron microscope. Near infrared scans were conducting using a spectrophotometer and related to remaining fabric tensile strength using multiple methods of analysis. The benefits and drawbacks of each NIR analysis method were discussed.

## 5.1. Conclusions

In this study outer shell fabrics consisting of 60/40% Kevlar®/PBI blends in the RS Natural, RS Black, and SCI PBI Max fabrics were subjected to thermal and UV exposure conditions. Major deteriorations in tensile strength were observed following both forms of ageing, but thermal ageing appears to be a more severe form of ageing by this measure.

Heat flux exposures were conducted from 0 – 70 kW/m$^2$ in order to simulate a range of firefighter working conditions. The length of thermal exposure was limited to a single time-controlled exposure for each heat flux. Lower heat flux exposures (10 – 15 kW/m$^2$) did not result in significant change of the fabrics, but significant loss of tensile strength was observed with increasing heat flux exposure (20 – 30 kW/m$^2$). Fabric strength levels fall below requirements (NFPA 1971 2013) for Ripstop fabrics following exposure to 35 kW/m$^2$ and 45 kW/m$^2$ for the PBI fabrics, respectively. Further decreases in tensile strength were observed in relation to increasing heat flux until a total loss of original tensile strength following exposure to 70 kW/m$^2$.

Ultraviolet light exposures were conducted from 0 – 160 SFH levels. The loss in strength of the UV aged specimens indicates photooxidative degradation of the fabrics. Tensile strength of the fabrics decreased with increased duration of UV exposure for all fabric types, but the remaining strength stayed above requirements (NFPA 1971 2013) until the highest levels of exposure considered in this study. These results confirm that UV sensitivity is an important portion of the ageing process of firefighter's protective clothing, but that a majority of losses in tensile strength of outer shell materials will depend on thermal exposure for the fabrics considered in this study. However, real-world UV exposures may be much longer and more varied in intensity (i.e. cloudy day in Saskatoon, SK. versus full sun in Phoenix, AZ).

A scanning electron microscope was used between magnification levels of 350 – 3000x to examine microstructural degradation due to thermal and UV ageing. From the thermally aged specimens a microstructural crack development process was found to occur. This process started with the development of microstructure cracks from crack initiation, progressed to partial thickness crack propagation, and full thickness cracks resultant from increasing thermal ageing exposure conditions. This crack development process could explain significant losses experienced in the tensile strength of the fabrics. Additionally, the overall shifting behaviour of NIR reflectance results could also be explained by increased absorbance due to the crack and hole development in the individual fibers. These cracks and holes would lower the reflectance values of incident light. This would be further compounded by the increased carbonization following the highest heat flux exposures. The UV exposed specimens showed a similar development of holes and increased/elongated striations in fabric microstructures with evidence

of increased brittleness of the surface structures. However, the full material loss and damage (e.g. charring and burning of surface) appeared less significant when compared to thermally aged microstructures.

A non-destructive evaluation study was conducted based on the spectral results obtained in the near infrared region. Near infrared reflectance readings were taken in the 400 – 2000 nm region, but focused to the 800 – 2000 nm region to avoid analysis of spectral regions with a significant sensitivity to colour change. Additionally, wavelength regions in 1880 – 2000 nm region found to be sensitive to moisture content of the fabric. Spectral reflectance results experienced significant change in thermally aged specimens. On the other hand, the reflectance results for UV aged specimens did not show significant change. Key wavelength regions related to chemical bonds (e.g. features located at 1130, 1520, 1660 nm) in the fabrics showed evidence of change with increased thermal ageing exposure conditions. Four different methods of evaluating the changes in spectral NIR reflectance results were examined and compared.

The spectral data obtained from NIR reflectance results was correlated to tensile strength using relations between percentage change in reflectance for key wavelengths, absorbance feature analysis (e.g. area or prominence changes), and the use of a normalized-difference index method. Each method was found to have positive and negative attributes. Using the percentage change in reflectance at a key wavelength location is quick and relatively easy, but due to the increasing or decreasing values of reflectance, these relations can become ambiguous and give varied results depending on the fabric being examined. Analysis of a feature area at key wavelength locations can be related to base chemical structures of the fabrics and these results were found to be consistent across different fabric types. However, the generation of significant and possibly confusing information combined with difficulties in assigning area bounds to changing areas or widths of reflectance features made this method less robust. This problem was reduced through evaluation of the local prominence or peak height of the spectral feature, but this third method could still be confusing and introduce ambiguity in some wavelength regions. For example, reflectance results with multiple overlapping Gaussian features could cause significant difficulty in interpreting results. The final method considered in this study consisted of examining slope changes between wavelength regions in the form of a normalized difference

index. This method showed the most promise at relating the level of ageing between the fabric types examined in this study and relies on two wavelength readings that could be easily obtained by a commercially viable device in the future. Future work related to improving retirement guidelines and the development of a predictive model for the evaluation firefighter's protective clothing should consider this normalized-difference index method of analysis.

## 5.2. Future Work

A number of important questions for future research studies were raised over the course of this current study. Increased variety and intensity in the ageing exposure process, further and more detailed microstructure examination, and the impact of ageing on moisture transfer and regain in protective clothing could all significantly contribute to the available literature.

The thermal ageing process considered was performed in a range of primarily radiative exposures, but only considered single exposures. The test matrix in future studies could be expanded to included smaller step increases in heat flux levels (e.g. more steps between critical 15 – 30 kW/m$^2$ region), varied durations for single-stage exposures, and the inclusion of multi-stage exposures (similar to Rezazadeh, 2014) in order to obtain more detailed information and data sets regarding the change in performance of these outer shell materials. Increasing the number of heat flux exposures in the critical region (e.g. 15 – 35 kW/m$^2$ conditions where the largest changes in tensile strength occur) could be key to understanding how firefighters' clothing ages when subjected to thermal exposure conditions in the field setting.

Ultraviolet light ageing was performed, but only at three time-controlled durations. The UV ageing process requires significant exposure time, but future studies could increase both the number of UV exposures considered and include multi-stage exposures. Additionally, information on the photooxidative process could be obtained through a detailed chemical analysis (e.g. thermogravimetric analysis combined with FTIR analysis of volatile by-products) of future UV aged protective fabrics. Combined ageing trials with both thermal and UV ageing procedures conducted on a single specimen could give more information on combined ageing processes.

Non-destructive SEM and NIR techniques were used to analyze aged fabrics. A larger amount of information on microstructure changes and proposed “crack propagation” processes could be obtained in future studies by considering synchrotron-based, atomic-force microscopy, and/or laser scanning confocal microscopy (Davis, et al. 2010) techniques of surface analysis. Performing this comprehensive microstructure examination could be combined with detailed analytical chemistry procedures to fully outline the thermochemical and mechanical ageing process experienced by outer shell fabrics in firefighters’ clothing.

A brief investigation of varying preconditioning humidity levels was performed. This portion of the current study revealed that the NIR region 1880 – 2000 nm is sensitive to entrained moisture. Future studies could consider a wider range of preconditioning environments. In this study information obtained could give new insight on how the ageing process impacts water retention and moisture regain (Chin, et al. 2007) that occurs in aged firefighters’ clothing. This information could be very useful for the development of a commercial device. It is likely that different fire departments will have different levels of ambient relative humidity and climate control systems in clothing storage areas depending on their geographic location.

# References


Abbott, N.J., and S. Schulman. 1976. "Protection from fire: non-flammable fabrics and coatings." *Journal of Industrial Textiles* 6 (1): 48-64.

Aidani, R., P. Dolez, and T. Vu-Khanh. 2011. "Effect of thermal aging on the mechanical and barrier properties of an e-PTFE/Nomex® moisture membrane used in firefighters' protective suits." *Journal of Applied Polymer Science* 121 (5): 3101-3110.

Aidani, R., P. Nguyen-Tri, Y. Malajati, J. Lara, and T. Vu-Khanh. 2013. "Photochemical aging of an e-PTFE/NOMEX® membrane used in firefighter protective clothing." *Polymer Degradation and Stability* 98 (7): 1300-1310.

An, S.K., R.L. Barker, and J.O. Stull. 1989. "Measurement of the flammability and thermal aging of chemical protective suit materials." *Chemical Protective Clothing Performance in Chemical Emergency Response, ASTM STP 1037*, 86-101.

Arrieta, C., E. David, P. Dolez, and T. Vu-Khanh. 2011b. "Hydrolytic and photochemical aging studies of a Kevlar®-PBI blend." *Polymer Degradation and Stability* 96 (8): 1411-1419.

Arrieta, C., E. David, P. Dolez, and T. Vu-Khanh. 2010. "Thermal aging of a blend of high-performance fibres." *Journal of Applied Polymer Science* 93 (5): 3031-3039.

Arrieta, C., E. David, P. Dolez, and T. Vu-Khanh. 2011a. "X-ray diffraction, Raman, and differential thermal analyses of the thermal aging of a Kevlar-PBI blend fabric." *Polymer Composites* 32 (3): 362-367.

ASTM D1230-10e1. 2016. *Standard test method for flammability of apparel textiles.* West Conshohocken, PA: American Society for Testing and Materials.

ASTM D1776/D1776M-16. 2016. *Standard practice for conditioning and testing textiles.* West Conshohocken, PA: American Society for Testing and Materials.

ASTM D2261-13. 2013. *Standard test method for tearing strength of fabrics by the tongue (Single rip) procedure (Constant-rate-of-extension tensile testing machine).* West Conshohocken, PA: American Society for Testing and Materials.

ASTM D3776/D3776M-09a. 2013. *Standard test methods for mass perunit area (weight) of fabric.* West Conshohocken, PA: American Society for Testing and Materials.

ASTM D5034-09. 2013. *Standard test method for breaking strength and elongation of textile fabrics (Grab test).* West Conshohocken, PA: American Society for Testing and Materials.

ASTM D5035-1. 2015. *Standard test method for breaking force and elongation of textile fabrics (strip method).* West Conshohocken, PA: American Society for Testing and Materials.

ASTM D6413/D6413M-15. 2015. *Standard test method for flame resistance of textiles (Vertical test).* West Conshohocken, PA: American Society for Testing and Materials.

ASTM D737-04. 2016. *Standard Test Method for Air Permeability of Textile Fabrics.* West Conshohocken, PA: American Society for Testing and Materials.

ASTM E104-02. 2012. *Standard practice for maintaining constant relative humidity by means of aqueous solutions.* West Conshohocken, PA: American Society for Testing and Materials.

ASTM E1131-08. 2014. *Standard test method for compositional analysis by thermogravimetry.* West Conshohocken, PA: American Society for Testing and Materials.

ASTM E1354-16a. 2016. *Standard test method for heat and visible smoke release rates for materials and products using an oxygen consumption calorimeter.* West Conshohocken, PA: American Society for Testing and Materials.

ASTM F1449-08. 2015. *Standard guide for industrial laundering of flame, thermal, and arc resistant clothing.* West Conshohocken, PA: American Society for Testing and Materials.

ASTM F1930-15. 2015. *Standard test method for evaluation of flame resistant clothing for protection against fire simulations using an instrumented manikin.* West Conshohocken, PA: American Society for Testing and Materials.

ASTM F1939-15. 2015. *Standard test method for radiant heat resistance of flame resistant clothing materials with continuous heating.* West Conshohocken, PA: American Society for Testing and Materials.

ASTM F2700-08. 2013. *Standard test method for unsteady-state heat transfer evaluation of flame resistant materials for clothing with continuous heating.* West Conshohocken, PA: American Society for Testing and Materials.

ASTM F2757-09. 2016. *Standard guide for home laundering care and maintenance of flame, thermal and arc resistant clothing.* West Conshohocken, PA: American Society for Testing and Materials.

Atalay, O., S. Bahadir, and F. Kalaoglu. 2015. "An analysis on the moisture and thermal protective performance of firefighter clothing based on different layer combinations and effect of washing on heat protection and vapour transfer performance." *Advances in Materials Science and Engineering* 2015 (540394).

Barnett, R., and K. Slater. 1991. "The progressive deterioration of textile materials, part V: the effects of weathering on fabric durability." *Journal of the Textile Institute* 82 (4): 417-425.

CAN/CGSB 4.2 No. 36-M89. 1997. *Textile Test Methods Air Permeability.* Ottawa, ON: Canadian General Standards Board.

CAN/CGSB-155.1. 2001. *Firefighters' protective clothing for protection against heat and flame.* CAN/CGSB Standard, Ottawa, ON: Canadian General Standards Board.

Chalmers, J.M., and P.R. Griffiths. 2001. *Handbook of vibrational spectroscopy.* New York, NY: John Wiley and Sons.

Chin, J., A. Forster, C. Clerici, L. Sung, M. Oudina, and K. Rice. 2007. "Temperature and humidity aging of poly( p-phenylene-2,6-benzobisoxazole) fibers: Chemical and physical characterization." *Polymer Degradation and Stability* 1234-1246.

Cinnamon, M.L. 2013. *Post use analysis of firefighter turnout gear-phase III.* MSc Thesis, Lexington, KY: University of Kentucky.

Clark, R.N. 1983. "Spectral properties of mixtures of montmorillonite and dark carbon grains: Implications for remote sensing minerals containing chemically and physically adsorbed water." *Journal of Geological Research* 88 (B12): 10635-10644.

Clark, R.N., and T.L. Roush. 1984. "Reflectance spectroscopy: Quantitative analysis techniques for remote sensing applications." *Journal of Geophysical Research* 89 (B7): 6329-6340.

Cloud, R.M., and P. Lowe. 1995. "Effects of field-wear abrasion on barrier properties of nonwoven fabrics." *Clothing and Textile Research Journal* 13 (3): 159-164.

Cui, Z., C. Ma, and N. Lv. 2015. "Effects of heat treatment on the mechanical and thermal performance of fabric used in firefighter protective clothing." *Fibres and Textiles in Eastern Europe* 23 (2): 74-78.

Davis, R., J. Chin, C. Lin, and S. Petit. 2010. "Accelerated weathering of polyaramid and polybenzimidazole firefighter protective clothing fabrics." *Polymer Degradation and Stability* 95 (9): 1642-1654.

Day, M., J.D. Cooney, and T. Suprunchuk. 1988. "Durability of firefighter's protective clothing to heat and light." *Textile Research Journal* 58 (3): 141-147.

Donnelly, M.K., W.D. Davis, J.R. Lawson, and M.J. Selepak. 2006. *Thermal environment for electronic equipment used by first responders.* NIST Technical Note 1474, Gaithersburg, MD: National Institute of Standards and Technology.

DuPont. 2016. *Protecting the DuPont™ Kevlar® brand.* Accessed June 27, 2017 . http://www.dupont.com/products-and-services/fabrics-fibers-nonwovens/fibers/articles/trademarks-licensing.html.

EN 367. 1992. *Protective clothing – Protection against heat and fire – Method of determining heat transmission on exposure to flame.* Brussels, Belgium: European Committee for Standardization.

EN 469. 2005. *Protective clothing for firefighters – Performance requirements for protective clothing for firefighting.* Brussels, Belgium: European Committee for Standardization.

Federal Trade Commission. 2009. *Generic names and definitions for manufactured fibres.* Washington. DC: National Archives and Records Administration.

Fortier, C., J. Montalvo, T. Von Hoven, M. Easson, J. Rodgers, and B. Condon. 2014. "Preliminary evidence of oxidation in standard oven drying of cotton: attenuated total reflectance/Fourier transform infrared spectroscopy, colorimetry, and particulate matter formation." *Textile Research Journal* 84: 157-173.

Frank, A.S. 1997. *Handbook of instrumental techniques for analytical chemistry.* Edited by A.S. Frank. Upper Saddle River, NJ: Prentice Hall.

Fulton, M., M. Fauchoux, D.A. Torvi, and A. Beitel. 2017a. "Comparison of temperatures measured during sprinklered and unsprinklered public fire demonstrations." *Proceedings of Combustion Institute - Canadian Section, Spring Technical Meeting.* Montreal, QC. (Paper #5, Fire Research Session, pages 1-6).

Fulton, M., M. Fauchoux, D.A. Torvi, and A. Beitel. 2017b. "Heat flux measurements during a full-scale house fire." *Proceedings of Combustion Institute - Canadian Section, Spring Technical Meeting* (Paper #1, Fire Research Session, pages 1-6).

Fulton, M., M. Rezazadeh, and D.A. Torvi. 2017. "Tests for evaluating textile ageing." In *Advanced Characterization and Testing of Textiles*. Cambridge, UK: Woodhead Publishing.

Garside, P., P. Wyeth, and X. Zhang. 2011. "Use of near IR spectroscopy and chemometrics to assess the tensile strength of historic silk." *e-PRESERVATIONScience* 8: 68-73.

Gau, Bo-cai. 1996. "NDWI - A normalized difference water index for remote sensing of vegetation liquid water from space." *Remote Sensing of Environment* 58 (3): 257-266.

Ghosh, S., M.D. Cannon, and R.B. Roy. 1990. "Quantitative analysis of durable press resin on cotton fabrics using near-infrared reflectance spectroscopy." *Textile Research Journal* 60 (3): 167-172.

Goddu, R.F., and D. Delker. 1960. "Spectra-structure correlations for near-infrared." *Analytical Chemistry* 32: 140-141.

Gu, X., B. Dickens, D. Stanley, W.E. Byrd, T. Nguyen, I. Vaca-Trigo, WQ. Meeker, J. Chin, and JW. Martin. 2008. "Linking accelerating laboratory test with outdoor performance results for a model epoxy coating system." In *Service Life Prediction of Polymeric Materials: Global Perspectives,* edited by JW. Martin, RA. Ryntz, J. Chin and R. Dickie, 3-28. Berlin, Germany: Springer.

Hadjianfar, M., D. Semnani, and M. Sheikhzadeh. 2010. "A new method for measuring luster index based on image processing." *Textile Research Journal* 80: 726-733.

Hedrick, S.E., R.M. Bennett, T.G. Rials, and S.S. Kelley. 2007. "Correlation of near-infrared spectroscopy measurements with the properties of treated wood." *Journal of Materials in Civil Engineering* 19 (4): 279-285.

Hewlett-Packard Company. 1999. *Agilent 34970A data acquisition/switch unit: Edition 3.* Palo Alto, CA, USA: Hewlett-Packard Company.

House, J., and J. Squire. 2004. "The effect of wear and washing on the protection afforded by the new Royal Navy fire fighters' protective hood." *International Journal of Clothing Science Technology* 16: 368-373.

Houshyar, S., R. Padhye, R. Nayak, and R.A. Shanks. 2015. "Deterioration of polyaramid and polybenzimidazole woven fabrics after ultraviolet irradiation." *Journal of Applied Polymer Science* 133 (9).

ISO 13506. 2008. *Protective clothing against heat and flame - Test method for complete garments - Prediction of burn injury using an instrumented manikin.* ISO Standard, Geneva, Switzerland: International Standards Organization.

ISO 6942. 2002. *Protective clothing - Protection against heat and fire - Method of test: Evaluation of materials and material assemblies when exposed to a source of radiant heat.* Geneva, Switzerland: International Standards Organization.

Iyer, R.V., A. Sudhakar, and K. Vijayan. 2006. "Decomposition behaviour of Kevlar 49 fibres: Part II. At T values < Td." *High Performance Polymers* 18 (4): pp. 495–517.

Iyer, R.V., and K. Vijayan. 1999. "Decomposition behaviour of Kevlar 49 fibres: Part I. at T≈Td." *Bulletin of Materials Science* 22 (7): 1013–1023.

Jain, A., and K. Vijayan. 2002. "Thermally induced structural changes in Nomex fibres." *Bulletin of Material Science* 25 (4): 341-346.

Johnson, M.L. (Ed.). 2005. *The Cambridge handbook of age and ageing.* Cambridge: The Cambridge University Press.

Kelley, S.S. 2003. Method of predicting mechanical properties of decayed wood. Kansas City, MO Patent US 6593572 B2.

Kludt, K.D. 2003. *Use of near infrared spectroscopy technology for predicting bending properties of clear wood specimens.* MSc Thesis, Pullman, WA.: Washington State University.

Loftin, D. 1992. *The durability of flame resistant fabrics in an industrial laundry environment: Performance of Protective Clothing: Fourth Volume, STP19205S.* West Conshohocken, PA: American Society for Testing and Materials, 775-784.

Makinen, H. 1992. *The effect of wear and laundering on flame-retardant fabrics: Performance of Protective Clothing: Fourth Volume, STP19203S.* West Conshohocken, PA: American Society for Testing and Materials, 754-765.

McClure, F. 2004. "Review: 204 years of near infrared technology 1800–2003." *Journal of Near Infrared Spectroscopy* 11 (6): 487-518.

McQuerry, M., S. Klausing, D. Cotterill, and E. Easter. 2015. "A post-use evaluation of turnout gear using NFPA 1971 standard on protective ensembles for structural fire fighting and NFPA 1851 on selection, care and maintenance." *Fire Technology* 51 (5): 1149-1166.

Mora, C.R. 2009. *Rapid techniques for screening wood properties in forest plantations.* PhD Thesis, Athens, GA: University of Georgia.

Mosquera, M.E.G., M. Jamond, A. Martinez-Alonzo, and J.M.D. Tascon. 1994. "Thermal transformations of Kevlar aramid fibers during pyrolysis: infrared and thermal analysis studies." *Chemistry of Materials* 6 (11): 1918-1924.

National Fire Protection Association. 2016. *Fire Statistics.* Accessed June 19, 2017. http://www.nfpa.org/news-and-research/fire-statistics-and-reports/fire-statistics.

Nazare, S., R.D. Davis, J.S. Peng, and J. Chin. 2012. *Accelerated weathering of firefighter protective clothing: delineating the impact of thermal, moisture, and ultraviolet light exposures.* NIST Technical Note 1746, Gaithersburg, MD: National Institute of Standards and Technology.

NFPA 1851. 2014. *Selection, care, and maintenance of protective ensembles for structural fire fighting and proximity fire fighting.* Quincy, MA: National Fire Protection Association.

NFPA 1971. 2013. *Standard on protective ensembles for structural fire fighting and proximity fire fighting.* Quincy, MA: National Fire Protection Association.

NFPA 2113. 2015. *Standard on selection, care, use, and maintenance of flame-resistant garments for protection of industrial personnel against short-duration thermal exposures.* Quincy, MA: National Fire Protection Association.

Onions, W.J., and K. Slater. 1967. "The automatic comparison of roving and yarn irregularities during drafting." *Journal of the Textile Institute* 58: 210 – 219.

Ozgen, B., and G. Pamuk. 2014. "Effects of thermal aging on Kevlar and Nomex fabrics." *Industria Textila* 65 (5): 254-262.

Pickett, J.E., and J.R. Sargent. 2009. "Sample temperatures during outdoor and laboratory weathering exposures." *Polymer Degradation and Stability* 94 (2): 189-195.

Poli, T., L. Toniolo, and A. Sansonetti. 2006. "Durability of protective polymers: the effect of UV and Thermal Ageing." *Macromolecules in Cultural Hertiage* 238 (1): 78-83.

Randall, D. 1998. *Instruments for the measurement of color.* AATCC Review 30 (2), Charlotte, NC: Datacolor International, pp. 20-26.

Rezazadeh, M. 2014. *Evaluation of performance of in-use firefighter's protective clothing using non-destructive tests.* PhD Thesis, Saskatoon, SK: University of Saskatchewan.

Rezazadeh, M., and D.A. Torvi. 2011. "Assessment of factors affecting the continuing performance of firefighters' protective clothing: a literature review." *Fire Technology* 47 (3): 565-599.

Richardson, E., G. Martin, P. Wyeth, and X. Zhang. 2008. "State of the art: non-invasive interrogation of textiles in museum collections." *Microchimica Acta* 162 (2): 303-312.

Rodgers, J., C. Fortier, J. Montalvo, X. Cui, S.Y. Kang, and V. Martin. 2010. "Near infrared measurements of cotton fiber micronaire by portable near infrared instrumentation." *Textile Research Journal* 80: 1503-1515.

Rossi, R.M., W. Bolli, and R. Stampfli. 2008. "Performance of firefighter's protective clothing after heat exposure." *International Journal of Occupational Safety and Ergonomics* 14 (1): 55-60.

Schwanninger, M., J.C. Rodrigues, and K. Fackler. 2011. "A review of band assignments in near infrared spectra of wood and wood components." *Journal of Near Infrared Spectroscopy* 19 (5): 287-308.

Shorter, G.W., and J.H. McGuire. 1958. *St. Lawernce burns summary report.* Report No. 158 of the Division of Building Research, Ottawa, ON: National Research Council Canada.

Shull, P.J. 2002. "Introduction to NDE." In *Nondestructive evaluation: theory, techniques, and applications*, edited by PJ. Shull, 1-15. New York, NY: Marcel Dekker Inc.

Sipe, J.E. 2004. *Development of an instrumented dynamic mannequin test to rate the thermal protective performance provided by protective clothing.* MSc thesis, Worcester, MA: Worcester Polytechnic Institute.

Slater, K. 1991. "Textile degradation." *Textile Progress* 21 (1): 1-150.

Slater, K. 1986. "The progressive deterioration of textile materials, part I: characteristics of degradation." *Journal of the Textile Institute* 77 (2): 76-87.

Slater, K. 1987. "The progressive deterioration of textile materials, part II: A comparison of abrasion testers." *Journal of Textile Institute* 78 (1): 13-22.

Staggs, J.E.J. 2011. "A reappraisal of convection heat transfer in the cone calorimeter." *Fire Safety Journal* 46 (3): 125-131.

Staggs, J.E.J. 2009. "Convection heat transfer in the cone calorimeter." *Fire Safety Journal* 44 (4): 469-474.

Stull, J., C. Dodgen, M. Connor, and R. McCarthy. 1996. *Evaluating the effectiveness of different laundry approaches for decontaminating structural fire fighting protective clothing: Performance of Protective Clothing: Fifth Volume, STP1237-EB.* West Conshohocken, PA: American Society for Testing and Materials, 447-468.

TA Instruments. 2006. *TGA Thermogravimetric Analyzer - Q series getting started guide, Revision K.* New Castle, DE: Waters LLC.

Thorpe, P. 2004. *Assessment of in-use firefighter's protective clothing.* MSc Thesis, Saskatoon, SK: University of Saskatchewan.

Threlfall, T.G., D.A. Torvi, and P.A. Thorpe. 2004. "Exterior Heat Flux Measurements During House Burn and Implications for Building Codes." *Combustion Institute Canadian Section Spring Technical Meeting.* Kingston, ON: CICS. (Paper #4, Session K, pages 1-6).

Timiras, P.L., W.B. Quay, and A. Vernadakis. 1995. *Hormones and aging.* Boca Raton, Florida: CRC Press.

Torvi, D.A. 1997. *Heat transfer in thin fibrous materials under high heat flux conditions.* Ph.D Thesis, Edmonton, AB: University of Alberta.

Torvi, D.A., M. Rezazadeh, and C. Bespflug. 2016. *Effects of convective and radiative heat sources on thermal response of single and multiple-layer protective fabrics in bench top tests: Tenth Symposium on Performance of Protective Clothing and Equipment: Risk Reduction through Research and Testing.* San Antonio, TX: American Society for Testing and Materials, 131-158.

Udayraj, P. Talukdar, A. Das, and R. Alagirusamy. 2016. "Heat and mass transfer through thermal protective clothing – A review." *International Journal of Thermal Sciences* 106 (0): 32-56.

Vanderschaaf, C.J., J.C. Batcheller, and D.A. Torvi. 2015. "Combined effects of laundering and abrasion on the protective performance of flame resistant fabrics." *Proceedings of Combustion Institute - Canadian Section, Spring Technical Meeting.* Saskatoon, SK. FS6 - FS11.

Veghte, J.H. 1988. *Firefighters' protective clothing: Design criteria, Second edition.* Dayton, OH: Lion Apparel.

Vogelpohl, T., and E.P. Easter. 1997. "Post-use evaluation of fire fighters turnout coats: Proceedings of the Fifth Scandinavian Symposium on Protective Clothing (NOKOBETEF)." *Proceedings of the Fifth Scandinavian Symposium on Protective Clothing (NOKOBETEF).* Elsinore, Denmark: General Workers Union. 68–73.

Vogelpohl, T.L. 1996. *Post-use evaluation of firefighter's turnout coats.* MSc Thesis, Lexington, KY: University of Kentucky.

Wang, M., and J. Li. 2015a. "Thermal protection retention of fire protective clothing after repeated flash fire exposure." *Journal of Industrial Textiles* 46 (3): 1-19.

Washer, G., T. Brooks, and R. Saulsberry. 2009. "Characterization of Kevlar using Raman spectroscopy." *Journal of Materials in Civil Engineering* 21 (5): 226-234.

Westad, F., A. Schmidt, and M. Kermit. 2008. "Incorporating chemical band-assignment in near infrared spectroscopy regression models." *Journal of Near Infrared Spectroscopy* 265-273.

Wijayasinghe, M. 2011. "Fire losses in Canada: Year 2007 and selected years." *Alberta Municipal Affairs: Office of the Fire Commissioner* 0-68.

Winnipeg Architecture. 1913. "Eatons Planbook, Page Twelve, Eadwin Plan E14." *Winnipeg Architecture.* Accessed June 2016. http://www.winnipegarchitecture.ca/wp-content/uploads/2014/10/Eaton-Plan-Book-of-Ideal-Homes.pdf.

Yang, L., Y. Wang, X. Zhou, J. Dai, and Z. Deng. 2012. "Experimental and numerical study of the effect of samlpe orientation of the pyrolysis and ignition of wood slabs exposed to radiation." *Journal of Fire Sciences* 211-223.

Yuen, R.K.K., G.H. Yeoh, G. de Vahl Davis, and E. Leonardi. 2007. "Modelling the pyrolysis of wet wood – II. Three-dimensional cone calorimeter simulation." *International Journal of Heat and Mass Transfer* 4387-4399.

Zhang, C., Q. Zhang, Y. Xue, G. Li, F. Liu, X. Ji, and L. Gao. 2014. "Effect of draw ratio on the morphologies and properties of BPDA/PMDA/ODA polyimide fibers." *Chemical Research in Chinese Universities* 30 (1): 163-167.

Zhang, F., T. Tiyip, J. Ding, M. Sawut, N. Tashpolat, H. Kung, G. Han, and D. Fui. 2012. "Spectral reflectance properties of major objects in desert oasis: a case study of the Weigan–Kuqa river delta oasis in Xinjiang, China." *Environmental Monitoring and Assessment* 184 (8): 5105-5199.

Zhang, H., J. Zhang, J. Chen, X. Hao, S. Wang, and X. Feng. 2006. "Effects of solar UV irradiation on the tensile properties and structure of PPTA fiber." *Polymer Degradation and Stability* 91 (11): 2761-2767.

Zhao, H., M. Zhang, S. Zhang, and J. Lu. 2012. "Influence of fiber characteristics and manufacturing process on the structure and properties of aramid paper." *Polymer-Plastics Technology and Engineering* 51 (2): 134-139.

Zhu, X., L. Yuan, G. Liang, and A. Gu. 2014. "Unique UV-resistant and surface active aramid fibers with simultaneously enhanced mechanical and thermal properties by chemically coating Ce0.8 Ca0.2 O1.8 having low photocatalytic activity." *Journal of Materials Chemistry A* 2 (29): 11286-11298.

# Appendices

## Appendix A: Calibration Data

The incident radiation level utilized in the thermal ageing process was a key parameter. Therefore, a pre-testing calibration of the working heat flux gauge (Model GTW-10-32-485A; Serial 1285515; Huntsville, AL) was performed on August 10, 2016 against a calibration heat flux gauge (Model GTW-10-32-485A; Serial 128559; Huntsville, AL) that is kept in reserve. Figure A.1 and A.2 show the calibration comparison for output voltage and incident cone calorimeter temperature. This calibration was used to adjust a calibration factor within the cone calorimeter's software.

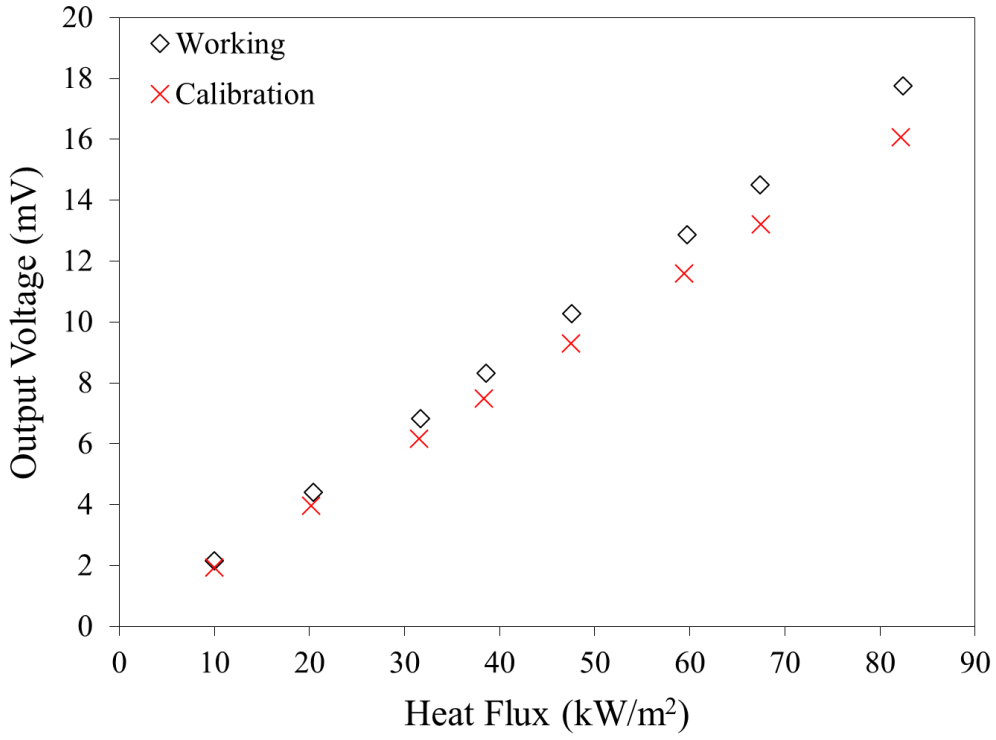


*Figure A.1 Calibration of the working heat flux gauge against a laboratory calibration reserve heat flux gauge for heat flux ranges from 0 – 80 kW/m$^2$*

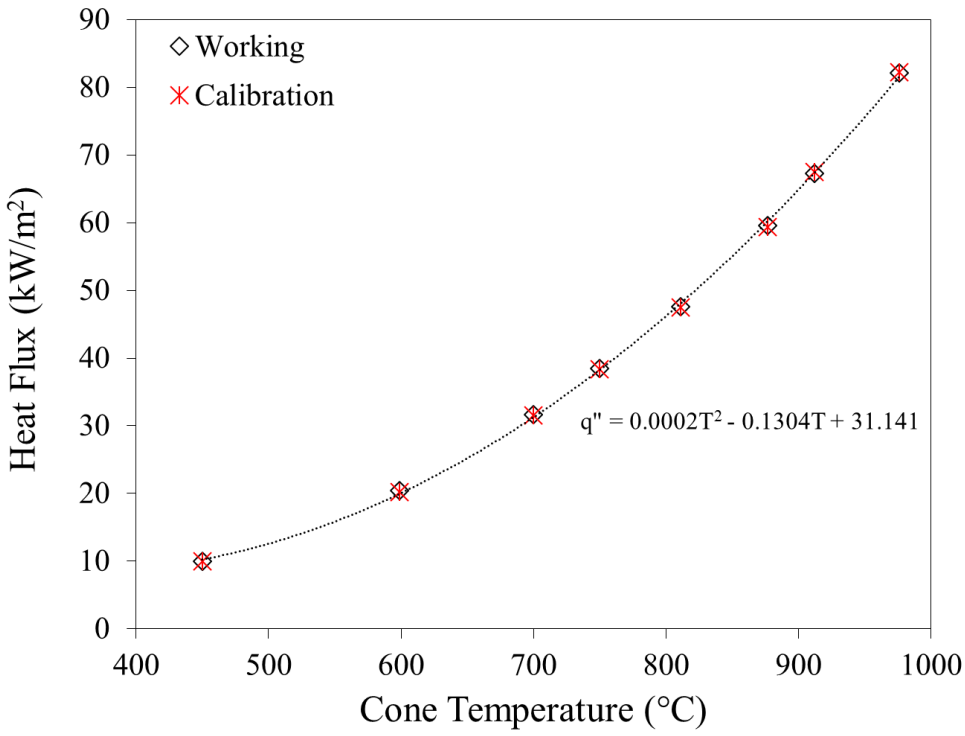


*Figure A.2 Calibration results for both working and calibration heat flux gauge response to incident thermal radiation from a cone calorimeter*

# Appendix B: Tensile Testing Trials

Tensile tests were conducted for RS Natural, RS Black, and SCI PBI Max fabric types following both UV and thermal ageing procedures. The remaining tensile strength indicates the impact of the ageing procedure performed on the specimen. Results given in the body of this thesis were averaged over five specimen results from each ageing procedure. Three results were obtained from the first specimen in the ageing category (e.g. strip A, B, and C of specimen 1 for 10 kW/m$^2$) and two were obtained from the second specimen (e.g. strip A and B from specimen 2 for 10 kW/m$^2$). This left a full four remaining 30 x 150 mm aged strips for further testing and evaluation procedures. Individual results for both thermal and UV aged tensile testing experiments for all three fabrics can be found in Figures B.1 – B.3. Decreases in tensile strength for UV testing seem to follow a defined trend while the thermal ageing trend appears to be more complex. Variability between trials seems to be fairly consistent and the overall grouping at individual ageing points is usually within 50 N. Considering the original unaged specimens have this same level of variability this can be considered an expected level of uncertainty.

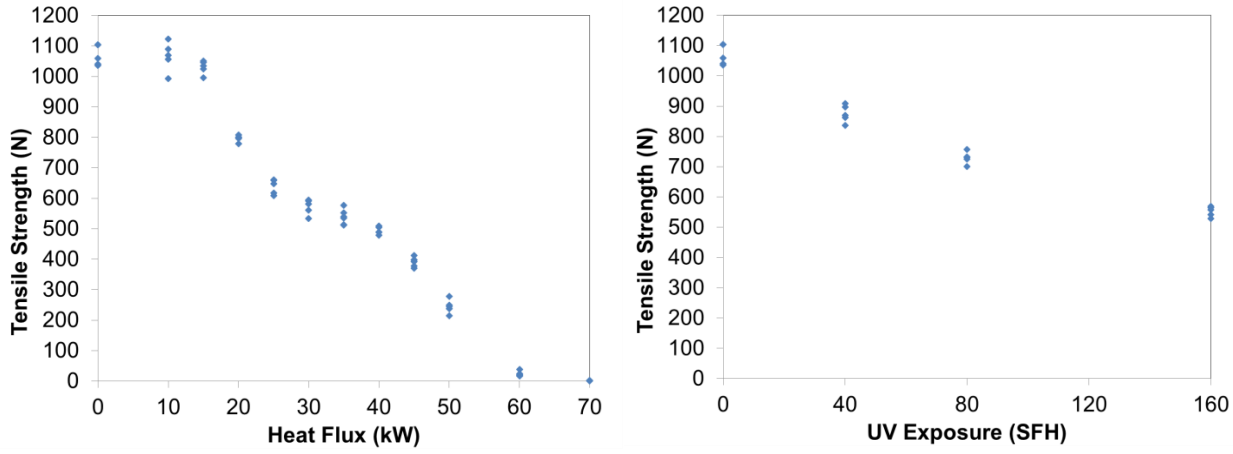


(a) (b)

*Figure B.1 RS Natural tensile testing results for (a) thermally aged and (b) UV aged specimens*

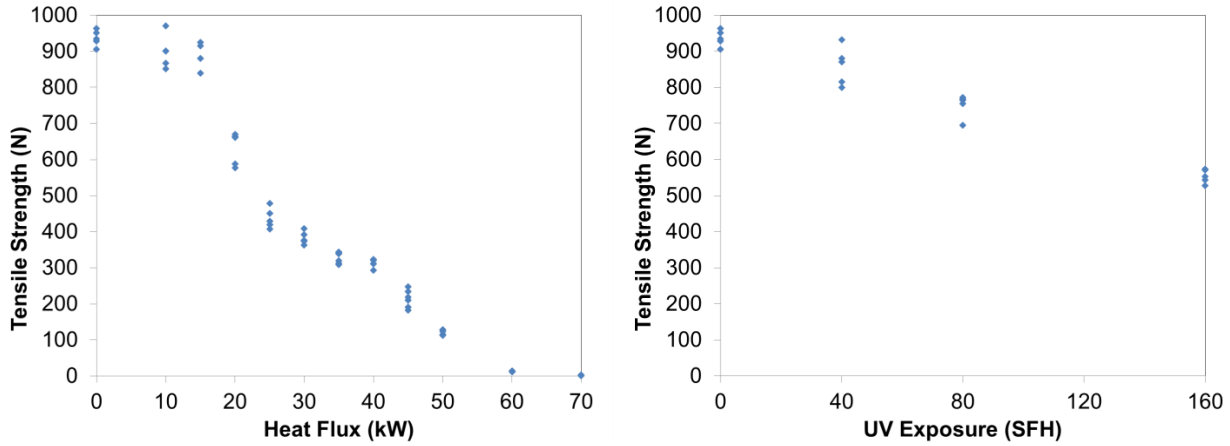


(a) (b)

*Figure B.2 RS Black tensile testing results for (a) thermally aged and (b) UV aged specimens*

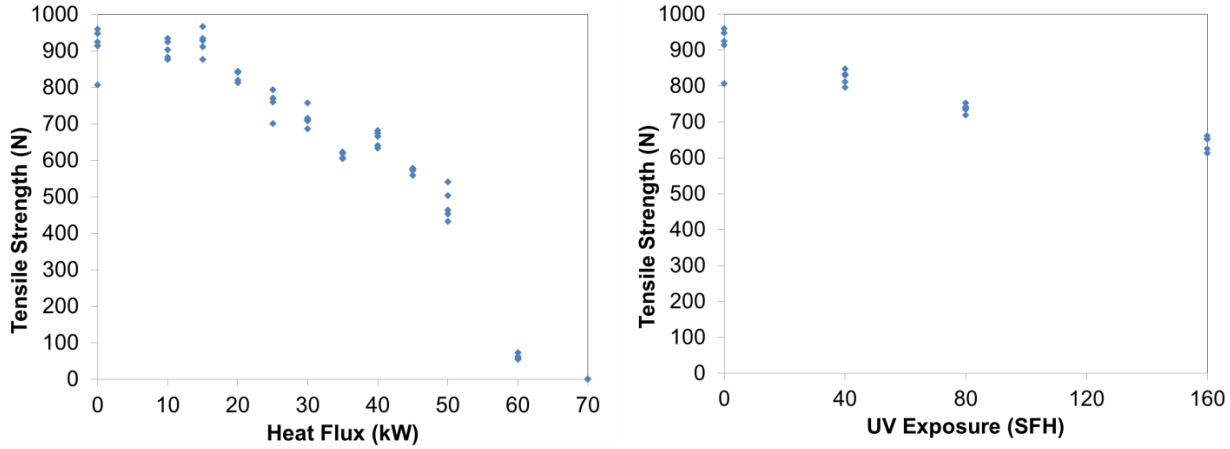


(a) (b)

*Figure B.3 SCI PBI Max tensile testing results for (a) thermally aged and (b) UV aged specimens*

# Appendix C: Initial Low Magnification SEM Images

The initial low magnification (350x) SEM images for, RS Natural, RS Black and SCI PBI Max fabrics are located in this section. Inexperience with the SEM device is evident from the quality of these initial images. Microstructure damage and surface feature changes that occur during the thermal and UV ageing process are similar to those described previously.

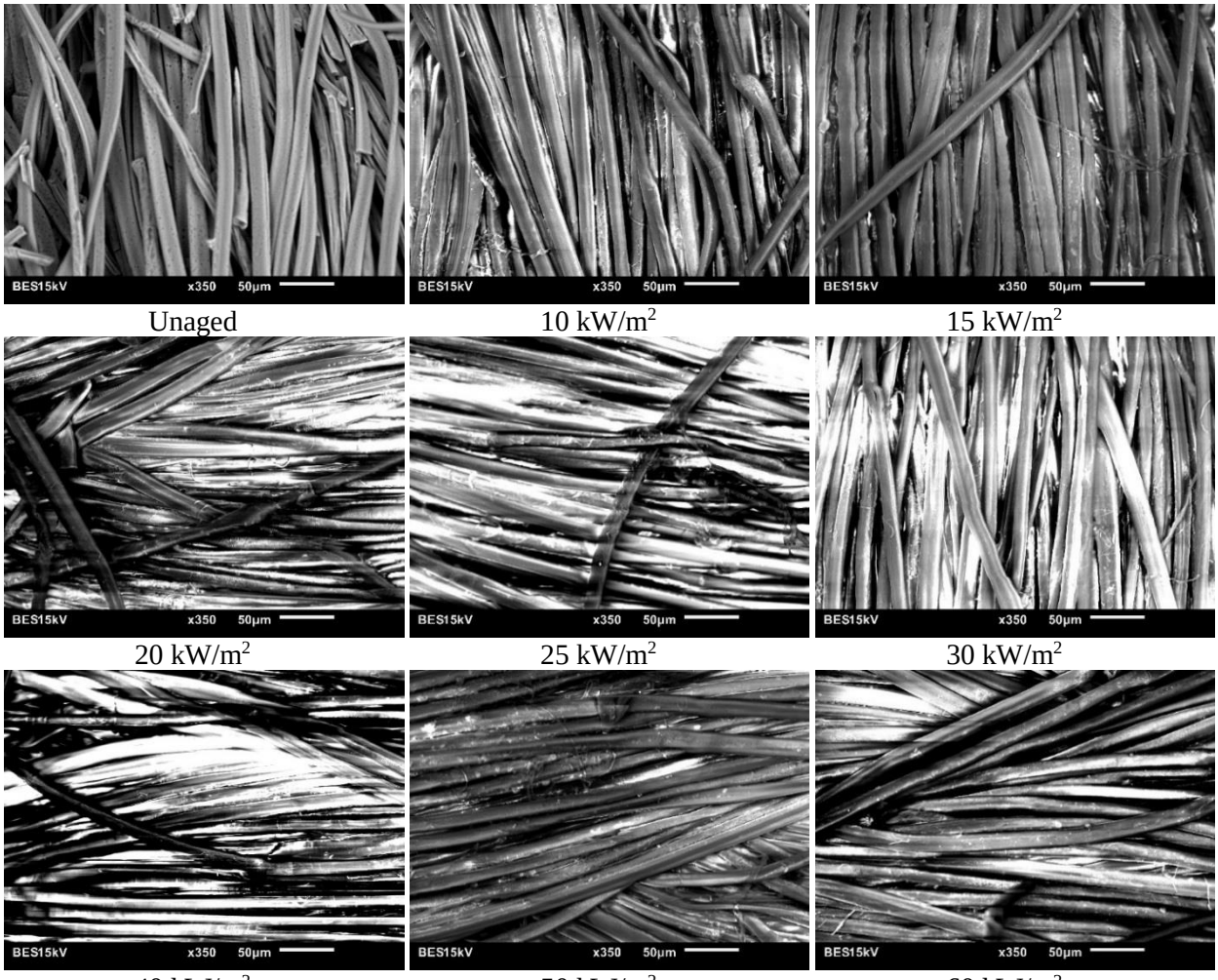


*Figure C.1 RS Natural SEM imaging for thermally and UV aged specimens*

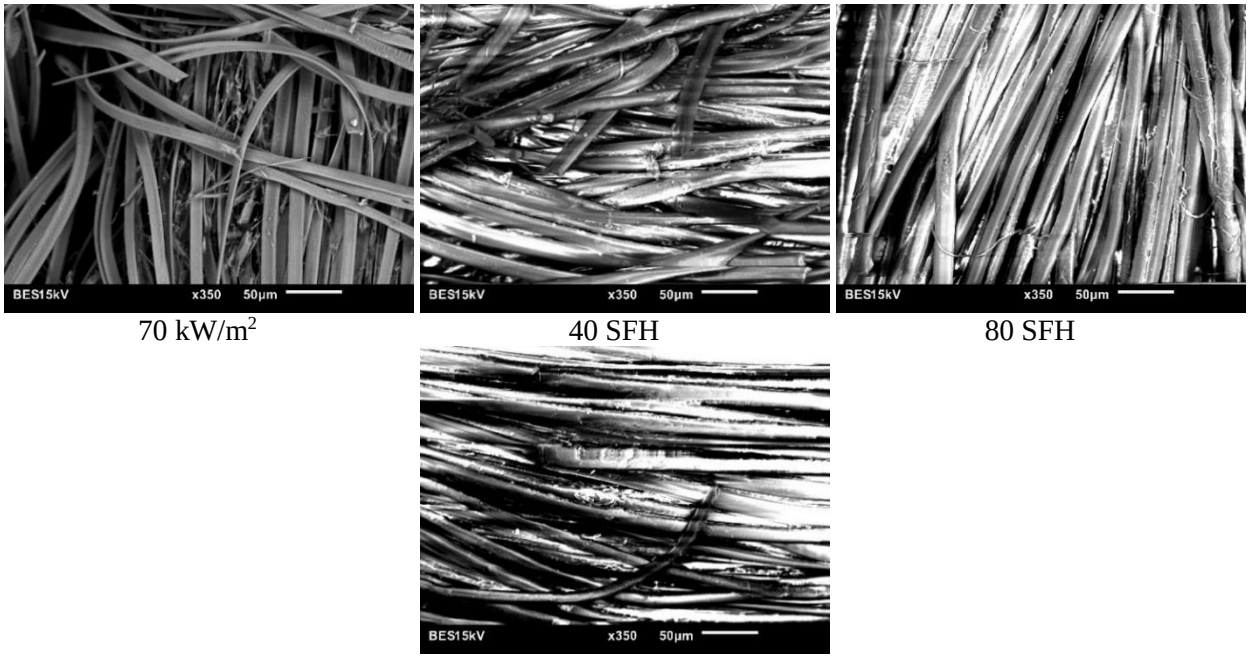


70 kW/m$^2$ 40 SFH 80 SFH

160 SFH

*Figure C.1 Continued*

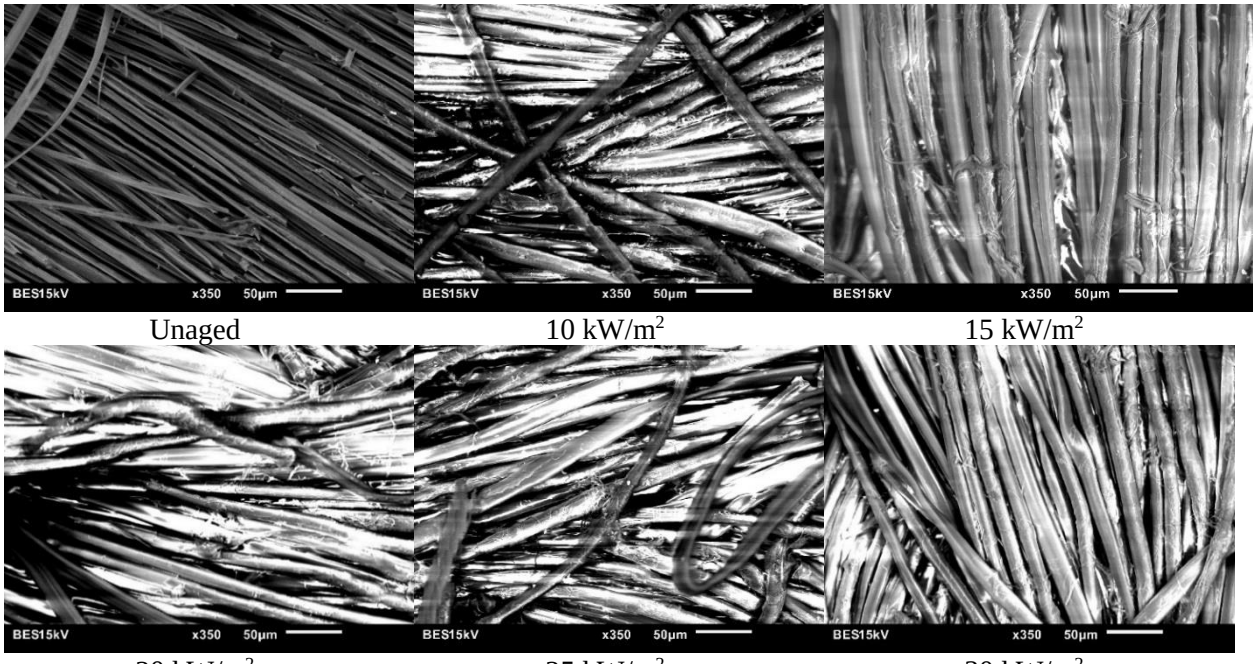


Unaged 10 kW/m$^2$ 15 kW/m$^2$

20 kW/m$^2$ 25 kW/m$^2$ 30 kW/m$^2$

*Figure C.2 RS Black SEM images for both thermally and UV aged specimens*

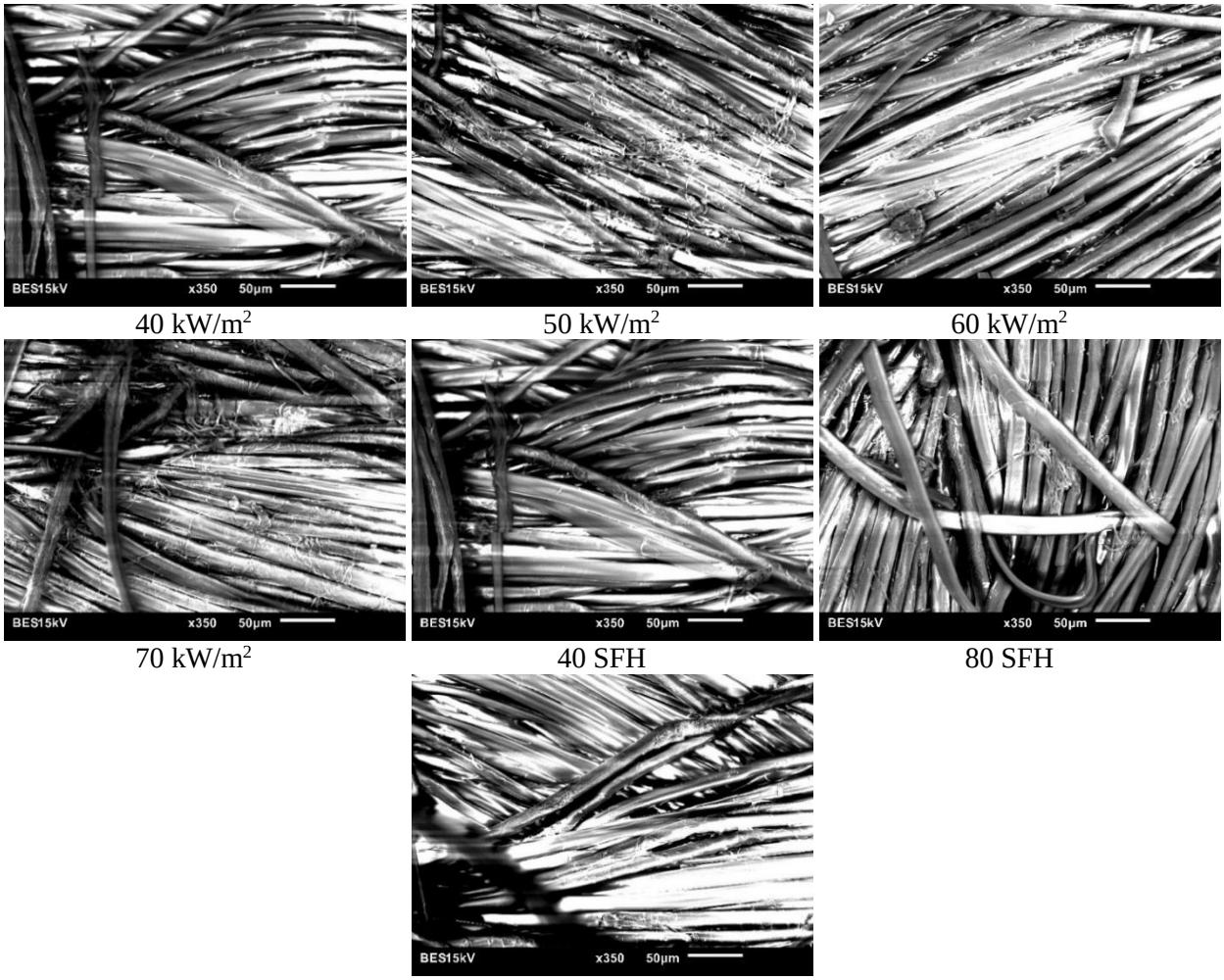


40 kW/m$^2$ 50 kW/m$^2$ 60 kW/m$^2$

70 kW/m$^2$ 40 SFH 80 SFH

160 SFH

*Figure C.2 Continued*

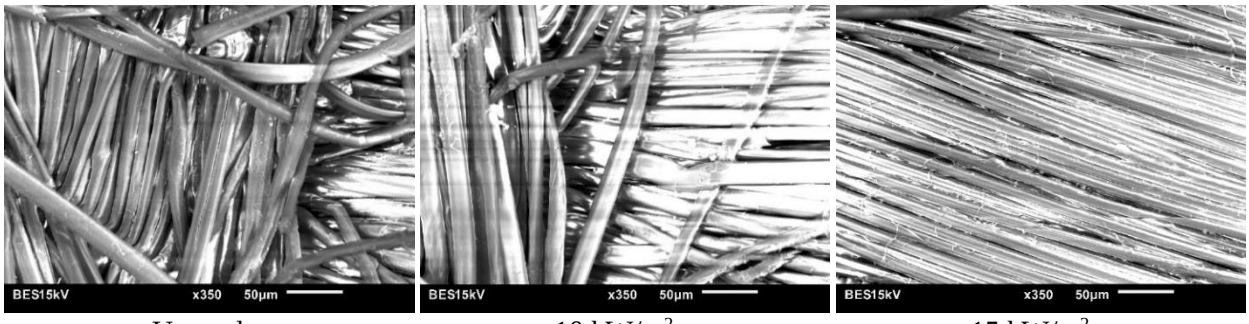


Unaged 10 kW/m$^2$ 15 kW/m$^2$

*Figure C.3 SCI PBI Max SEM imaging for thermally and UV aged specimens*

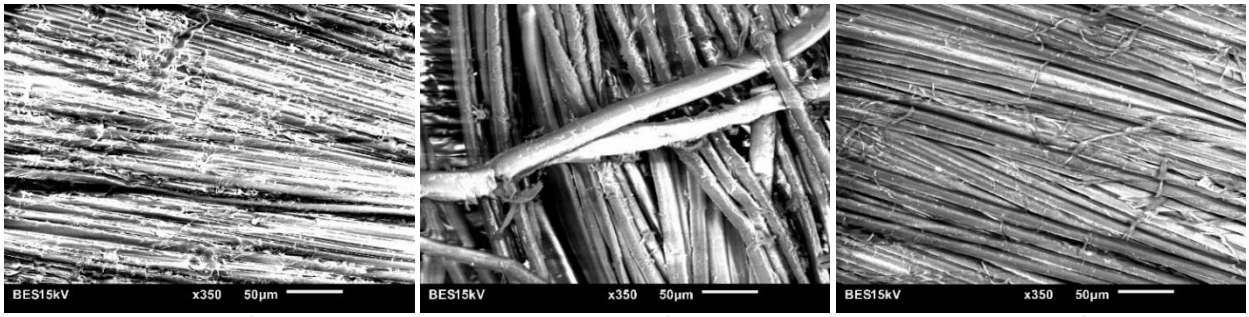


20 kW/m$^2$ 25 kW/m$^2$ 30 kW/m$^2$

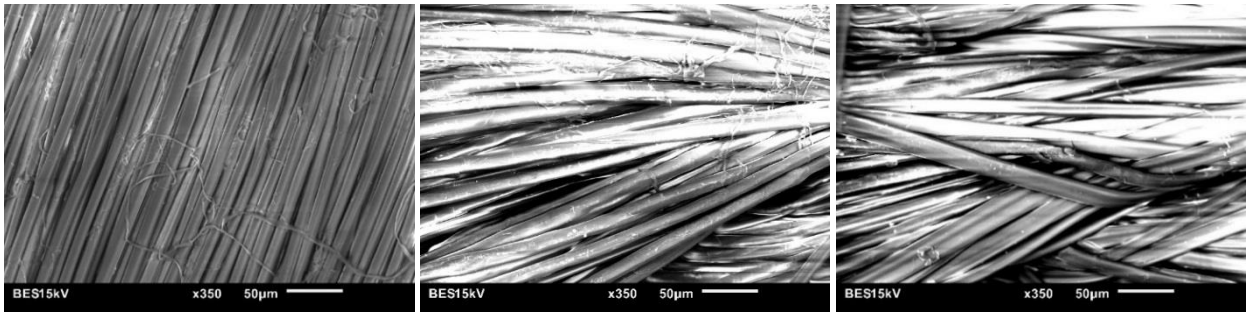


40 kW/m$^2$ 50 kW/m$^2$ 60 kW/m$^2$

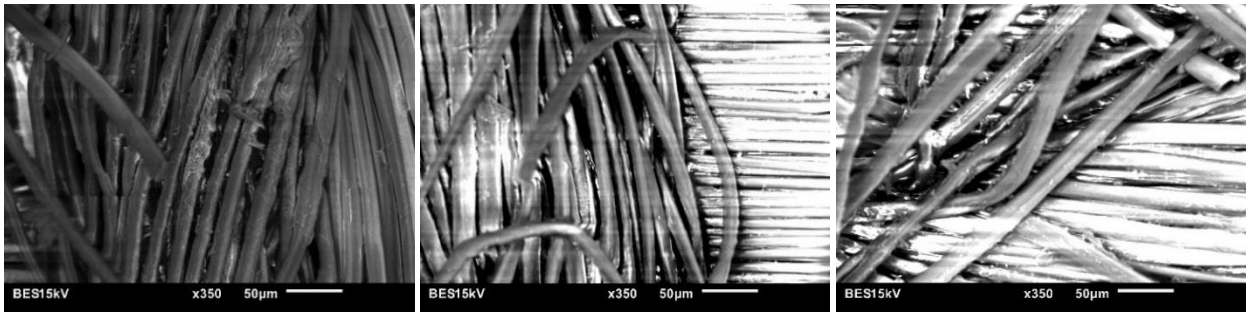


70 kW/m$^2$ 40 SFH 80 SFH

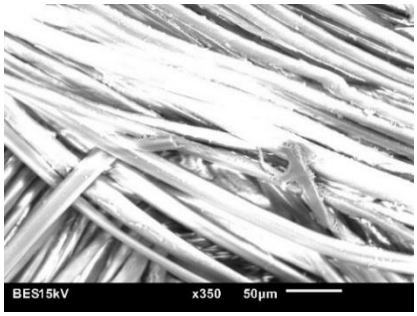


160 SFH

*Figure C.3 Continued*

# Appendix D: Absorbance Feature Analysis from MatLab

The following section contains original absorbance peak height, local peak prominence, width, and wavelength location analysis for all three fabric types obtained from a modified MatLab "findpeaks" function. The UV aged absorbance feature data from MatLab is also contained in this section.

A minimum peak prominence of 0.01 was initially selected in order to eliminate the inclusion of smaller peak features. Investigating a relaxation change in peak prominence to 0.005 was then used to gain a few additional data points. Further relaxation to 0.001 and 0.0025 minimum peak prominence failed to provide additional data points in this study. The following graphs highlight the absorbance local peak prominence, width, and wavelength location the RS Natural, RS Black, and SCI PBI Max fabrics following ageing procedures.

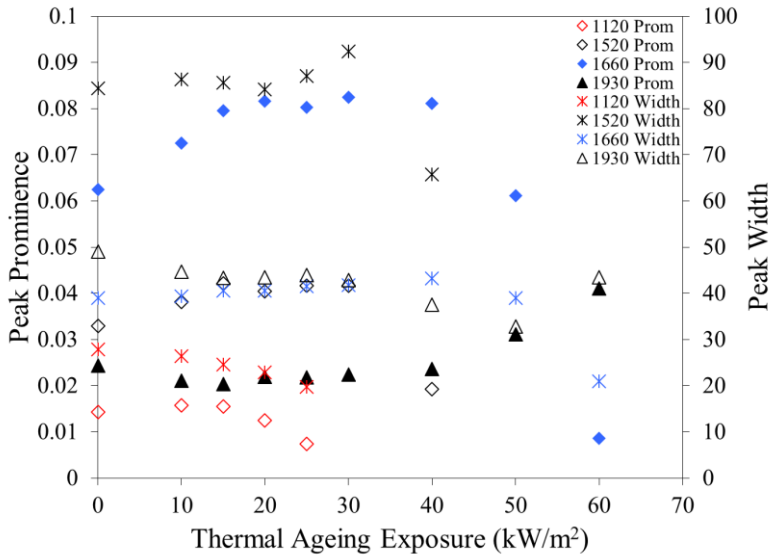


(a)

*Figure D.1 Local peak prominence and peak width changes in relation to thermal ageing exposure for (a) RS Natural, (b) RS Black, and (c) SCI PBI Max fabrics at 1130, 1520, 1660, and 1930 nm absorbance feature wavelength regions*

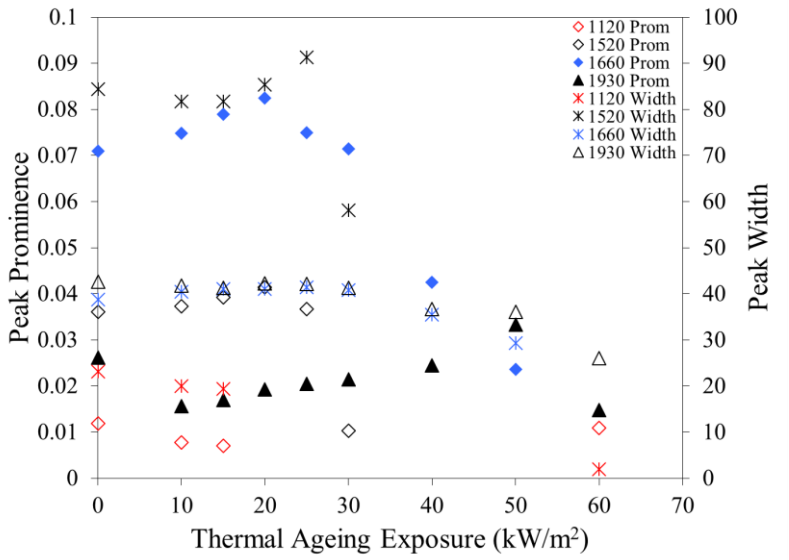


(b)

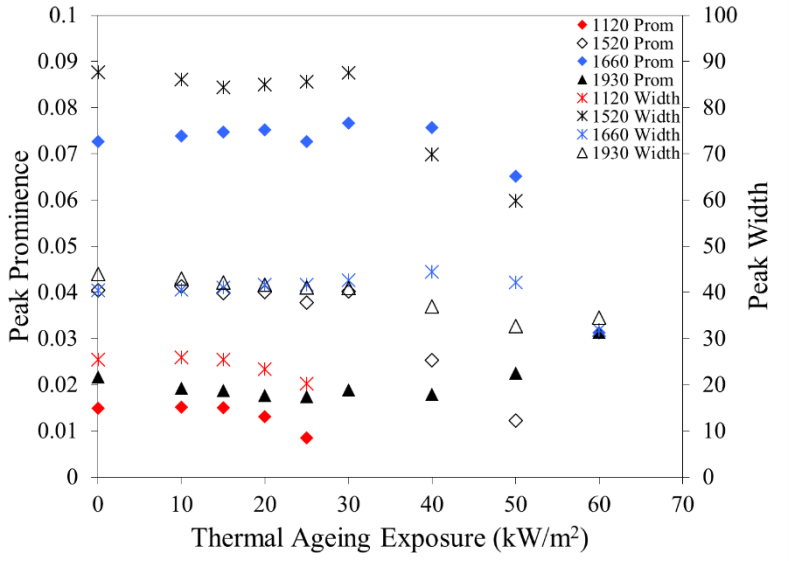


(c)

*Figure D.1 Continued*

The same method of analysis can be applied to absorbance peaks following UV ageing. The absorbance feature changes at the previously examined key wavelength regions (1130, 1520, 1660, and 1930 nm) are examined in Figure D.0.10 for UV aged specimens.

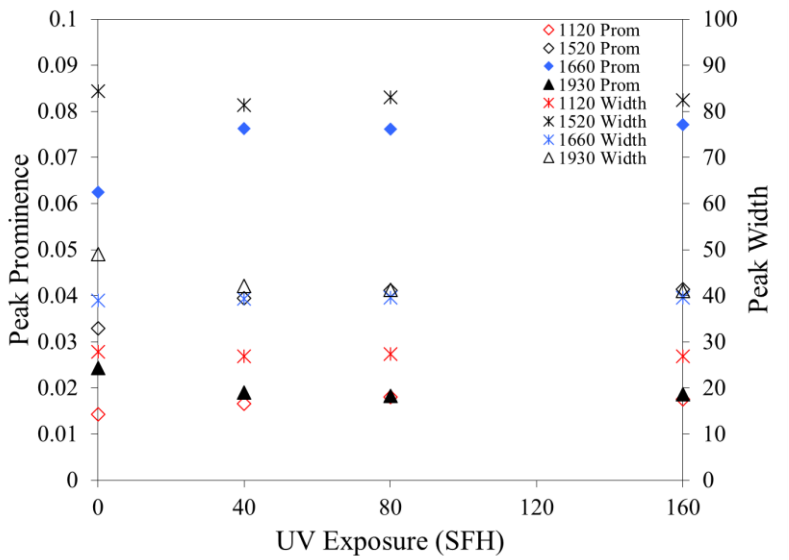


(a)

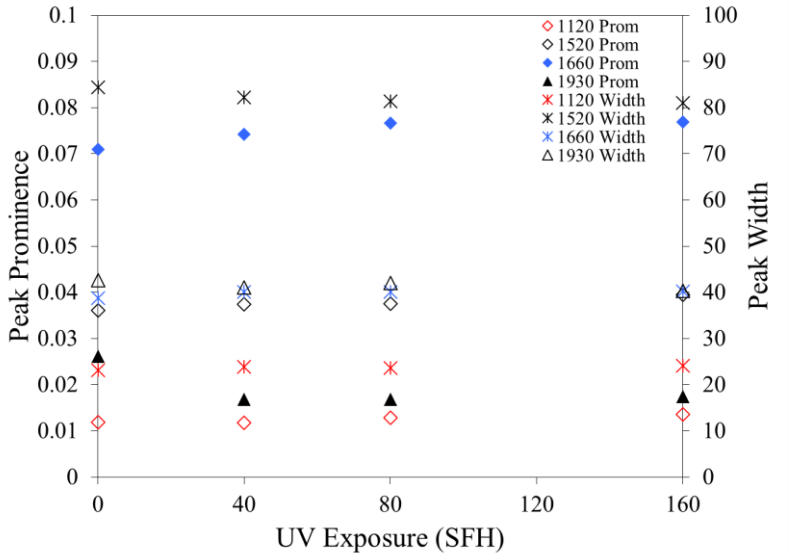


(b)

*Figure D.2 Local peak prominence and peak width changes in relation to UV ageing exposure for (a) RS Natural, (b) RS Black, and (c) SCI PBI Max fabrics at 1130, 1520, 1660, and 1930 nm absorbance feature wavelength regions*

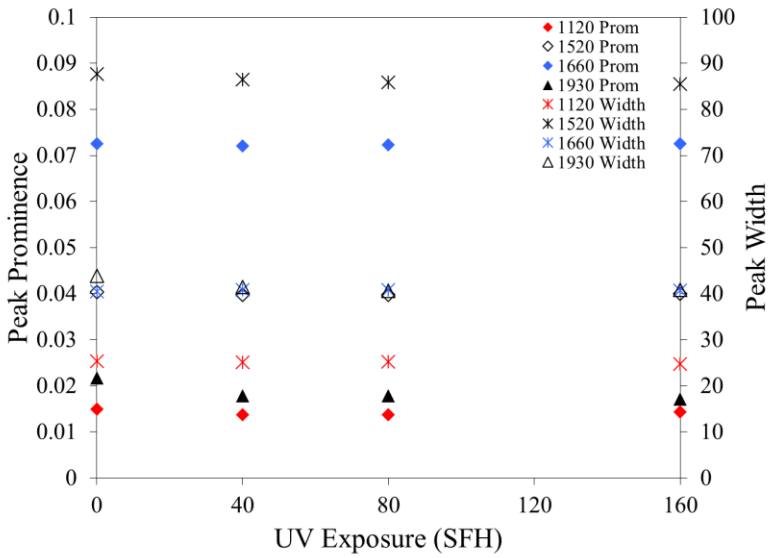


(c)

*Figure D.2 Continued*

# Appendix E: Continuum Removal Procedure

The following section contains details on the continuum removal process (also called baseline normalization) performed to compare the absorbance feature areas in Section 4.2.2. A straight-line segment was used to create a right trapezoid area that was removed prior to comparison of the individual areas. The sketch in Figure E.1 shows an example of two trapezoidal areas that would be removed through this method during analysis. The bounds in this example sketch have been shifted slightly for improved clarity (i.e. bounds would be the same in actual removal process completed in this study).

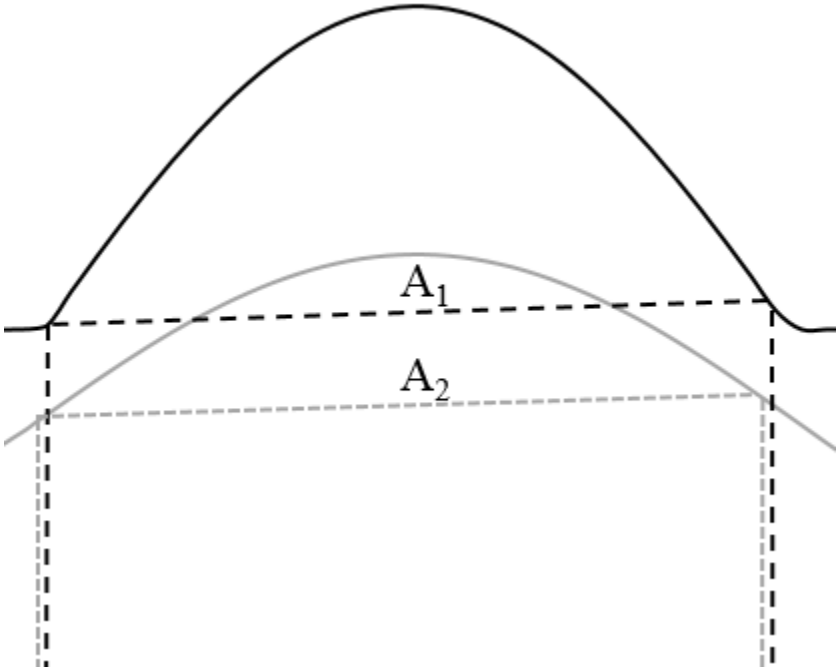


*Figure E.1 Sketch of straight-line trapezoid method of continuum removal*